# Influence of carbon content and sintering temperature on the green and sintered properties of cemented carbide tool grades

Thandazi Makhosazana Maseko

A dissertation submitted to the Faculty of Engineering and the Built Environment, University of the Witwatersrand, Johannesburg, in fulfilment of the requirements for the degree of Master of Science in Engineering.

October 2014

# Declaration

I declare that this report is my own unaided work. It is to be submitted for the Masters of Science in Engineering at the University of the Witwatersrand, Johannesburg. This report has never been submitted before for any degree or examination in any other University.

Student Name: Thandazi Maseko; Student No.: 0614453N

Student Signature: ……

# Abstract

A research study was done on four different cemented carbide cutting tool grades, which had different Co contents and different compositions of additional carbides such as TiC, TaC, NbC, $Cr_3C_2$ and TiCN. The tool grades were manufactured using the powder metallurgy process. The aims of the research were to investigate how carbon content and sintering temperature influences the material properties, and if possible to select the optimum parameters to yield the best sintered properties for each tool grade. The chemical analysis of the starting and milled powders with three different C contents were done using X-ray Fluorescence (XRF) and Inductively Coupled Plasma- Optical Emission Spectroscopy (ICP-OES), with phase identification and morphology done using X-Ray Diffraction (XRD) and Scanning Electron Microscopy (SEM) analysis. The milled and dried powders were pressed and sintered at three different sintering temperatures. Microstructural characterization of the sintered alloys included phase analysis, and measurement of the WC grain size, WC contiguity and Co binder mean free path. The hardness, toughness, coercivity, density, porosity and magnetic cobalt was determined using relevant standards. In general, as the C content increased, graphite formed in the alloys which resulted in lower hardness and toughness. The hardnesses of the different grades were affected in different ways and were dependent on the level of mixed carbides added and the Co content. It was also clear that as the Co content increased with the increase in C level, the hardness of the alloys decreased. The density for all the alloys decreased with an increase in C content. The porosity for all the alloys increased with an increase in C content. As the sintering temperature increased grain growth increased. However, with the addition of $Cr_3C_2$, which is a grain growth inhibitor, some alloys could be sintered at higher temperatures with limited grain growth. For all four tool grades the best material properties were obtained with the stoichiometric C content. With respect to sintering temperature, two grades showed the best properties at 1430°C while the other two grades had their best properties at 1510°C.

## Acknowledgements

I would love to say a very special thanks

*To:*

*My supervisor Prof. Natasha Sacks:* for believing in me and her supervision and support throughout the MSc.

*Pilot Tools:* for providing the project, materials and facilities to run the experiments for the project.

*Andrew Sekgobela (Pilot Tools):* for his tireless lab work assistance.

*My family and friends:* for their unconditional love and support as well as their prayers.

*Above all GOD:* for giving me the strength to carry on each day until the end of the MSc.

# Table of Contents

# List of Figures

# List of Tables

# Chapter 1

## Introduction

Cemented carbide is classified as a hardmetal because it exhibits high hardness values [1]. These hardmetals are manufactured using powder metallurgy processes, which include mixing, wet milling, drying, pressing and sintering [1]. This production process allows the alloys to be manufactured into different sizes and shapes depending on the application, which includes drill bit inserts, cutting tools and forming dies [2, 3]. A fundamental feature of the cemented carbide materials is the potential to vary its composition, so that the resulting physical and chemical properties ensure maximum resistance to wear, deformation, fracture, corrosion and oxidation. The common type of cemented carbide is based on the WC-Co system. In this alloy the WC phase provides the high hardness and wear resistance while the Co phase provides the toughness and impact strength [2]. Mixed carbides such as TiC, TaC, NbC and $Cr_2C_3$ may be added to the WC-Co to improve its performance for specific applications.

During sintering of the cemented carbides the stoichiometric carbon required is typically 6.13 wt %C of the WC and not the whole WC-Co system [4]. Excess carbon causes the formation of free carbon in the microstructure of cemented carbide during sintering which may be removed during sintering thereby increasing porosity levels known as type C graphite porosity. The addition of less than 6.13 wt% C generally leads to the formation of eta phase which is known to compromise the mechanical properties of the alloy when present in high amounts [3]. The carbon levels are also known to influence phase evolution during sintering and thus directly impact the final sintered material properties. For example, it has been shown that a high carbon content enhances shrinkage of the WC-Co material while a low carbon content delays shrinkage during sintering [5]. Thus the carbon content strongly influences the performance of the material during application. Sintering temperature is another factor that influences the properties of hardmetals. Frykholm et al [6] stated that as the sintering temperature of a WC-Co alloy increases, grain growth is promoted which leads to a decrease in alloy hardness [6]. If the sintering temperature is too low the alloy does not fully densify. It has also been shown that the optimum sintering temperature is dependent on the composition of the cemented carbides [6].

Therefore, in this research project, a systematic study on the influence of carbon content and sintering temperature on the production, green and sintered properties of four cemented carbide tool grades was conducted.

## 1.1. Aims and Objectives

The main aim of the research was to develop and improve the sintering properties of commercial cemented carbide tools. Another aim of this research project was to determine the optimum carbon level and sintering temperature for four commercial cemented carbide tool grades; the grades were chosen from the simple system to the complex system of WC-Co. The test conditions of the research were chosen in order to be of relevance to the present cemented carbide industry.

The aim was achieved through the following objectives:

- Sintering each tool grade at three commercial temperatures.
- Investigating the influence of carbon on phase evolution by adjusting the carbon levels during the initial stage of mixing.
- Characterizing the powder, green and sintered material properties.
- Establishing relationships between carbon levels, sintering temperature and material properties.

## 1.2. Structure of dissertation

This dissertation is structured as follows: Chapter 1 explains the significance of the research work. Chapter 2 reviews published literature on the production of cemented carbides, the influence of carbon levels and sintering temperature, as well as the properties of the alloys. Chapter 3 describes the experimental procedures followed during the project. The results are presented in Chapter 4 and discussed in Chapter 5. Chapters 6 and 7 provide the conclusions and recommendations for future work, respectively. Finally a list of references and relevant appendices are provided.

# Chapter 2

## Literature Review

This chapter provides a review of published research work that has been done on the subject under investigation in the present work. This chapter will describe hardmetals in general, how they are manufactured, the effect or influence of carbon content and sintering temperature, as well as the sintered properties of these cemented carbides.

### 2.1. Hardmetals

Hardmetals are tungsten-carbide-cobalt composites, which are manufactured using powder metallurgy processes and are the most commonly used in the cutting tool industry. The word 'cemented' refers to the tungsten carbide (WC) particles being cemented in the metallic binder forming a metallurgical bond [1]. The WC phase usually ranges from 70-97% of the total weight of the alloy and is mixed with a binder material, predominantly cobalt (Co), but nickel (Ni) may also be used [1]. According to Sandvik [7] the metal cutting tools have a Co composition that typically ranges from 6 - 17 wt.% Co. This composite also belongs to the family called cermets, which is derived from WC being a ceramic material (*cer*) and Co a metallic material (*met*) [8]. Ceramics are known to be very hard, while metals are known for their good toughness properties; thus the combination of these two materials provides a unique compound or alloy of two very important mechanical properties.

Fig. 2.1 is a pseudo-phase diagram showing how the two materials combine to form the desired composite at various temperatures. It also shows the eutectic point at 1320℃, which is where the Co starts to transform to a liquid phase [3].

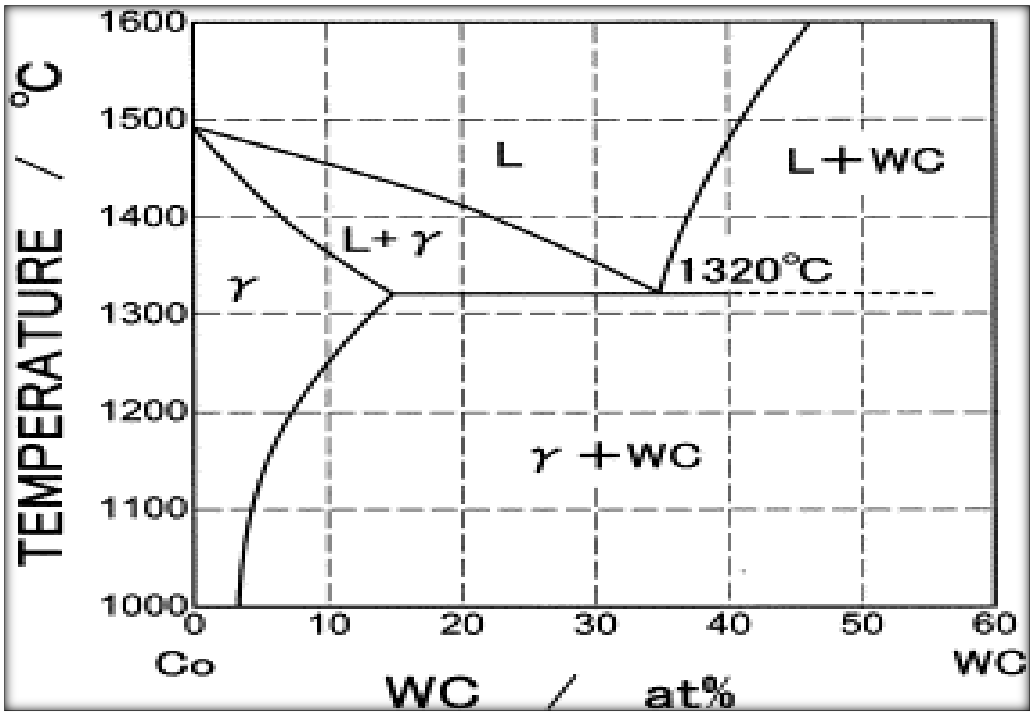


Fig. 2.1: A pseudo-binary phase diagram in the system of Co and WC [3].

Tungsten carbide has a high melting point of 2870°C, as shown in Fig. 2.2 which is the binary phase diagram of W-C, which clearly shows the location of the systems liquidus line [3]. Tungsten carbide is also extremely hard (1700-2400 Vickers number) and has a low electrical resistivity (~$2\times10^{-7}$ Ohm/m). It has a hexagonal close-packed (HCP) crystal structure as shown in Fig. 2.3. The carbon (C) in the WC crystal structure is fixed at interstitial sites and enhances the hardness of the material and allows good wettability by the Co binder [7].

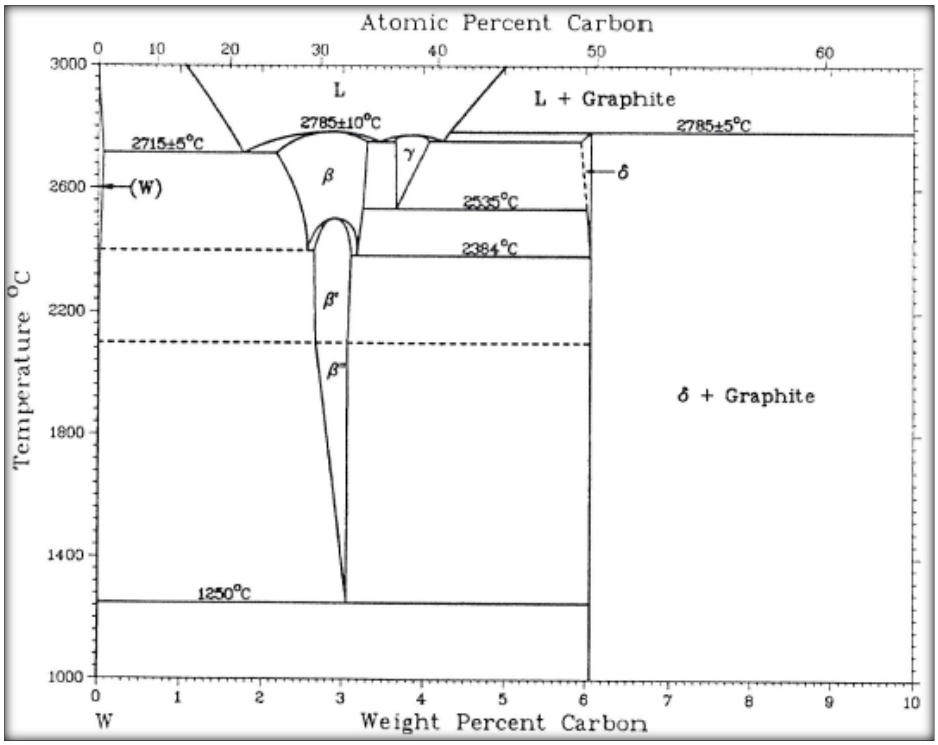


Fig. 2.2: Binary phase diagram of W-C system [3].

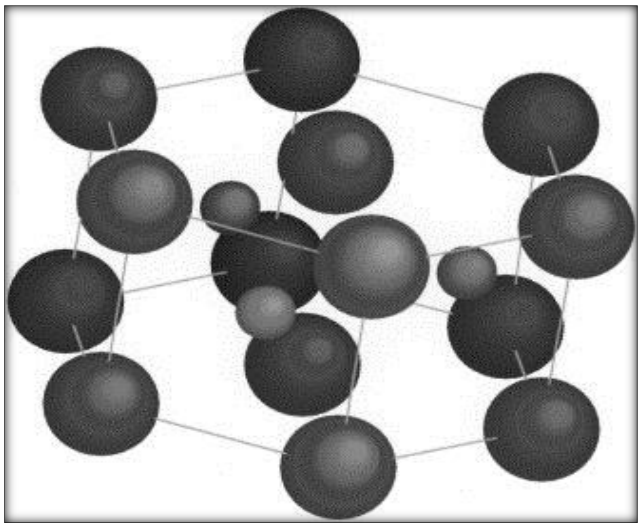

Fig. 2.3: Schematic image of the WC HCP crystal structure. Large spheres are W and small spheres C [4].

Cobalt is a ferromagnetic metal which is commonly found as a compound rather than an element. It has an atomic number of 27 and is between iron (Fe) and Ni on the periodic table, which are the other binders often used for cemented WC systems. Cobalt has a melting point of 1495℃ a density of 8.90 g/cm$^3$ and heat capacity of 24.81 J/mol.K [9].

It has two allotropic forms; below 417°C it shows a hexagonal close-packed (HCP) structure and above this temperature up to its melting point is represented by a face centred cubic (FCC) structure [10]. Fig. 2.4 is a schematic of the Co HCPcrystal structure [5].

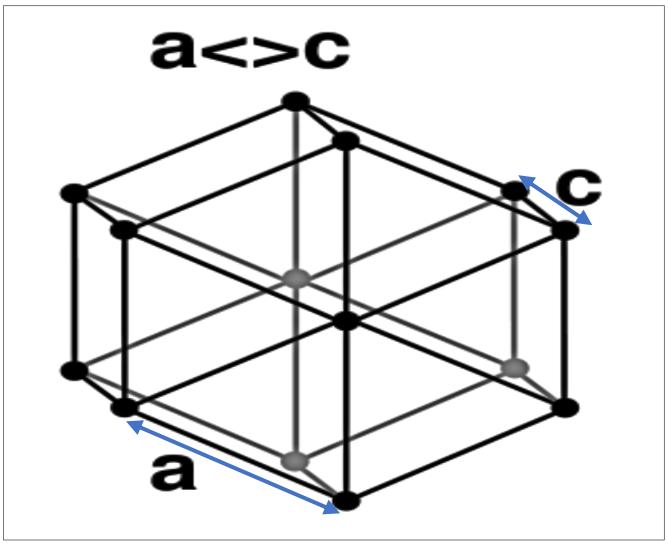


Fig. 2.4: Schematic of the Co crystal structure [5].

Depending on the application of the material, sometimes small amounts of additional metals are added to the basic WC-Co composite to improve the performance of the material. The typical metals that are added and their respective properties are [8]:

- TiC, Ti(C, N): predominantly added to increase the hardness. The addition of these metals also limits crack propagation into the bulk which may cause failure. The addition of these metals lead to the formation of a gradient zone at the outer edges of the microstructure, leaving this area rich in the binder phase and depleted of the mixed carbides as seen in Fig. 2.5 [6]. This creates a tough surface zone in an insert prior to coating.

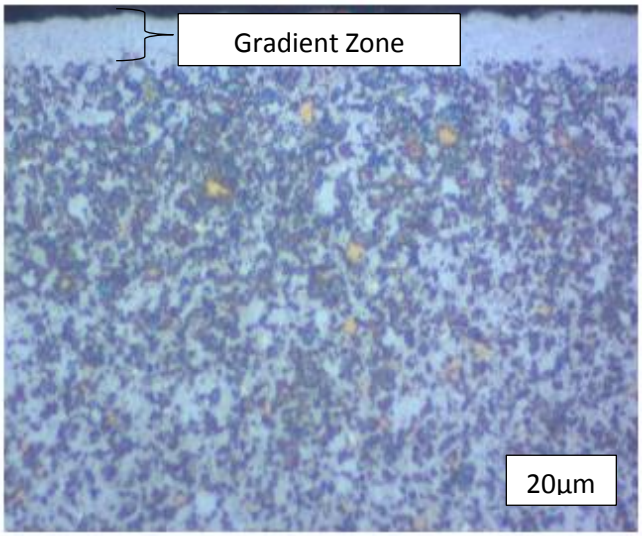


Fig. 2.5: WC-Co system with gradient zone where: (a) shows it under an optical microscope [6].

- (Ta, Nb)C: These mixed carbides also increase wear resistance, thermal shock resistance and high temperature perfomance. When added in high quantities they also slightly decrease the hardness of the carbide [11]. The decrease in transverse rupture strength is remarkably high for (Ta, Nb) C contents exceeding 20 wt%. They are also used to improve the oxidation and corrosion resistance.
- VC, $Cr_3C_2$: these carbides are grain growth inhibitors which lead to increased hardness. They are also used to improve the oxidation and corrosion resistance [12]. The addition of Cr significantly lowers the initial melting point, but also broadens the melting range, in particular at low carbon levels [13].
- $Mo_2C$: this carbide improves the wettability of Ti(C, N) when added.

## 2.2. Manufacturing process

Cemented tungsten carbide – cobalt alloys are manufactured using powder metallurgy processes which have three major steps, namely: mixing and blending, compaction and sintering. Fig. 2.6 is a basic flow sheet for the production process. Some of the reasons for using powder metallurgy to manufacture cemented tungsten carbides include [3]:

- WC does not melt. According to Fig. 2.2 it is seen that the melting point of WC is at 2785±10°C, while the production of the alloys occurs at the melting point of the binder phase which is much lower. The melting point is too high and it becomes too expensive because of energy consumption.
- The component materials retain their original properties;
- It is economical when producing large volumes of small parts, requiring close tolerances, with minimum finishing operations.

The limitations of powder metallurgy include [1]:

- Requires high pressure capacities;
- The powders must have very specific and carefully controlled characteristics. Deviations may lead to a non-uniform sintered density which would compromise the final properties.

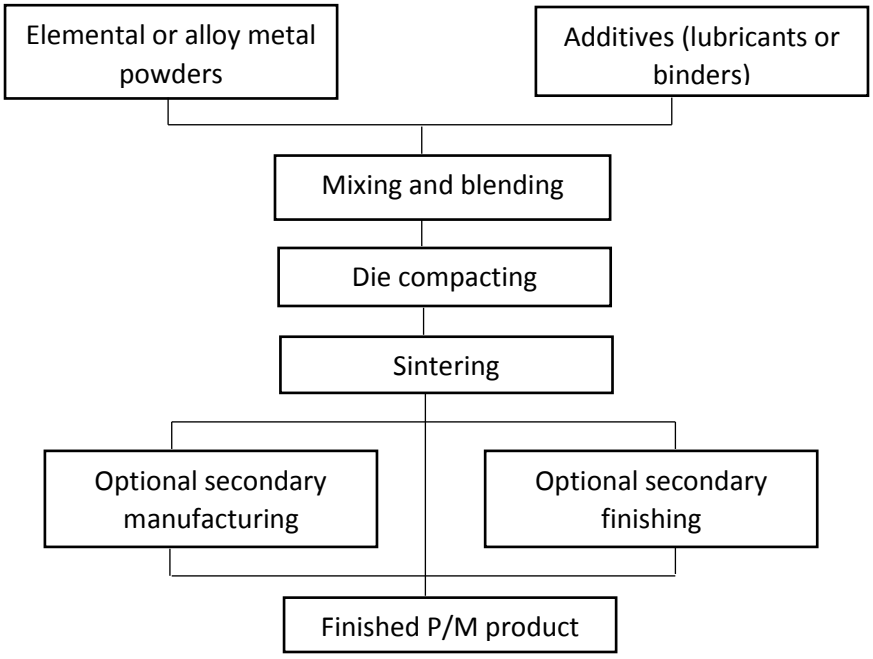


Fig. 2.6: Powder metallurgy block flowsheet [3].

### 2.2.1. Mixing and milling

Different powders are mixed to form a homogeneous mixture. Different mixers can be used to achieve this process. Fig. 2.7 shows a typical mixer, as well as a schematic of the powder particles, as they are mixed together. The mixing can also be done using various types of milling media. Different mills can be used such as ball mills and attritor mills. In attritor milling mechanical alloying is achieved by high energy ball milling under conditions such that the powders are not only fragmented but also re-welded together [14].

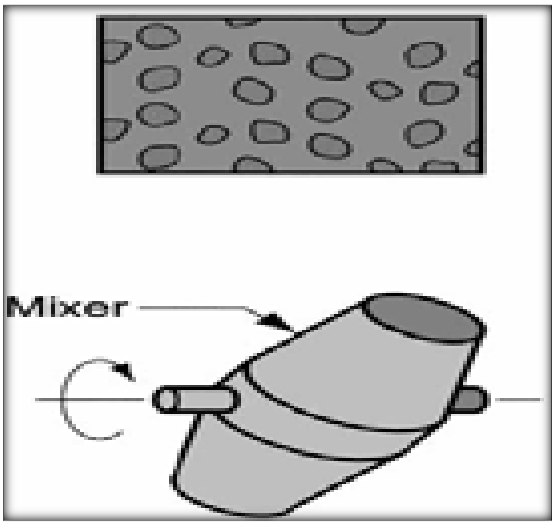


Fig. 2.7: The mixer and particle distribution of powder [4].

Ball milling is the commonly applied comminution method in the cemented carbide industry. This process is carried out mainly to mix/blend the carbides with the binder metal using lubricants. The lubricants usually consist of paraffin wax or polyethylene glycol (PEG), which are introduced to enhance the pressing properties of the materials [2]. The uniformity of the mixture after milling influences the mechanical properties and reduces the level of porosity in the sintered products. The important purpose of ball milling, apart from particle size reduction, is to ensure that every carbide particle is coated with cobalt [1, 2].

Conventional ball milling of hardmetal powders is carried out in simple, cylindrical, rotating ball mills [2]. These mills vary in size over a range, but little difference is observed in their milling action. Larger mills appear to be more effective than small ones. However, from an efficiency point of view, vibratory milling is best because the balls tend to rotate individually, as well as in unison. For the best results carbide balls should be used to limit contamination.

Ball mills and attritor mills are preferably lined with carbide and typically carry a charge of carbide balls of 2.5 to 3 times the weight of the powder charge [2]. Because of the significantly high milling energy, a liquid is introduced when carrying out the process in order to protect the powder from oxidizing and limiting increases in temperature. Wet milling of the carbides is normally carried out using an organic liquid such as acetone, hexane or alcohol. Liquid is also used to ensure sufficient mixing. The milled slurry mixture is dried using either a spray dryer which leaves the powder as granules, or it can be oven dried in a vacuum. The drying process is employed to remove the organic liquid, and spray drying is used to granuate the powder making it suitable for pressing [2].

### 2.2.2. Pressing

The blended powders are then pressed in dies, under high pressure into the required shape. After compaction the product is called a green compact; the word green meaning not yet fully processed. Fig. 2.8 shows typical steps during compaction, beginning with step 1 where the powder is transported to the presser and charged into the die (step 2) after which compaction begins (step 3). In step 4 compaction is complete and the part is then ejected (step 5). As a result of compaction, the density of the part, called the green density, is much greater than the starting material density [15, 16].

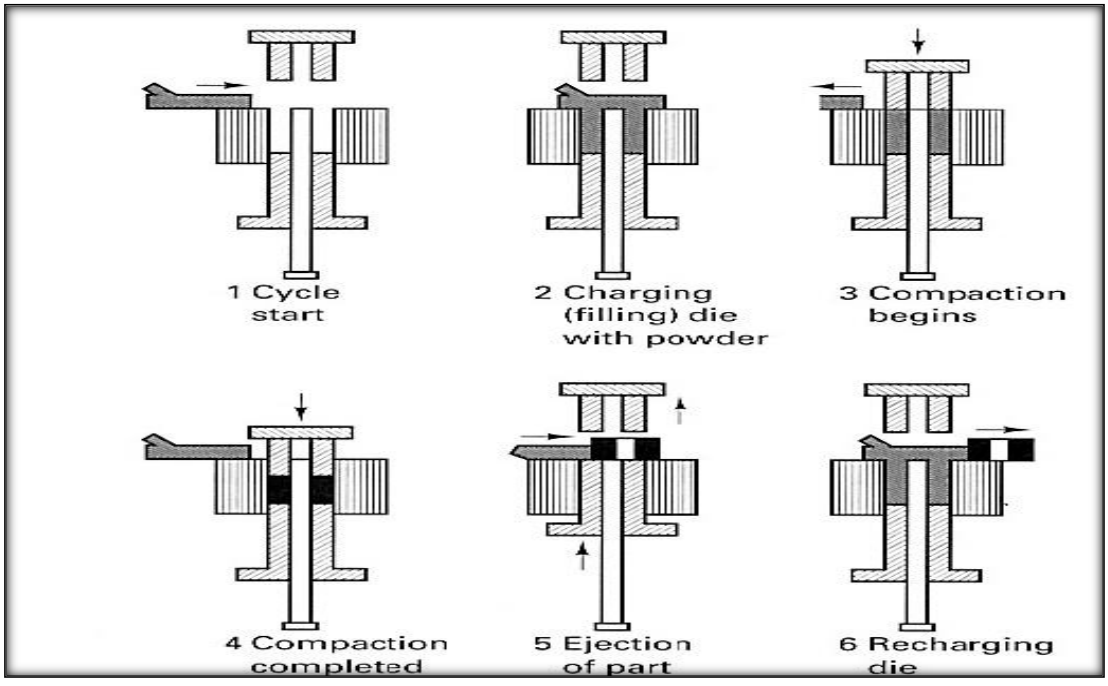


Fig. 2.8: Typical steps in compaction [7].

### 2.2.3. Sintering

The compacted powders will be bonded together when heated to temperatures in excess of about half of the absolute melting temperature; this phenomenon is referred to as sintering [1]. Characteristic of all forms of sintering is a reduction in surface area which assists in strengthening of the compact. The green compact is sintered at temperatures below the WC melting temperature, usually 1400°C, which is just above the Co melting point [4]. During sintering, diffusion occurs, and the pores either diminish in size or close up, as seen in Fig. 2.9. Sintering results in densification of the green compact, which improves its mechanical properties.

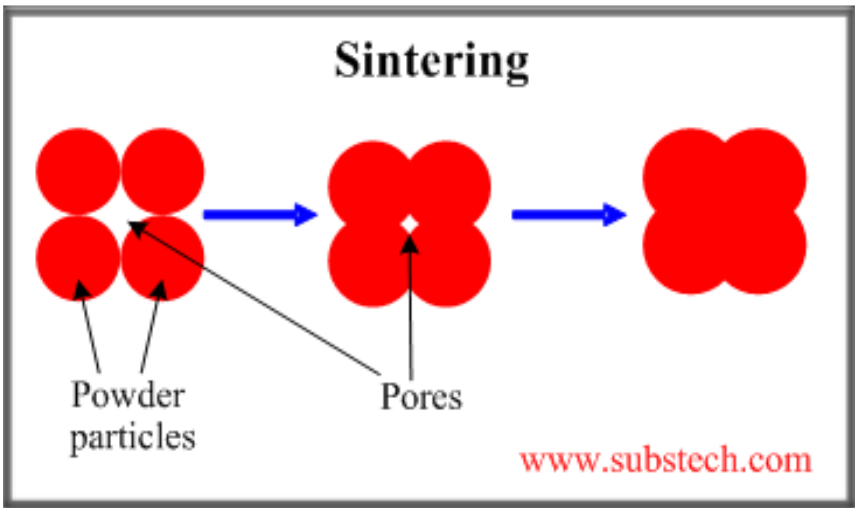


Fig. 2.9: Sintering process [17].

There are different sintering methods that can be employed to form the cemented carbide alloys which include solid phase sintering and liquid phase sintering. In this review the focus will be on the liquid sintering of the cemented carbides as this was the method used in this research project. During liquid phase sintering, a liquid co-exists with a particulate solid at the sintering temperature and the liquid phase usually enhances the rate of inter-particle bonding [18]. During sintering the excess surface energy attributed to porosity, is decreased by means of matter transport, which becomes kinetically possible at high temperature.

Within the main classes of liquid phase sintering, there are several possible variants dependent on the material characteristics, i.e. the solid may be soluble or insoluble in the liquid. Such a difference greatly affects the rate of sintering and the microstructure evolution.

Other major factors relate to the interfacial energies between the liquid and solid phases (wetting versus non-wetting liquids) and relative penetration of the liquid along solid- solid grain boundaries. These variants coupled to the processing options like particle size, sintering temperature, time, atmosphere, and green density have further large effects on the type of material formed [18].

Sintering occurs in a continuous process, usually in three stages, namely [8]:

- Preheating, for removing the lubricant and other organic materials;
- Sintering, where diffusion occurs;
- Cooling, when the sintered parts cool down.

Fig. 2.10 is a schematic of the sintering process which indicates the initial stage where the mixed powders are heated to the temperature where melting initiates and solid phase sintering is attained. Then the particles and liquid phase rearranges themselves where after solution re-precipitation occurs, followed by the final densification of the alloy.

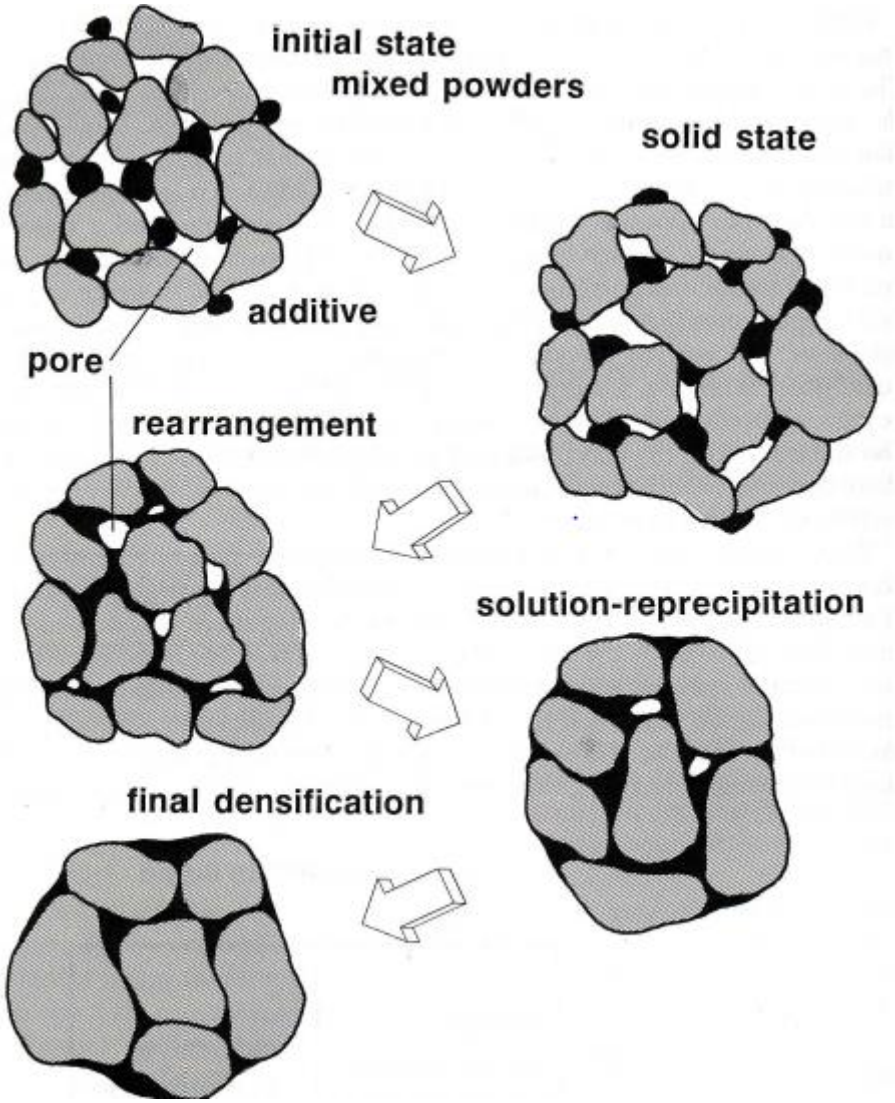


Fig. 2.10: Sintering stages [2].

During sintering Ostwald ripening occurs where the large grains become larger. Neck growth between two particles in contact is a crucial aspect of sintering. Fig. 2.11 illustrates it best.

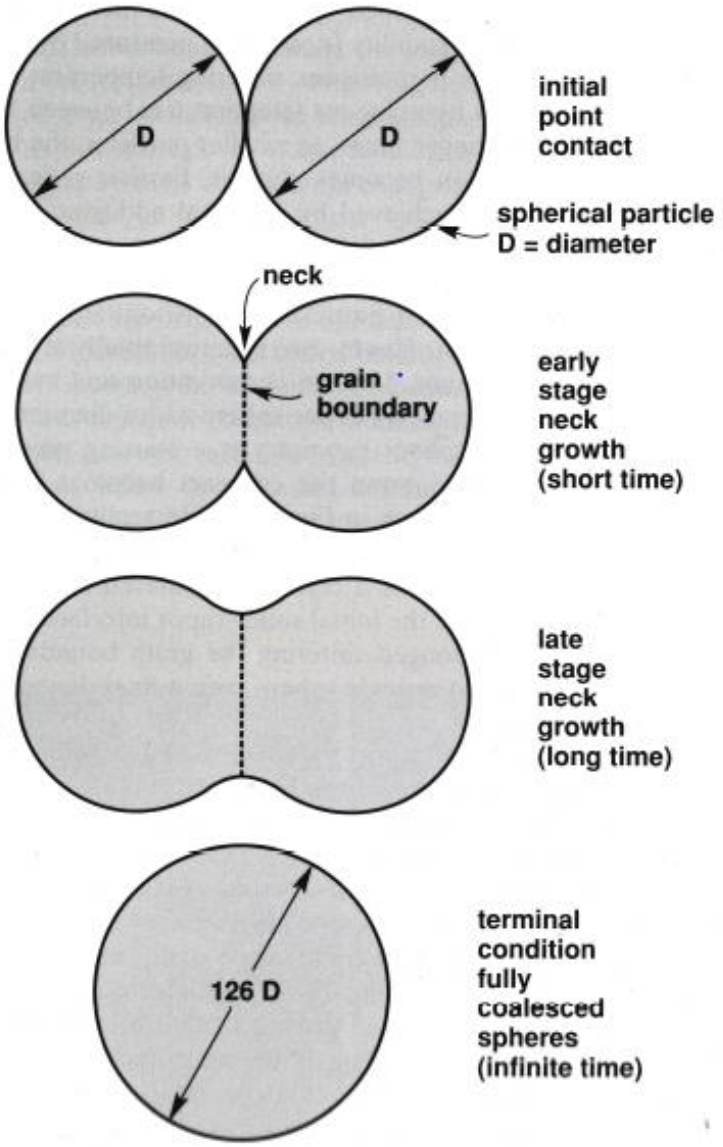


Fig. 2.11: Two sphere sintering model [2].

### 2.3. Effect of carbon content

Carbon influences the physical and mechanical properties of the sintered material. In stoichiometric proportions, the total amount of carbon in the carbide composite is 6.12 wt% [1]. This is calculated from the atomic ratio of WC which is c/w = 1/1 = 1. The molecular weight of W is 184 g/mol, whilst the molecular weight of C is 12 g/mol. Thus the C content in WC is 6.13 wt.%. A carbon deficiency in the microstructure leads to the formation of lower carbides which are brittle, such as the η-phase [2, 19]. When the carbon content is less than 6.13 wt.% the hardness of the alloy may also increase, whilst the toughness of the alloy decreases. If an excessive amount of carbon is present, then free carbon will appear along the grain boundaries [1]. These carbon rich areas will disrupt the WC-Co matrix and affect the properties of the material. Excess carbon will influence the grain size of the final alloy, and it is also classified according to ASTM standard B276-91[20] as type C porosity [2]. Since the carbon content can be changed substantially during sintering by reactions with oxygen-containing phases, and by carbon exchange reactions with the metallic content in the initial material, control of the composition of the starting powder, as well as the furnace atmosphere, is essential to produce high-quality powder metallurgy parts.

The C content also affects the sintering temperature and the formation of the first liquid or melt [18]. As a result a certain temperature range can be defined in which the metallic binder (Co) is only partly molten during the isothermal sintering process [13]. The lowest value of melt formation can be expected in the case of excess C, whereas the highest value can be expected in the case of deficient C. Melt formation at certain C levels can occur within a certain temperature range, which implies, that other than in the case of a melting point, melt formation takes place gradually with time/temperature during heating over a certain temperature range [21]. Only at the end of this range, will all the Co be transformed into liquid. When mixed carbides are added, it can be expected that they will interfere with the liquid formation and will therefore have an influence on the optimal sintering range.

By varying the C content, the sintered properties of the alloy are influenced. According to the work done by Cura et al [21] the effect of C content on the density is given in Fig. 2.12. The upper curve represents the theoretical densities of the studied compositions and the curves

below it represent the densities of the compacts consolidated with different techniques. In the presence of 0.2 wt. % C, the measured density of the material was very close to its theoretical density; which indicates almost full densification. At all other C contents, the densities were slightly lower than the theoretical density values. The measured density of the hot isostatically pressed (HIPed) material was 13.40 g/cm$^3$ and it increased slightly in the presence of 0.2 wt.% C to 13.43 g/cm$^3$. When the carbon amount was 0.4 wt.% C the densities of all the compositions, regardless of the production technique dropped significantly [21].

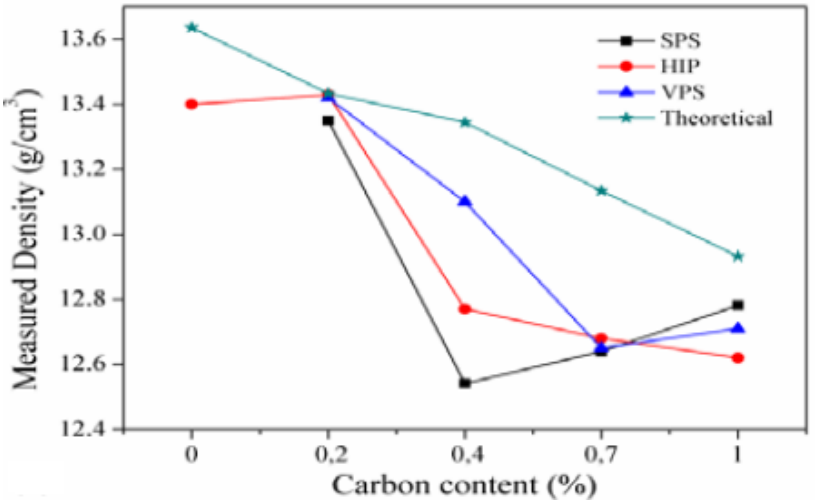


Fig. 2.12: Effect of C content on the density [21].

## 2.4. Material properties of hardmetals

There are many properties that can be analysed on cemented carbide; however, here only mechanical properties and magnetic properties will be discussed.

### 2.4.1. Mechanical properties

Cemented tungsten carbides are used for their excellent combination of hardness and fracture toughness, thus these properties will be briefly reviewed. Several factors which influence these properties include the chemical composition of the starting components, carbon levels, density and microstructural properties such as the WC grain size, Co mean free path and WC contiguity [4].

***Hardness***

Hardness is a measure of the resistance to plastic deformation [22]. Since the carbide phase has a relatively hard and brittle character, and the binder phase is soft and ductile, the hardness of the alloy is primarily accounted for by the carbide phase [1]. Therefore the main factors which influence hardness are the cobalt volume fraction and particle size of the carbide phase as reflected in Fig. 2.13 [16]. An increase in the carbide grain size leads to a decrease in the hardness, a decrease in the cobalt volume fraction leads to an increase in hardness .

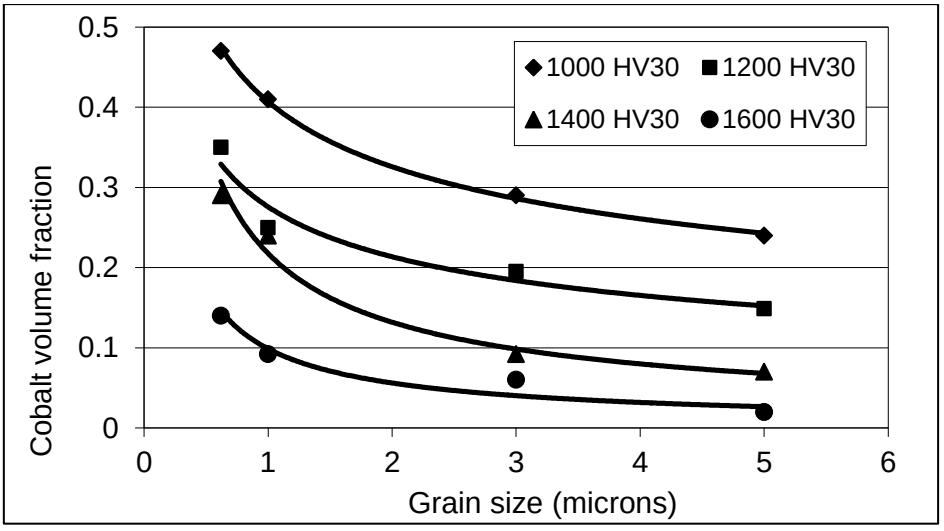


Fig. 2.13: Mechanical properties with respect to grain size and Co content [16].

***Fracture toughness***

Fracture toughness is a measure of the energy required for crack initiation and propagation [23]. Brittle materials are known to have a high hardness and low fracture toughness; hence fracture toughness generally exhibits an inverse relation to hardness. The effect of C content on fracture toughness is illustrated in Fig. 2.14 which shows that the type of sintering method influences the relationship. There is also no general trend of increasing toughness with increasing C content.

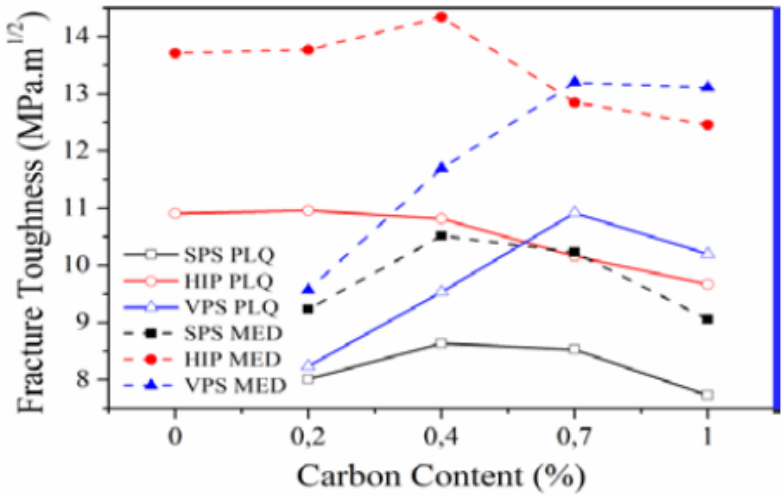


Fig. 2.14: Effect of C content on fracture toughness [21].

### 2.4.2. Magnetic properties

The magnetic properties of cemented tungsten carbides are generally measured in industry as a quality control measure. It is well known that the carbon content greatly influences the magnetic properties, hence a brief review will be given of the two main magnetic properties, namely coercivity and saturation magnetization.

***Coercivity***

Coercivity is the intensity of the applied magnetic field required to reduce the magnetization of a material to zero after the magnetization of the sample has been driven to saturation [24]. Thus coercivity measures the resistance of a ferromagnetic material, i.e. the Co phase, to becoming demagnetized. It is usually measured in units of Oersteds or ampere/meter and is denoted $H_C$ [24]. Coercivity is influenced by the C content, WC grain size, cobalt content and the sintering temperature [25]. The coercive force of the cobalt phase increases with the amount of tungsten dissolved in it, due to solution and precipitation hardening [2].

### *Saturation Magnetization*

Saturation magnetization (SatMag) is used to measure the magnetism of a sample [21]. In the tungsten carbide - cobalt system the only ferromagnetic phase is the Co based binder, hence this property is measured in Co percentage. The sintering temperature must be considered for cemented carbides containing substantial amounts of cubic carbides, when utilizing SatMag as a tool for carbon balance adjustments or sintering furnace monitoring [19]. The solubility of other cubic carbides (Ti, Nb, Ta, etc.) forming metallic elements in the binder phase is quite low, and will have no significant effect on SatMag and the solubility of WC [2]. The amount of tungsten in solution or precipitated in the binder phase decreases the magnetism of the alloy. This is due to the effect of the carbon content on the overall alloy system. It is known from stoichiometry that the ratio of W: C is 1:1, so if there is less carbon in the alloy this means that there is W that does not have any carbon to bond with, so it will precipitate on the binder phase forming an eta phase and thereby reduces the magnetism of the alloy, as there is less pure cobalt in the system [10].

# Chapter 3

## Experimental Procedure

This chapter describes the details of the experimental procedure followed to produce and characterize the properties of the sintered alloys used in this study. Detailed descriptions of the different tests that were performed in order to investigate the effect of carbon level and sintering temperature on the green and sintered properties of the alloys are given. The chapter is divided into three main sections namely, powder characterization, production of the alloys and sintered alloy characterization.

### 3.1. Powder characterization

The starting powders were characterized using ICP, XRF, XRD and SEM to confirm the composition and phases present and to detect if any impurities were present.

#### 3.1.1. Powders

WC, TiCN, $Cr_3C_2$, mixed carbides and Co powders were mixed to produce four different alloys that were studied in this project. Table 3.1 lists the composition of each alloy. Additional W and C powders were used to adjust the carbon level of the final alloy composition in order to assess the influence of C content on the alloy properties.

Table 3.1: Composition of the cemented carbide cutting tool grades in wt %.

| | **WC** | **Co** | **$Cr_3C_2$** | **TiCN** | **Mixed carbides** |
|---|---|---|---|---|---|
| **Alloy A** | 94.0 | 6.0 | - | - | - |
| **Alloy B** | 85.5 | 6.6 | - | 2.5 | 5.4 |
| **Alloy C** | 85.0 | 5.0 | 0.3 | 2.5 | 7.2 |
| **Alloy D** | 79.3 | 9.5 | - | 2.5 | 8.7 |

### 3.1.2. X-Ray Fluorescence (XRF)

This analysis was done to conduct elemental and chemical analysis of each powder. An 8 g powder sample was pressed at 10 tons pressure in a 20 mm backing cup without binder and analyzed using a Rigaku ZSX Primus II using EZ Scan semi-quantitative analysis. The source was a Rhodium tube using the WDXRF method. The results of the elements present in each powder were given in their oxide form from which the elemental composition was calculated.

### 3.1.3. Inductively Coupled Plasma (ICP) -Optical Emission Spectroscopy (OES)

This analysis was used to detect impurities that may be present in the powders as well as to compliment the XRF results since fluorine is the lowest element that can be analyzed with XRF. ICP was also used to identify the total amount of C in each mixed alloy powder since the C content was varied as mentioned in Section 3.1.1. The oxygen level for each powder was also analyzed. A 5 g powder sample was analyzed using a SLS-ICP method.

### 3.1.4. X-Ray Diffraction (XRD) analysis

This analysis was used to identify the phases present in each powder. A Bruker D2 machine was used according to the parameters specified in Table 3.2. Peaks were identified using PANalytical X'pert High Score software.

Table 3.2: XRD analysis operating conditions.

| | |
|---|---|
| Start position [$^0$2Th.] | 10.0020 |
| End position [$^0$2Th.] | 90.0040 |
| Step size [$^0$2Th.] | 0.0260 |
| Anode material | Co |
| Generator settings | 30kV. 10mA |

### 3.1.5. Scanning Electron Microscopy (SEM)

This analysis was done to characterize the powder morphology and energy-dispersive x-ray spectroscopy (EDS) of each powder was also done to confirm the elements present. A few grams of powder was attached to a carbon tape and then analyzed in a FEI NanoNevo SEM200 using various magnifications.

## 3.2. Production of the alloys

The alloys were produced using a commercial powder metallurgy process which has three main stages, namely, mixing and milling, pressing and sintering.

### 3.2.1. Mixing and milling

The starting powders for each alloy grade, as listed in Table 3.1, were mixed together in a 1 kg mill which was lined with WC. To enhance the milling and pressing properties of the powder, additives such as dispersant and a PEG lubricant were added. After mixing, milling was conducted under wet conditions, in which alcohol was added. The milling medium was added in the ratio of 3:1 and the targeted particle size was 1.8 µm. The particle size was measured using a Microtrac S3500 Particle Analyser and the analysis was determined using Microtrac Flex 10.3.15 software. Every hour during milling, a powder sample was subjected to particle analysis until the target particle size was attained. Milling curves were generated using the hourly sampling data for each alloy grade.

Per alloy, W and C were added during mixing to adjust the carbon content in such a way that carbon deficient and excess carbon grades were achieved respectively. In Chapter 2 it was stated that the standard C content in WC-Co alloys is 6.12 wt. %. Thus for the C deficient alloys a total C content of 5.9 wt. % was chosen while for excess C grades a total C content of 6.3 wt. % was chosen. Carbon balance calculations were done prior to mixing to calculate the exact amounts of W and C to be added to achieve the selected carbon contents. A summary of the calculations can be found in Appendix A.

### 3.2.2. Pressing

The milled slurry was then oven dried and pressed into the required test piece dimensions using commercial production processes under a pressure of 14 tons. These pressed test pieces are referred to as 'green compacts' in this dissertation. The weight and dimensions of the green compacts were measured using an AY120 SHIMADZLI electronic balance and Vernier callipers respectively. A total of 10 samples per alloy grade were pressed and subjected to further testing and the results averaged for each analyses.

The material properties of the green compacts were characterised prior to sintering using the techniques described below.

#### 3.2.2.1. Green density

The density of the green compacts was determined using MPIF standard 42 [26]. A sample was submerged in hot oil of 25-65 cSt at 82$\pm$5 °C for 4 hrs, and the mass before and after oil immersion was recorded. After oil immersion, the sample was gently wiped to avoid mass loss of the compacted powders. The density was then determined using a Sartorius analytical balance. The specimen was first weighed in air (A), thereafter weighed as oil impregnated (B) and finally in water (C). Three readings were taken per sample. The green density was calculated according to Eqn. 3.1 [26].

$$\text{Green density} = \frac{A\rho_w}{B-C} \qquad \text{Eqn. 3.1}$$

Where: A = green mass (g)

B = oil impregnated mass (g)

C = mass in water (g)

$\rho_w$ = density of water (g/cm$^3$)

#### 3.2.2.2. Porosity

Porosity measures the percentage of pores present in the specimen. It was calculated using Eqn. 3.2 [26].

$$\text{Porosity} = \frac{M_{wt} - M_a}{M_{wt} - M_w} \times 100\ \% \qquad \text{Eqn. 3.2}$$

Where: $M_a$ = mass of specimen in air (g)

$M_w$ = mass of specimen in water (g)

$M_{wt}$ = wet mass of specimen (g)

#### 3.2.2.3. Phase analysis and morphology

SEM images of the green compacts were taken to characterize their morphology, while EDS and XRD were used to confirm the elements and phases, and to assess if any changes occurred during the milling and pressing processes.

### 3.2.3. Sintering

The green compacts were sintered in a sinter-HIP furnace under a pressure of 45 bar, at three different temperatures, namely 1340°C, 1430°C and 1510°C. This was done to assess the influence of sintering temperature on the properties of the alloys.

## 3.3. Sintered alloy characterization

The sintered alloys were analyzed to characterize the microstructure and to determine the physical and mechanical properties.

### 3.3.1. Sample preparation

Prior to the analysis, the sintered samples were ground and polished according to the procedure outlined in Table 3.3.

Table 3.3: Grinding and polishing stages.

| Step | Disc | Diamond paste (μm) | Time (min) |
|---|---|---|---|
| 1 | Struers MD Piano 220 | $H_2O$ | 15 |
| 2 | Struers MD Piano 1200 | $H_2O$ | 6 |
| 3 | Struers MD Allegro | 9 | 6 |
| 4 | Struers MD Dac | 3 | 6 |
| 5 | Struers MD Nap | 1 | 5 |

### 3.3.2. Microstructural characterization

The polished samples were etched in Murakami's reagent solution (10 g NaOH + 10 g $K_3Fe(CN)_6$) to reveal the microstructure of the alloys. The characterization was done using SEM and EDS on the sample cross sections to see how the increase in C content and sintering temperature affected the microstructure. The WC grain size of the alloys was calculated using IJ image analysis software, which calculates the mean grain size and the grain size distribution in pixels which were converted into μm using Excel. An average of five readings was done on each image for verification of the results. The binder mean free path (BMFP) was also measured using the IJ image analysis software. The WC contiguity was calculated using Eqn. 3.3 [1].

$$C = 1 - \frac{l_{carbide} V_{binder}}{l_{binder} V_{carbide}} \qquad \text{Eqn. 3.3}$$

Where C= Contiguity

$l_{carbide}$= mean carbide grain size (mm)

$l_{binder}$= binder mean free path (mm)

$V_{carbide}$= volume fraction of the carbide phase (mm)

$V_{binder}$= volume fraction of the binder phase (mm)

### 3.3.3. Phase analysis

XRD was used to identify the phases present in each alloy using the procedure outlined in Section 3.1.4.

### 3.3.4. Sintered density and porosity

The density was determined using the Archimedes principle. The samples were initially weighed in air, then again whilst immersed in water, using an AY120 SHIMADZLI electronic balance. The density was calculated using Eqn. 3.4. Ten samples were tested and each measurement was repeated twice per sample.

$$\rho_s = \rho_w \frac{M_w}{M_a - M_w} \qquad \text{Eqn. 3.4}$$

Where: $\rho_s$= density of sample (g/cm$^3$)

$\rho_w$= density of water (g/cm$^3$)

$M_w$= mass of sample in water (g)

$M_a$= mass of sample in air (g)

The porosity was calculated according to the procedure outlined in Section 3.2.2.2.

### 3.3.5. Coercivity

Coercivity measures the strength of the magnetic field required to demagnetize a fully magnetized cemented carbide sample. The samples coercivity was measured according to ISO3326 [27] using a DR. Forster Koerzimat 1.0965 machine.

This property is influenced by the WC grain size, composition and binder content. The units of coercivity from this method are oesterds (Oe) which is then converted to SI units according to Eqn. 3.5. Ten samples were analyzed and the average was then taken.

$$\mathrm{Oe} = \frac{1000}{4\times\pi}\ \mathrm{A.m^{-1}} \qquad \text{Eqn. 3.5}$$

### 3.3.6. Magnetic cobalt

The magnetic properties of Co in a cemented carbide alloy are affected by the amount of C present. Therefore this analysis was done to assess if the different C levels introduced into the alloys would influence the Co content. A Sigma-meter, model no. S60/55980 was used to measure the amount of Co present. Ten samples per alloy were measured and the average value reported.

### 3.3.7. Vickers hardness

Vickers hardness was measured using a 30 kg load, in a Mityutoyo machine, model no. AVK-CO, according to ISO 3878 [28]. Three samples were randomly selected and three indentations were done per sample from which the average hardness was calculated using Eqn. 3.6.

$$\mathrm{HV} = \frac{1.854\mathrm{F}}{\mathrm{d^2}} \qquad \text{Eqn. 3.6}$$

Where F = indentation load (kg)

d = average indentation diagonal (mm)

HV = Vickers hardness number (kg / (mm) $^2$)

### 3.3.8. Hardness profiles

Hardness profiles were done on one sample per grade, for each C content and sintering temperature. These profiles were done on the cross-sections of the samples, using a load of 2 kg with the hardness being calculated according to Eqn. 3.6 given above.

### 3.3.9. Fracture Toughness

Fracture toughness describes the ability of a material containing a crack to resist fracture. The Palmqvist method [25] was used to calculate the fracture toughness of the sintered samples with respect to Shetty et al's equation, given below. This method is based on the lengths of the cracks emanating from the corners of a Vickers hardness indentation. The samples that were analyzed for hardness were used; where, the average length of the cracks is then used to determine the fracture toughness according to Eqn. 3.7 [25].

$$K_{IC} = A_1\sqrt{\frac{HV \times P}{\sum_1^4 a}} \quad MPa.\sqrt{m} \qquad \text{Eqn. 3.7}$$

Where $A_1 = 887x10^{-7}$

HV = Vickers hardness (MPa)

P = indentation load (N)

a = mean radial crack length (m)

$K_{IC}$ = toughness ($MPa.\sqrt{m}$)

# Chapter 4

## Results

This chapter gives detailed results of the experiments that were conducted according to Chapter 3. The chapter is divided into three main sections. Section 4.1 will report on the powder characterization results, section 4.2 presents the green compacts characterization results and section 4.3 provides the sintered alloys characterization results.

### 4.1. Powder characterization

This section presents the characterization results of the starting powders and the milled powders.

#### 4.1.1. Starting powders

The summary (considering the main elements according to Table 3.1) of the XRF and ICP analysis of the six starting powders are shown in Tables 4.1 and 4.2 respectively. The detailed chemical analyses of these tests are provided in Appendix B. Where MC-1 and MC-2 represent mixed carbides 1 (1:1 = WC: TiC) and 2 (0.2:0.4:0.4= NbC: TaC: TiC) respectively.

Table 4.1: XRF analysis of the starting powders in (wt %).

| | **WC** | **Co** | **MC-1** | **MC-2** | **TiCN** |
|---|---|---|---|---|---|
| **C** | - | - | - | - | - |
| **Ti** | 0.194 | 0.021 | 32.081 | 13.415 | 58.956 |
| **Ta** | 0.000 | 0.000 | 0.032 | 31.340 | 0.012 |
| **Nb** | 0.000 | 0.000 | 0.011 | 4.262 | 0.050 |
| **W** | 78.842 | 0.688 | 36.685 | 25.344 | 0.725 |
| **Co** | 0.095 | 67.849 | 0.036 | 0.158 | 0.096 |

Table 4.2: ICP analysis of the starting powders in (wt %).

| | **WC** | **Co** | **MC-1** | **MC-2** | **TiCN** |
|---|---|---|---|---|---|
| **C** | 6.420 | 0.084 | 12.940 | 9.020 | 10.440 |
| **Ti** | 0.035 | 0.005 | 43.200 | 11.510 | 88.500 |
| **Ta** | 0.094 | 0.005 | 0.005 | 40.330 | 0.005 |
| **Nb** | 0.012 | 0.005 | 0.033 | 4.750 | 0.487 |
| **W** | 94.990 | 0.005 | 43.150 | 33.140 | 0.005 |
| **Co** | 0.400 | 99.000 | 0.210 | 0.470 | 0.130 |

Table 4.1 and 4.2 report the chemical composition of the major elements of the starting powders and the traces of certain elements. Table 4.1 does not show the amount of C present in the powders as the WDXRF machine can only analyse periodic table elements from fluorine onwards. Table 4.2 shows all the elements that were expected according to Table 3.1. Comparing Tables 4.1 and 4.2, ICP results are more detailed than that of the XRF results, ICP results give traces of each element present in the samples, while XRF results does not report on some of the elements. For an example XRF shows 0% of Nb and Ta in the Co sample, whilst in ICP both elements are said to be 0.005%.

The XRD analysis of the powders is presented in Fig. 4.1, confirming the major phases expected, which are WC, TiC, Co and $Cr_3C_2$. No deleterious phases or impurities were detected in these analyses.

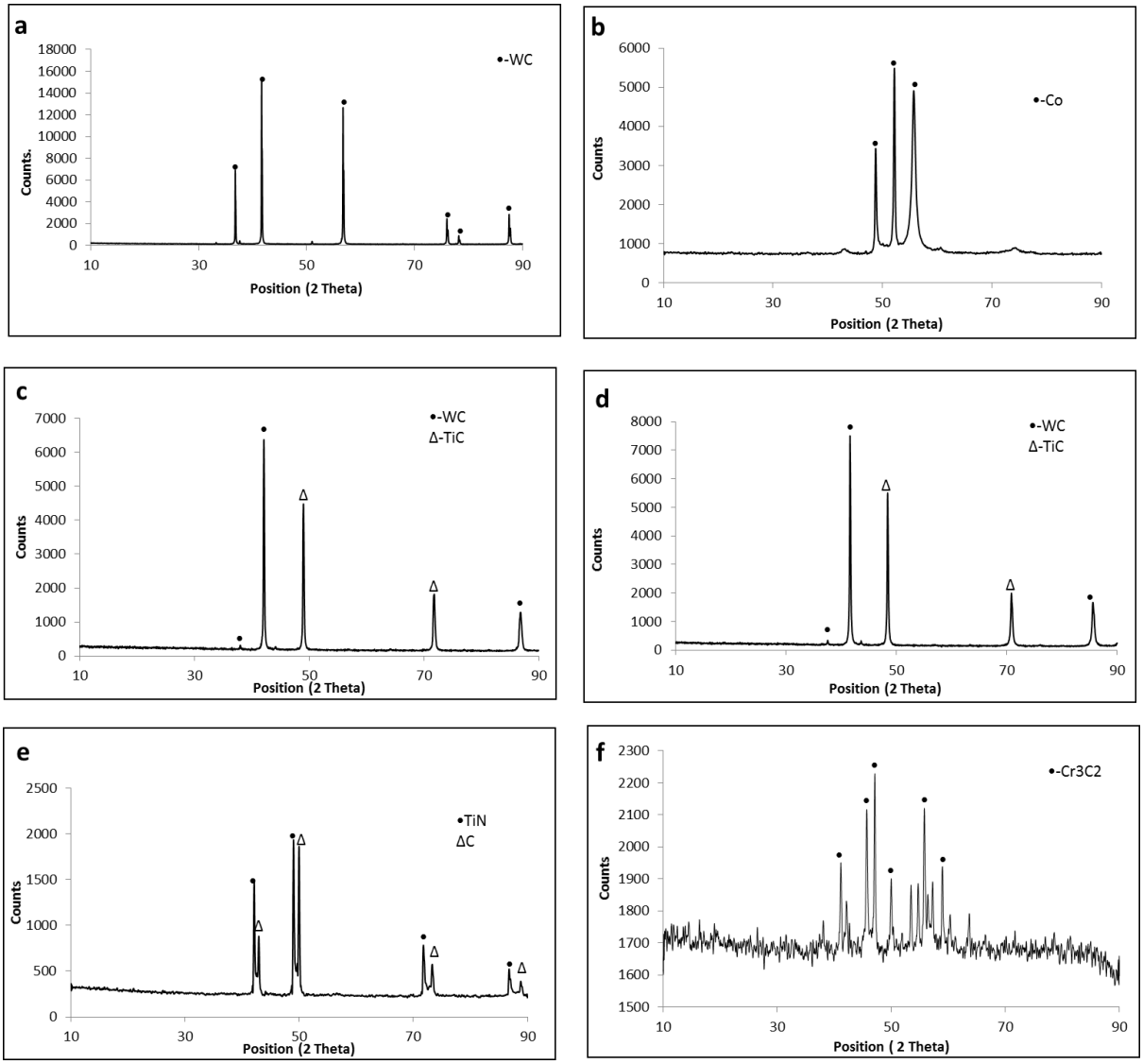


Fig. 4.1: XRD analysis for the starting powders. (a) WC, (b) Co, (c) MC-1, (d) MC-2, (e) TiCN and (f) $Cr_3C_2$.

Fig. 4.2 is SEM images showing the morphology of the powders. The WC (Fig. 4.2(a)) and Co (Fig. 4.2(b)) powders have a predominantly spherical morphology while the remaining four powders have irregular shaped particles, with some minor flaked shaped particles present. The EDS spectra of the powders are listed in Appendix C. These results confirmed the major elements as characterized using the XRF and ICP analyses.

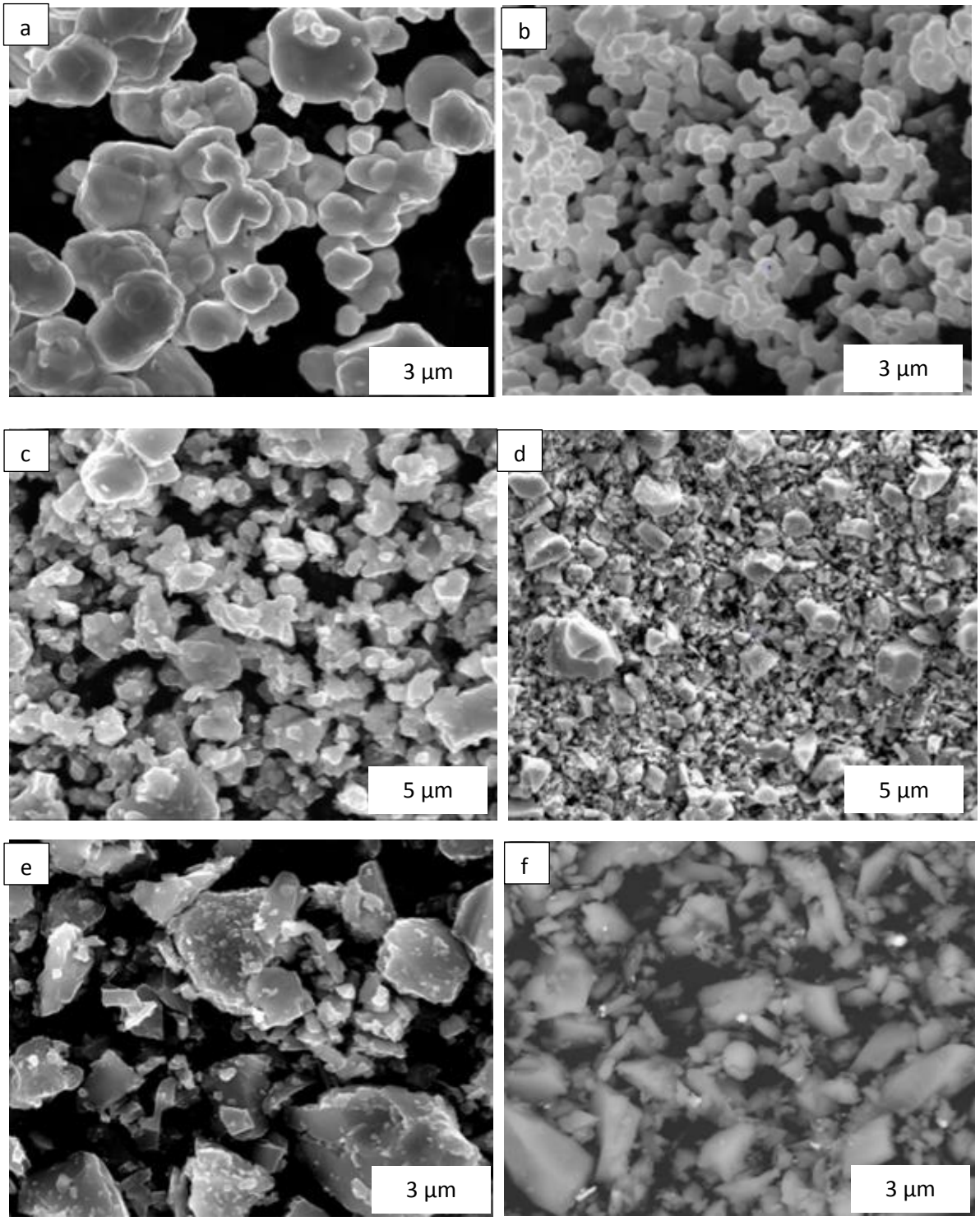


Fig.4.2: SEM analysis for the starting powders: (a) WC, (b) Co, (c) MC-1, (d) MC-2, (e) TiCN and (f) $Cr_3C_2$.

### 4.1.2. Milled powders

The starting powders were mixed according to the compositions listed in Table 3.1 in section 3.2.1. to produce the four alloy grades for this project. After mixing, the powders were milled to obtain a mean volume diameter of 1.8 µm. During the milling process a sample of the powder slurry was taken for particle size analysis every hour to assess how far the milling had progressed in terms of achieving the target particle size. Fig. 4.3. summarizes the milling curves for the four alloys.

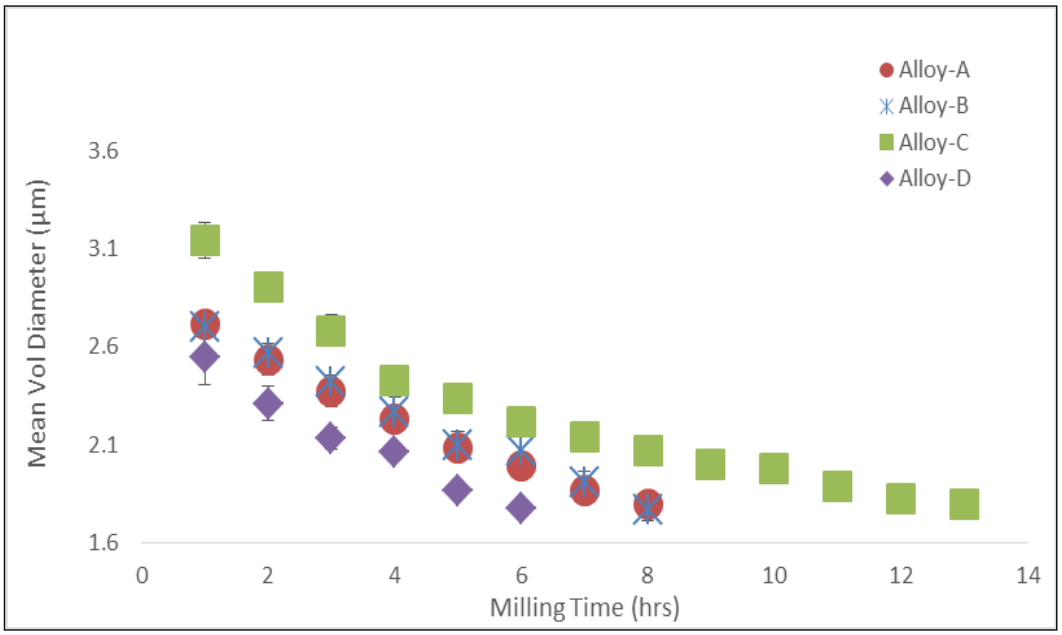


Fig. 4.3: Powder volume diameter as a function of milling time.

From Fig. 4.3 it is observed that as the milling time increased, the mean powder volume diameter decreased. The higher the amounts of Co and mixed carbides introduced into the cemented carbide system, the easier it was to mill the powder to the required size. This can be seen by comparing alloy-B (lowest) which has 5.4 wt. % mixed carbides and 5 wt%Co to alloy-D (highest) which has 8.7 wt. % mixed carbide and 9.5wt%Co respectively. This trend is also due to the low amount of hard WC phase present.

After the powders were milled and had their C levels adjusted as described in section 3.2.1, the milled powders were characterized using the tests described in section 3.1.

A powder nomenclature, as listed in Table 4.3, was designed to simplify identification of the different powder grades.

Table 4.3: Powder nomenclature.

| Symbol | Name |
|---|---|
| A | Alloy A (WC-6wt%Co) |
| B | Alloy B (WC-6.6wt%Co-B) |
| C | Alloy C ( WC-5wt% Co-C) |
| D | Alloy D (WC-9.5wt% Co-D) |
| d | Carbon deficient |
| s | Standard carbon |
| e | Excess carbon |

A summary of the XRF and ICP analysis of the milled powders is reported in Tables 4.4 and 4.5 respectively, and the detailed analyses is provided in Appendix B.

Table 4.4: XRF analysis of the milled powders in (wt %).

| | **A-d** | **A-s** | **A-e** | **B-d** | **B-s** | **B-e** | **C-d** | **C-s** | **C-e** | **D-d** | **D-s** | **D-e** |
|---|---|---|---|---|---|---|---|---|---|---|---|---|
| **W** | 71.32 | 71.30 | 71.37 | 62.69 | 63.44 | 62.33 | 63.12 | 62.28 | 61.80 | 57.13 | 58.46 | 57.83 |
| **C** | - | - | - | - | - | - | - | - | - | - | - | - |
| **Co** | 6.28 | 6.23 | 6.35 | 6.60 | 6.39 | 6.31 | 4.66 | 4.95 | 4.90 | 8.74 | 7.80 | 8.39 |
| **Ti** | 0.00 | 0.07 | 0.07 | 4.36 | 4.15 | 5.02 | 6.56 | 6.72 | 6.88 | 6.99 | 7.02 | 6.74 |
| **Ta** | 0.00 | 0.00 | 0.00 | 2.26 | 2.18 | 2.28 | 1.52 | 1.61 | 1.66 | 1.93 | 1.99 | 1.93 |
| **Nb** | 0.00 | 0.00 | 0.00 | 0.29 | 0.30 | 0.30 | 0.21 | 0.21 | 0.21 | 0.23 | 0.23 | 0.23 |
| **Cr** | 0.00 | 0.00 | 0.00 | 0.00 | 0.00 | 0.00 | 0.29 | 0.32 | 0.31 | 0.00 | 0.00 | 0.00 |

Table 4.5: ICP analysis of the milled powders in (wt %).

| | **A-d** | **A-s** | **A-e** | **B-d** | **B-s** | **B-e** | **C-d** | **C-s** | **C-e** | **D-d** | **D-s** | **D-e** |
|---|---|---|---|---|---|---|---|---|---|---|---|---|
| **W** | 83.7 | 80.25 | 84.09 | 74.96 | 72.72 | 76.86 | 77.03 | 73.03 | 77.89 | 73.5 | 75.83 | 70.78 |
| **C** | 6.02 | 6.32 | 6.58 | 6.49 | 6.76 | 6.90 | 7.03 | 7.54 | 7.72 | 6.91 | 7.47 | 8.09 |
| **Co** | 6.23 | 6 | 6.38 | 6.54 | 6.28 | 6.52 | 4.79 | 4.72 | 4.38 | 9.18 | 9.64 | 9.74 |
| **Ti** | 0.03 | 0.03 | 0.03 | 3.63 | 3.68 | 3.99 | 5.76 | 5.26 | 5.36 | 6.6 | 5.75 | 6.49 |
| **Ta** | 0.08 | 0.08 | 0.08 | 0.78 | 0.79 | 0.84 | 0.61 | 0.59 | 0.56 | 0.77 | 0.69 | 0.75 |
| **Nb** | 0.01 | 0.01 | 0.02 | 0.59 | 0.61 | 0.61 | 0.43 | 0.44 | 0.41 | 0.51 | 0.50 | 0.50 |
| **Cr** | 0.01 | 0.01 | 0.01 | 0.01 | 0.01 | 0.01 | 0.19 | 0.19 | 0.19 | 0.02 | 0.02 | 0.02 |

From Tables 4.4 and 4.5 the ICP results show trace elements while XRF show the main elements of each powder. For example the XRF of alloy-A reports only on the WC and Co while ICP reports traces of the other elements (Nb, Ta, Ti and Cr). Also XRF shows Cr in alloy-C which corresponds to the chemical composition in Table 3.1 and ICP reports traces of Cr for all the alloys. The XRF and ICP of Co show similar values, which are in the range of the values reported in Table 3.1.

The XRD analysis of the milled powders is reported in Appendix D. No phase changes occurred. The SEM images confirm the reduction in powder size as indicated by Fig. 4.4.

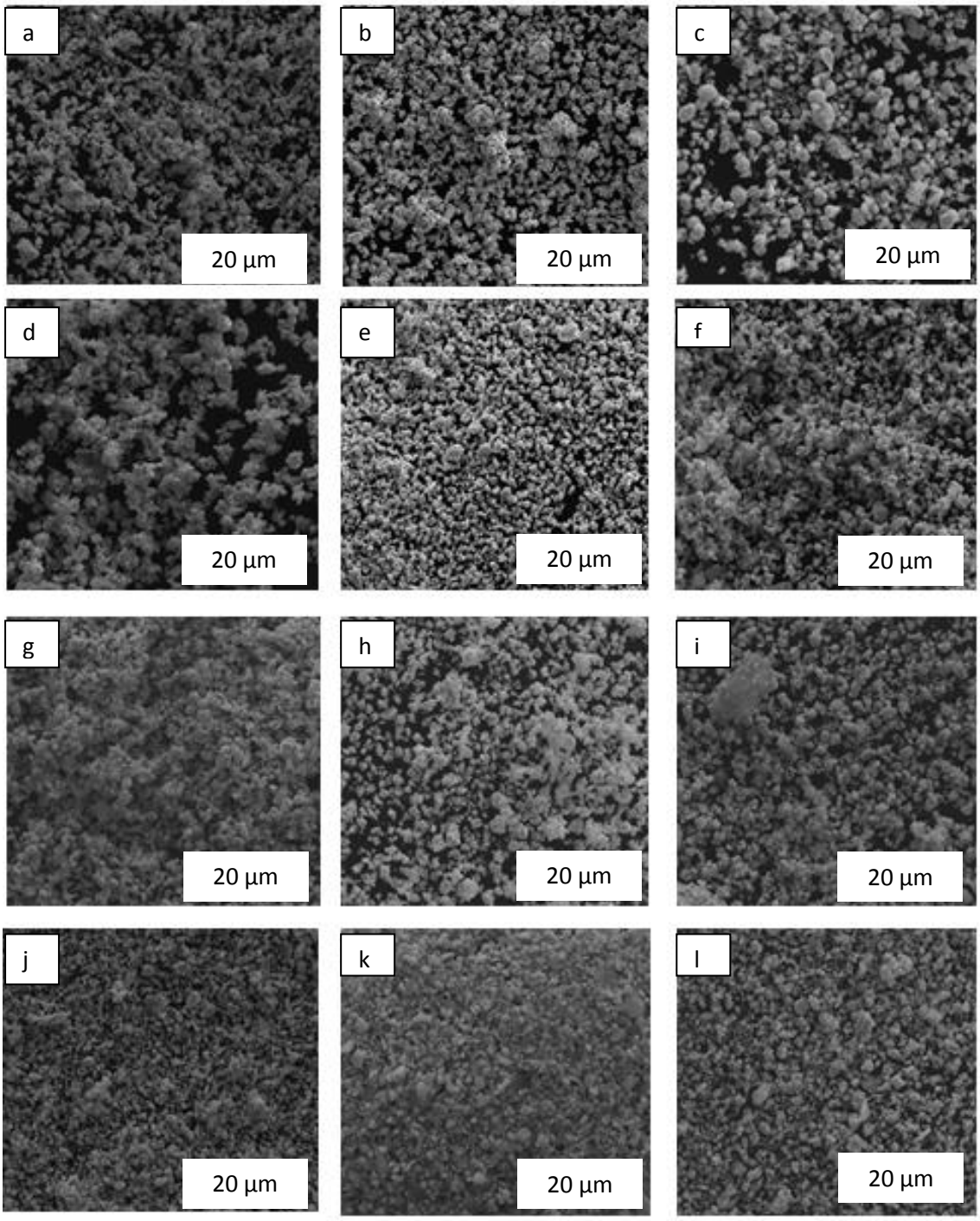


Fig. 4.4: SEM analysis for the milled powders: (a-c) Alloy-A with deficient to excess C, (d-f) Alloy-B with deficient to excess C, (g-i) Alloy-C with deficient to excess C, (j-l) Alloy-D with deficient to excess C.

## 4.2. Green compacts characterization

The milled and spray dried powders for the different alloys were pressed into green compacts and then characterized according to the tests described in section 3.2.2. The following nomenclature was used to distinguish between the different C levels of each alloy:

- D = carbon deficient alloy
- S = standard carbon alloy
- E = excess carbon alloy

### 4.2.1. XRD analyses

Figs. 4.5 to 4.8 show the phases identified in each of the green compacts using XRD. The adjustment of the C levels did not cause any major changes in the peaks; the XRD spectrum each alloy patterns were similar. The only new peak in the spectra, namely a W peak, is the result of the additional tungsten powder that was added to reduce the carbon level to produce the C-deficient alloys.

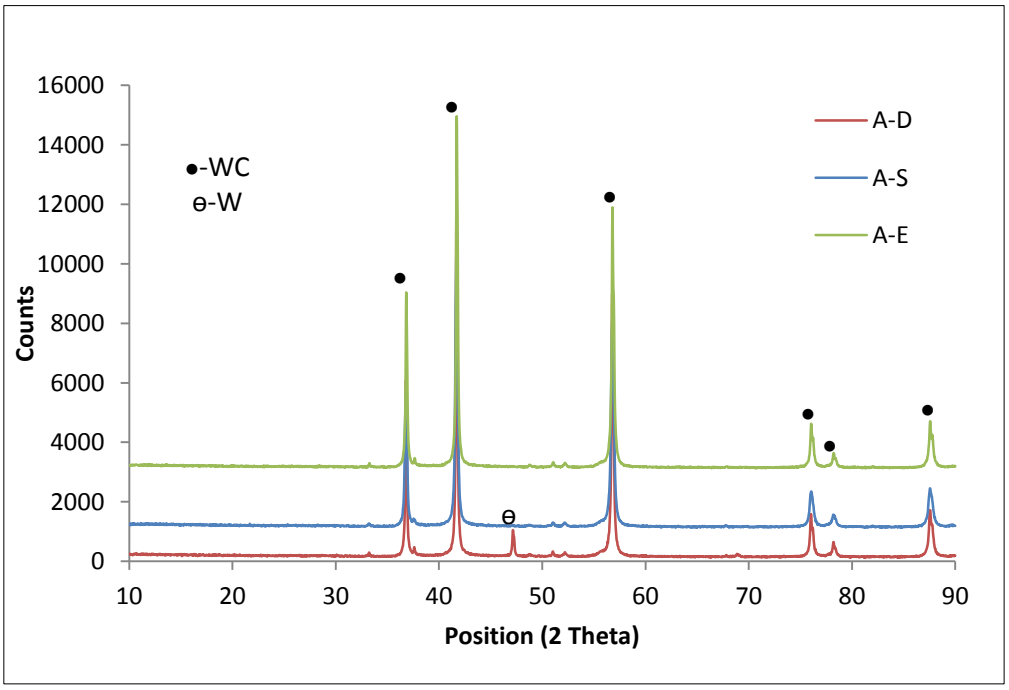


Fig. 4.5: XRD analysis of Alloy-A in its green state.

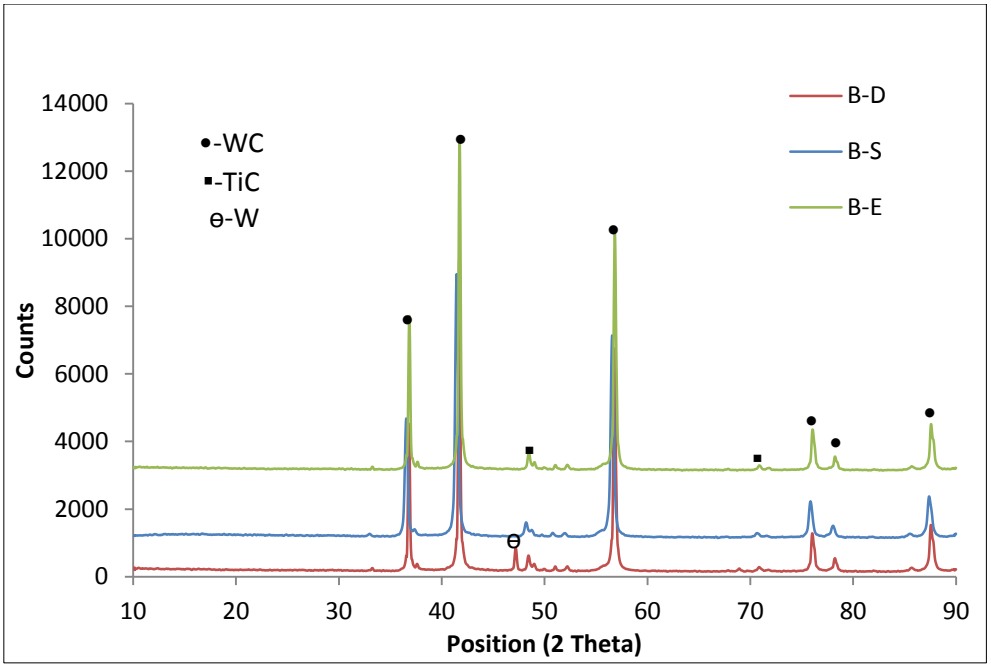


Fig. 4.6: XRD analysis of Alloy-B at its green state.

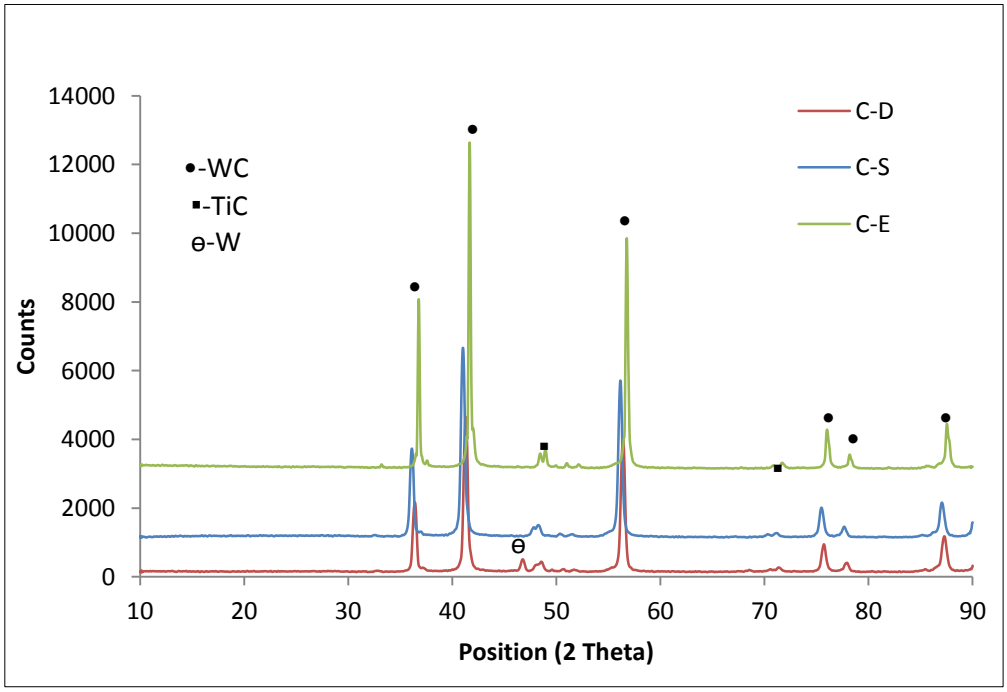


Fig. 4.7: XRD analysis of Alloy-C at its green state.

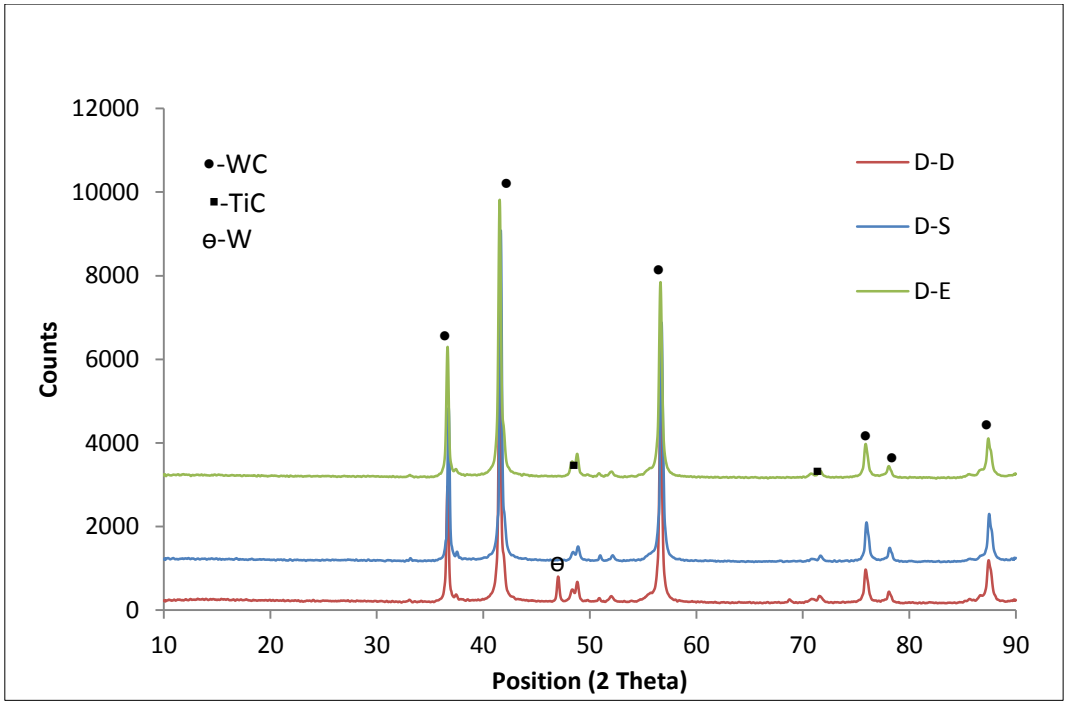


Fig. 4.8: XRD analysis of Alloy-D at its green state.

### 4.2.2. SEM analysis

Figs. 4.9 to 4.12 show the morphology and EDS spectra of the green compacts for the standard-carbon alloys. The SEM and EDS analyses of the C-deficient and excess-C alloys were found to be similar to those of the standard-C alloys and were therefore placed in Appendix E.

Alloy-A shows a microstructure that is predominately WC and only W in EDS graph concurs. Alloy-B shows more of the WC phase. Alloy-A and alloy-B show far different microstructures as compared to alloy-C and alloy-D. The last two alloys show the presence of the TaC and other carbides.

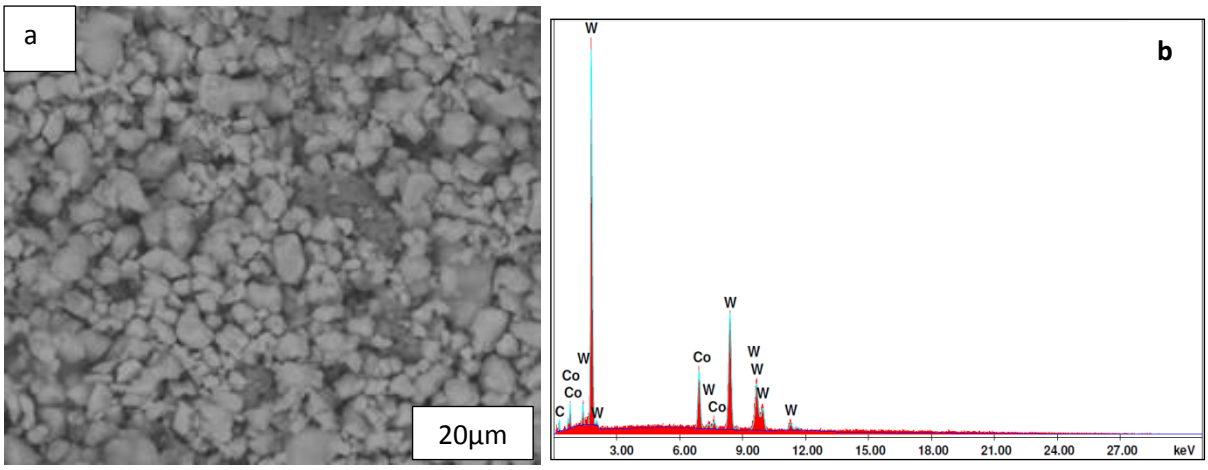


Fig. 4.9: (a) SEM and (b) EDS of Alloy-A for the standard-C level.

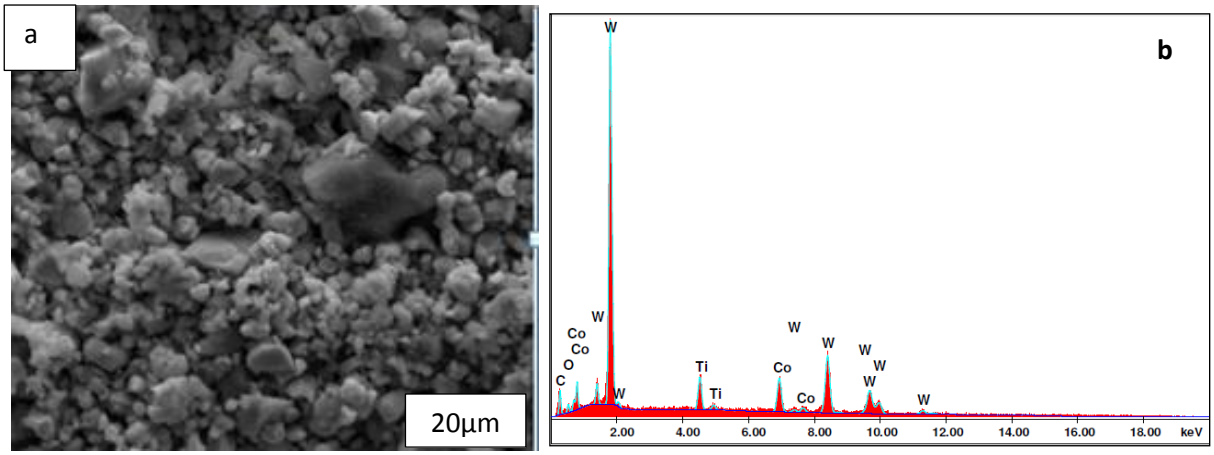


Fig. 4.10: (a) SEM and (b) EDS of Alloy-B for the standard-C level.

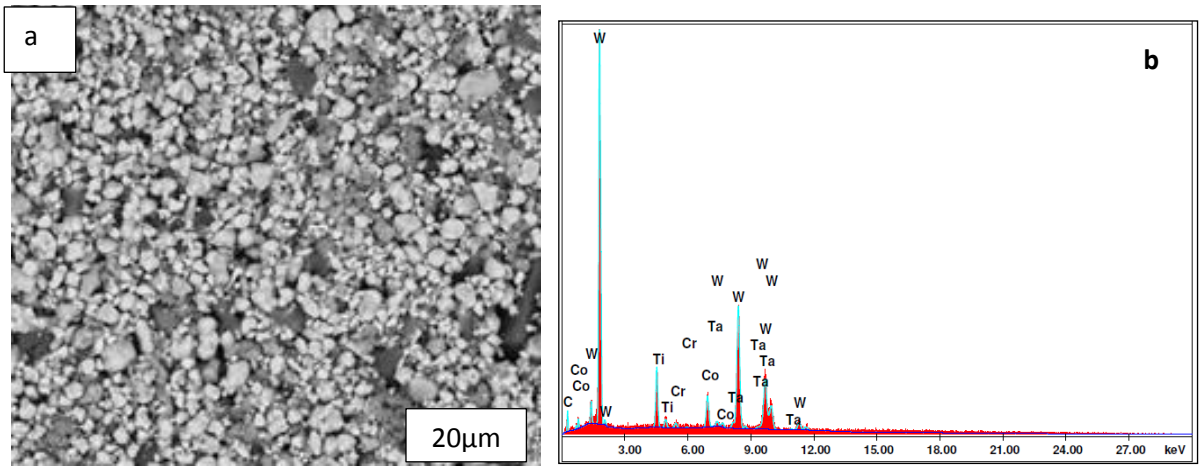


Fig. 4.11: (a) SEM and (b) EDS of Alloy-C for the standard-C level.

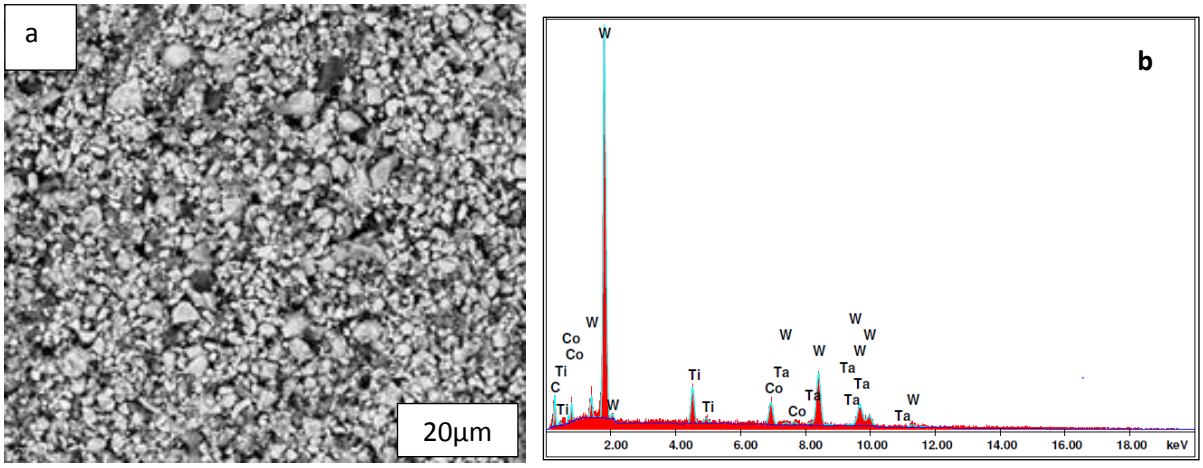


Fig. 4.12: (a) SEM and (b) EDS of Alloy-D for the standard-C level.

### 4.2.3. Green density and porosity

The green density and porosity was done according to the tests described in section 3.2.2. When the green compacts were impregnated with the oil many of the samples cracked before the required immersion time was reached. This is due to the temperature increase which increases the pressure within the sample as it elongates. Table 4.6 shows the density and porosity values for each alloy.

Table 4.6: Green density and porosity.

| | | **Def. C** | **Std. C** | **Exc. C** |
|---|---|---|---|---|
| **Alloy-A** | $\rho_s$ (g/cm$^3$) | 8.95 | 8.92 | 8.90 |
| | Porosity (%) | 18.46 | 18.20 | 17.63 |
| **Alloy-B** | $\rho_s$ (g/cm$^3$) | 8.28 | 8.30 | 8.25 |
| | Porosity (%) | 15.63 | 16.34 | 17.54 |
| **Alloy-C** | $\rho_s$ (g/cm$^3$) | 8.11 | 8.11 | 8.11 |
| | Porosity (%) | 15.28 | 14.82 | 14.48 |
| **Alloy-D** | $\rho_s$ (g/cm$^3$) | 8.07 | 7.99 | 8.00 |
| | Porosity % | 10.35 | 14.76 | 16.55 |

From Table 4.6 it was observed that the green density decreases with an increase in C level for all the alloys, it was also seen that the porosity was decreasing with an increase in C level for all the alloys. Alloy-A has the highest density when compared with the other alloys and alloy-D has the lowest density. Based on the results the binder content showed an influence on the green density as alloy-D has 9.5% of Co. This shows that the addition of the different mixed carbides leads to lighter and less porous alloys.

## 4.3. Sintered alloys characterization

The green compacts of all four alloys were sintered at two different sintering temperatures (1430°C and 1510°C) while the green compacts of alloys A and B were also subjected to a third sintering temperature (1340°C). The characterization of the sintered alloys was done according to the methods described in Section 3.3.

### 4.3.1. Microstructural characterization

In this section the SEM analysis (backscattered) of the microstructures will be reported per alloy for all the sintering conditions. The presence of eta phase and graphite in the microstructures was noted. This analyses is followed by the results of the WC grain sizes, WC contiguity and Co mean free paths for all the alloys.

In Figs. 4.13 to 4.20 the three levels of C and three different sintering temperatures are always represented by the same sub-figure number, as follows:

- (a), (d), (g) are C deficient
- (b), (e), (h) are standard C
- (c), (f), (i) are excess C
- (a), (b), (c) were sintered at 1430 °C
- (d), (e), (f) were sintered at 1510 °C
- (g), (h), (i) were sintered at 1340 °C

The SEM images for Alloy A are shown in Fig. 4.13 in plan view and in Fig. 4.14 in cross-sectional view. At all three sintering temperatures, as the C level increased, the grain structure became denser or more closely packed and the number of Co pools decreased. There were small traces of precipitated graphite (refer to Fig. 4.12(c)) on the alloys with excess C levels as well as a fairly good distribution of the binder throughout the microstructure. Overall it was observed that for all the different C levels, there was WC grain growth as the sintering temperature increased.

It was also evident that as the sintering temperature increased the amount of graphite precipitated and the amount of Co pools decreased, resulting in a good binder distribution. The graphite in the excess C alloys appears to be higher in concentration in the cross-sectional views compared to the plan view images.

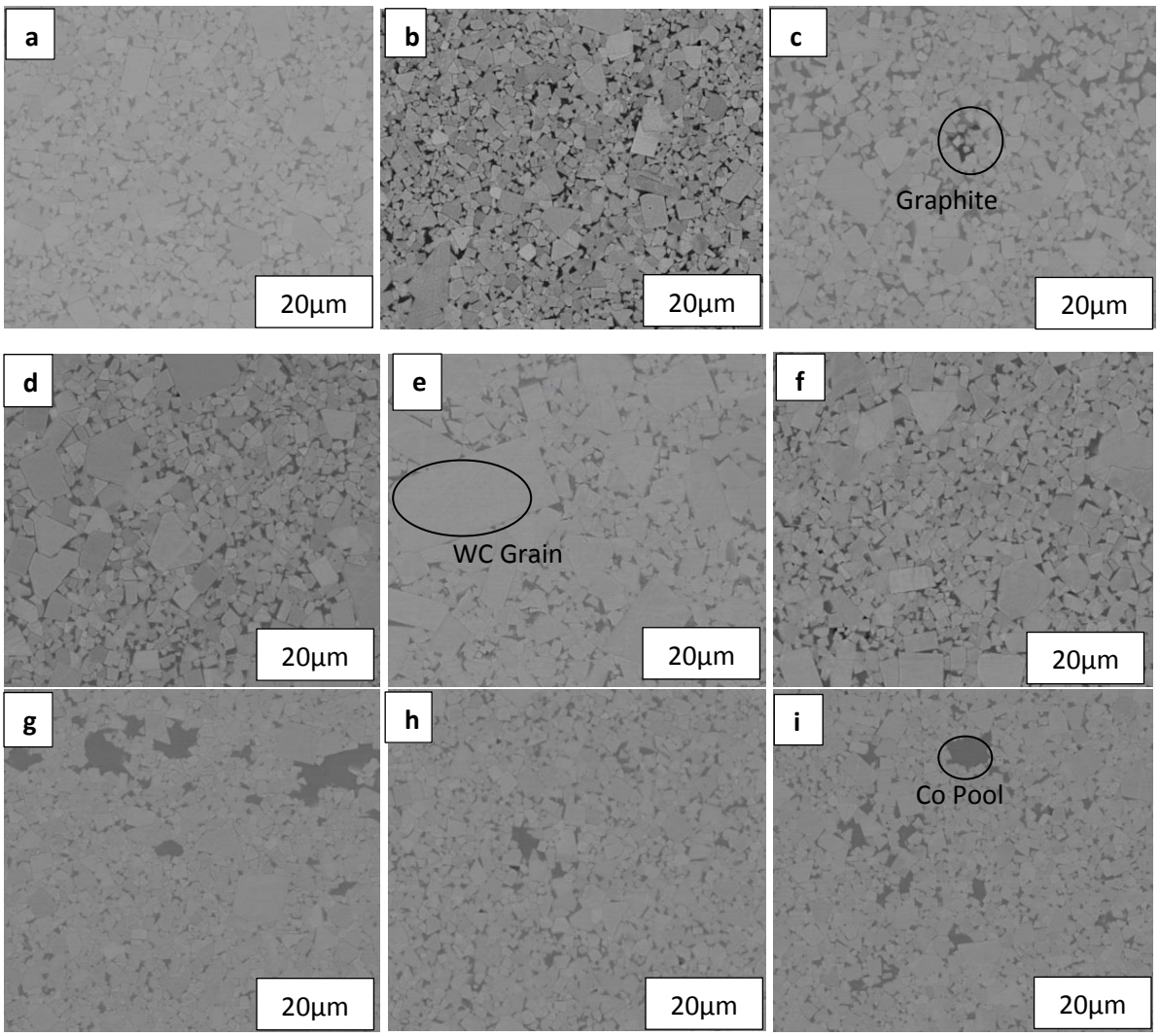


Fig. 4.13: Plan view SEM images of the sintered alloy A samples.

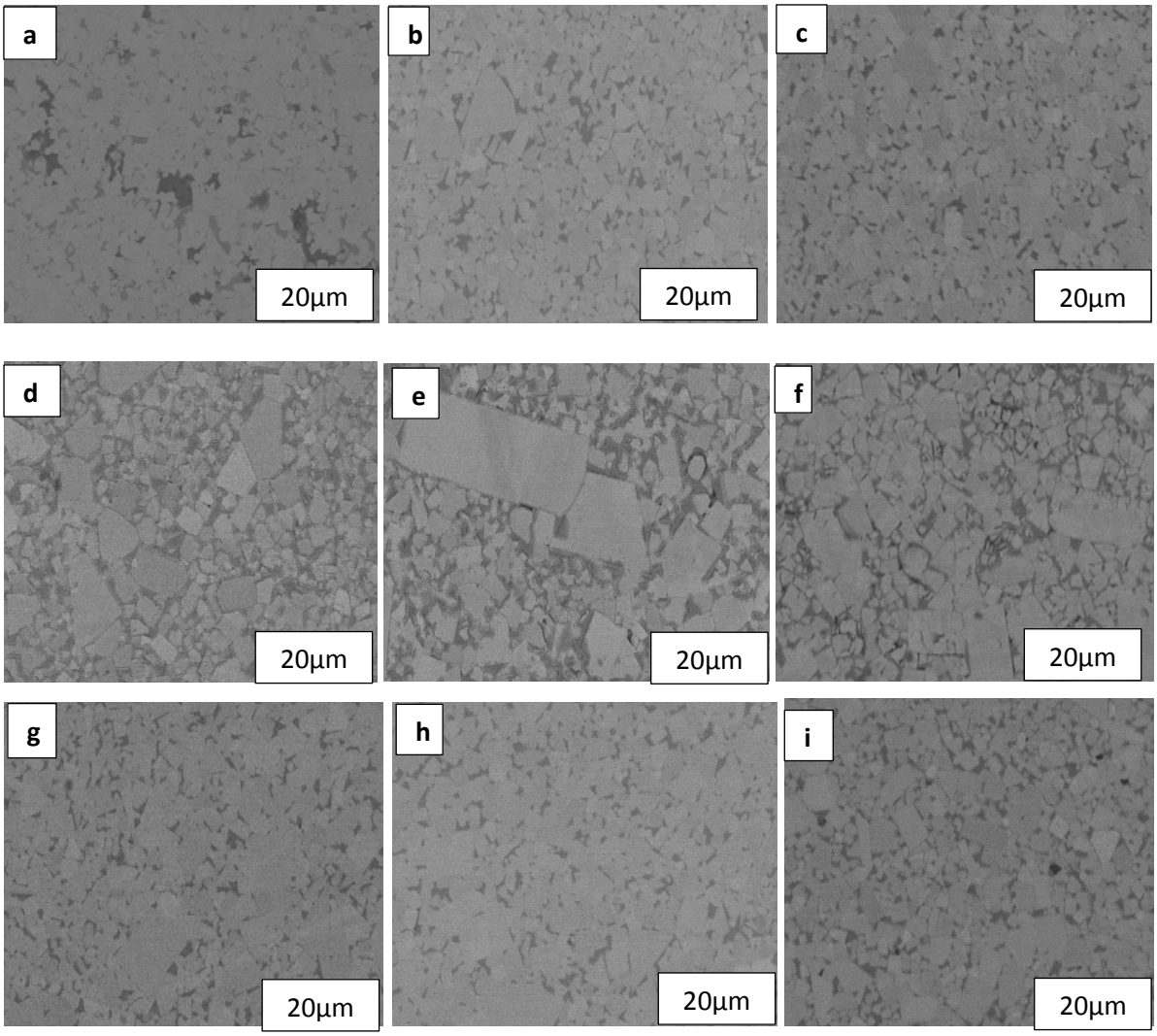


Fig. 4.14: cross-sectional view SEM images of the sintered alloy A samples.

The SEM images for Alloy B are shown in Fig. 4.15 in plain view and in Fig. 4.16 in cross-sectional view. At $1340^0$C the grains were not fully formed. As the sintering temperature increased, the grains started to have a defined grain structure; i.e. the grain shapes were clear. The sizes of the mixed crystals were fairly large at the lowest sintering temperature and reduced in size as the sintering temperature increased. An interesting feature in all the alloys was that some of the TiCN grains were completely surrounded by clusters of TiC grains as seen in Fig. 4.15 i. However this feature was not present at the highest sintering temperature. It was also interesting to note that in this alloy, increasing the sintering temperature did not cause the same degree of grain growth as was observed in Alloy A.

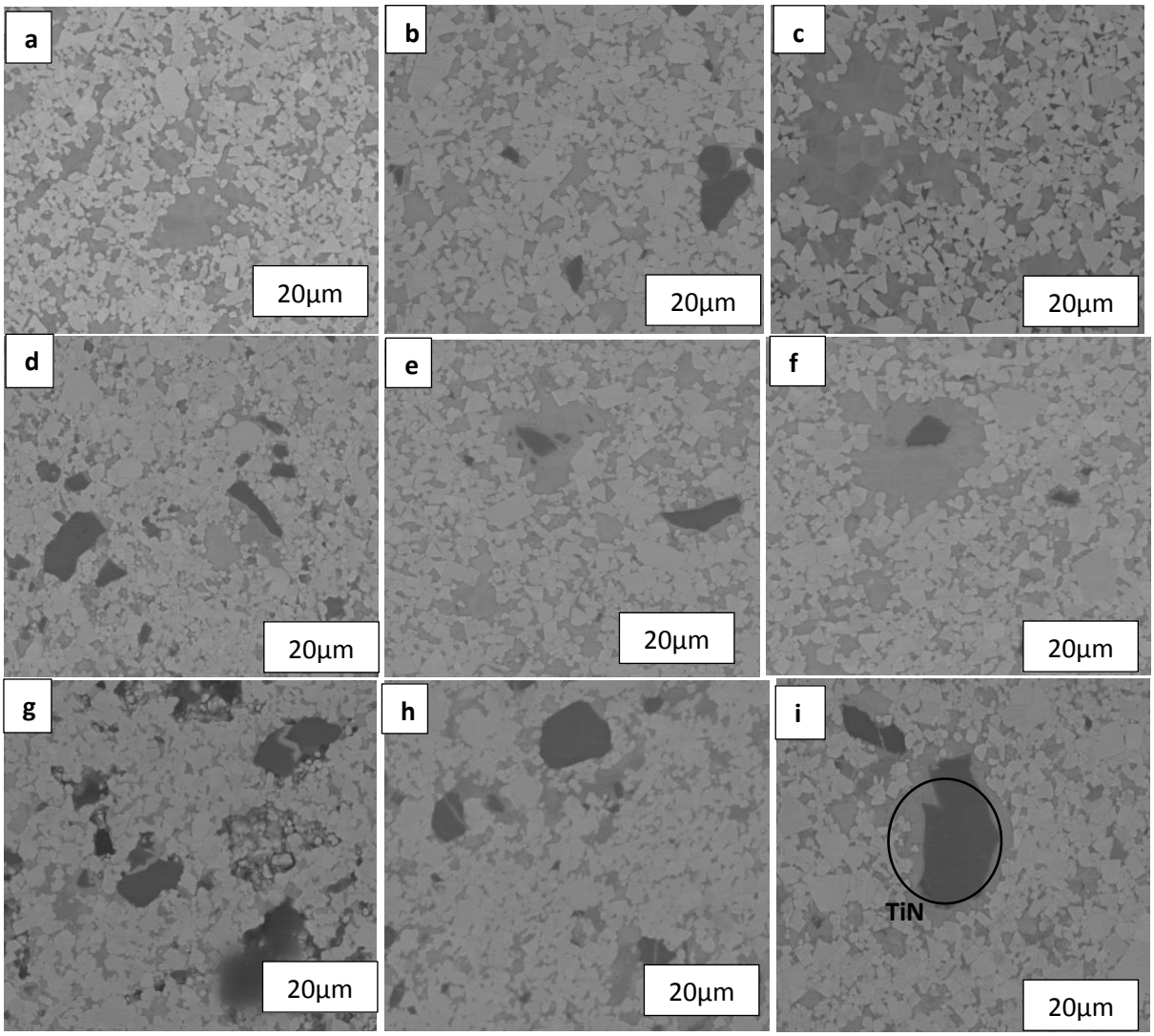


Fig.4.15: Plan view SEM images of the sintered alloy B samples.

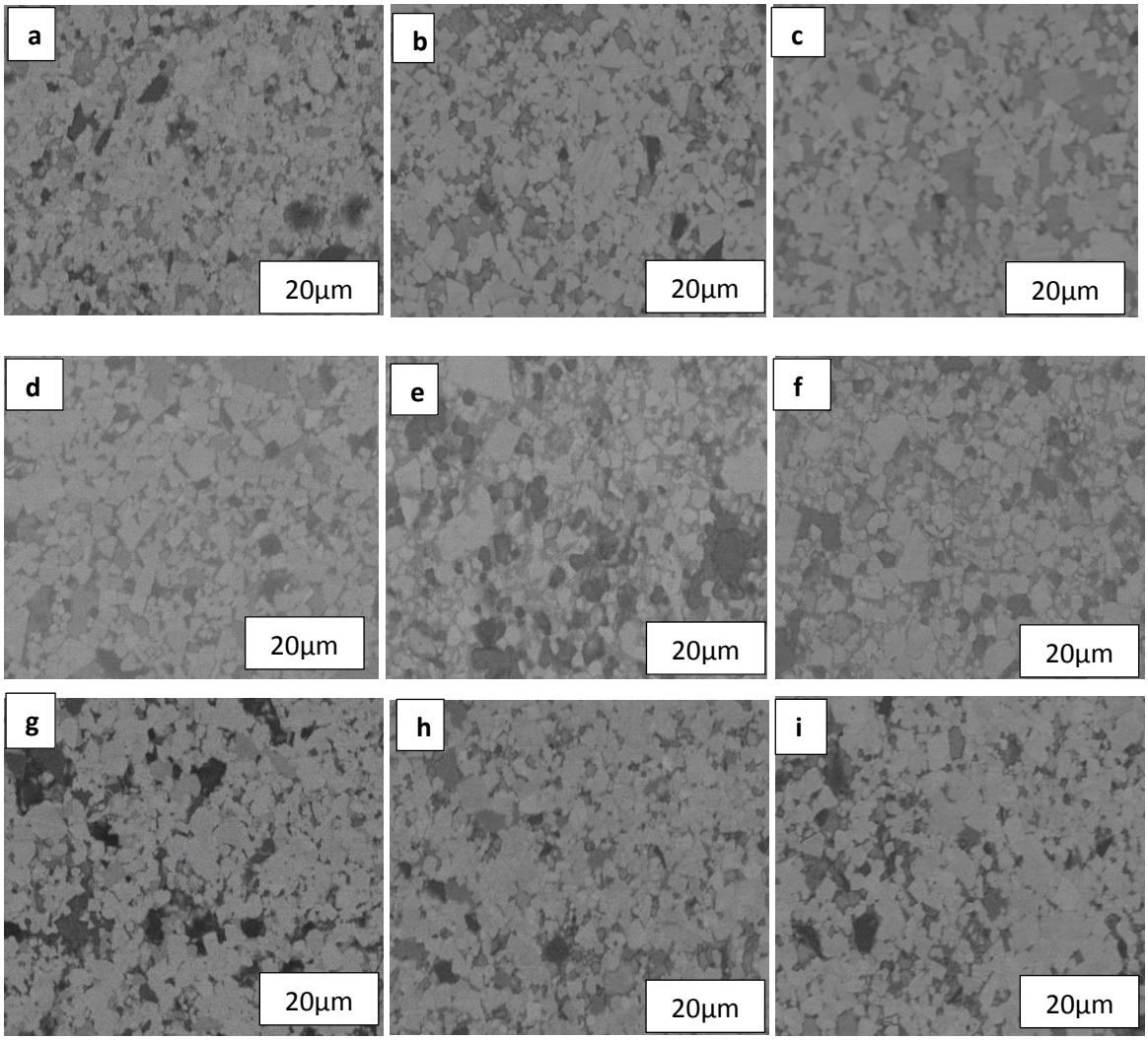


Fig. 4.16: Cross-sectional view SEM images of the sintered alloy B samples.

The SEM images for Alloy C are shown in Fig. 4.17 in plan view and in Fig. 4.18 in cross-sectional view. The grain structure of the alloy was well defined at both sintering temperatures (1430°C and 1510°C) and all three C levels. A slight increase in grain growth was observed as the sintering temperature was increased. TiC grains were also observed in this alloy.

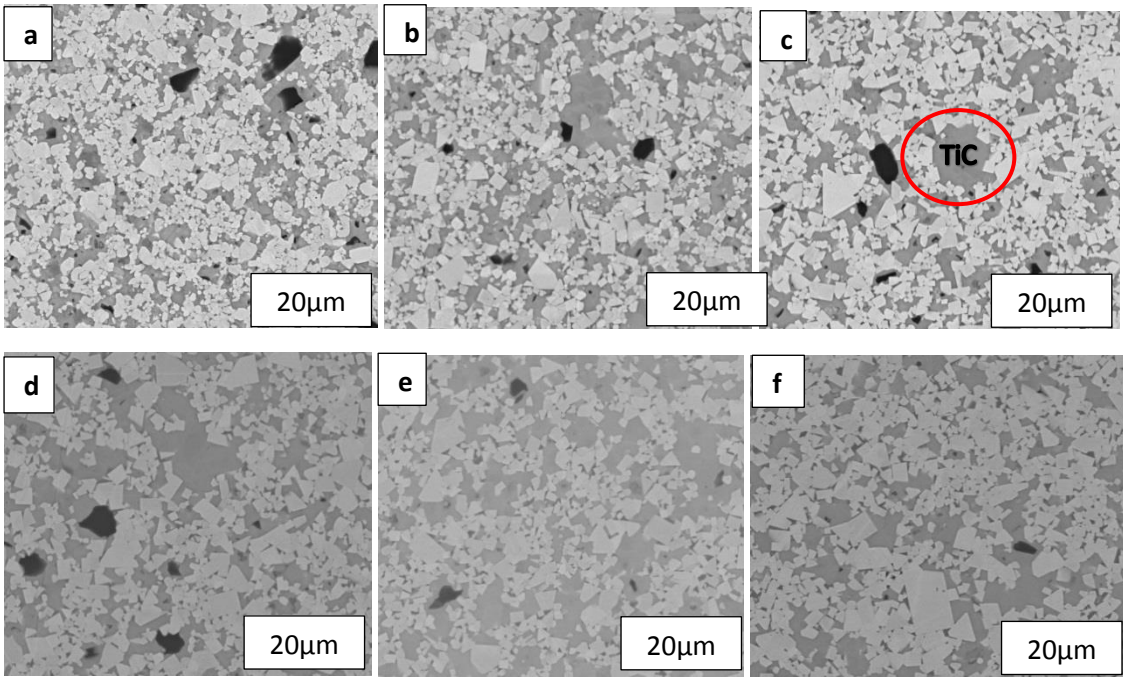


Fig. 4.17: Plan view SEM images of the sintered alloy C samples.

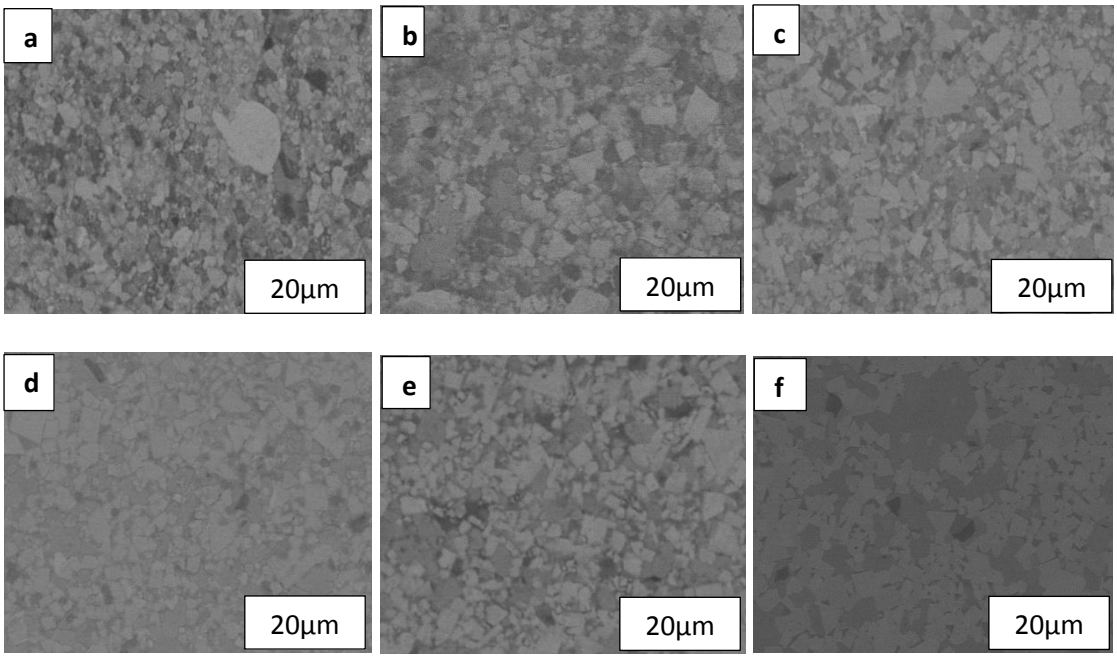


Fig. 4.18: Cross-sectional view SEM images of the sintered alloy C samples.

The SEM images for Alloy D are shown in Fig. 4.19 in plan view and in Fig. 4.20 in cross-sectional view. There is evidence of clear grain growth as the sintering temperature increased for all the C levels of this alloy. In this alloy as the C level increased the number of Co pools increased in the microstructure.

The clustering of the mixed crystals was also evident in this grade although here the size of the clusters appears to increase as the C level increases see Fig. 19 e.

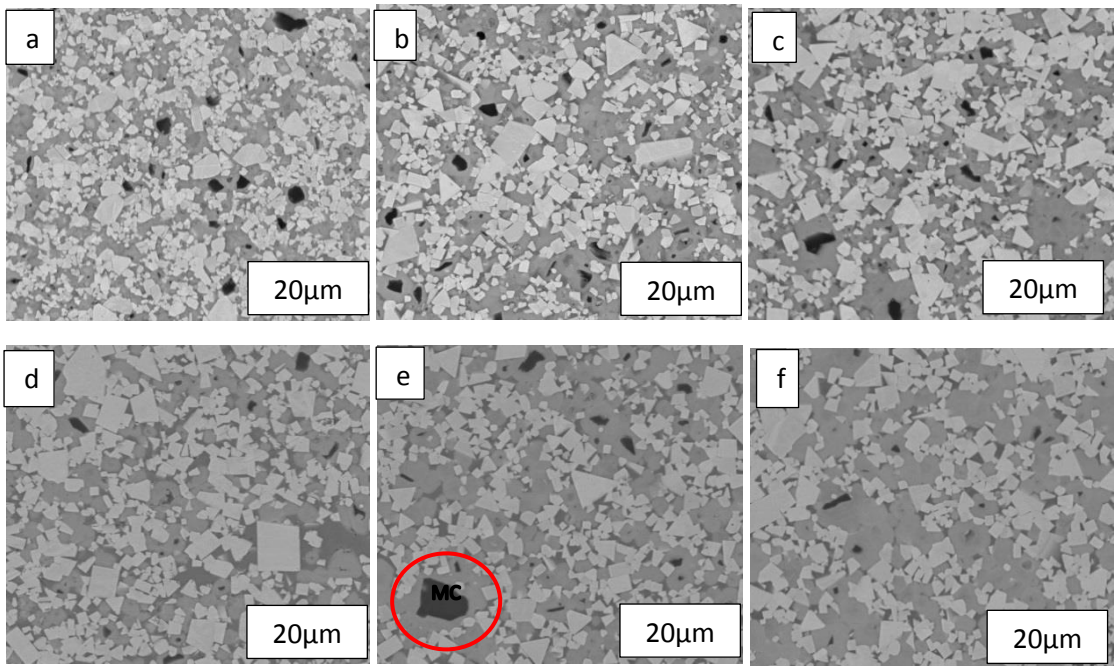


Fig. 4.19: Plan view SEM images of the sintered alloy D samples.

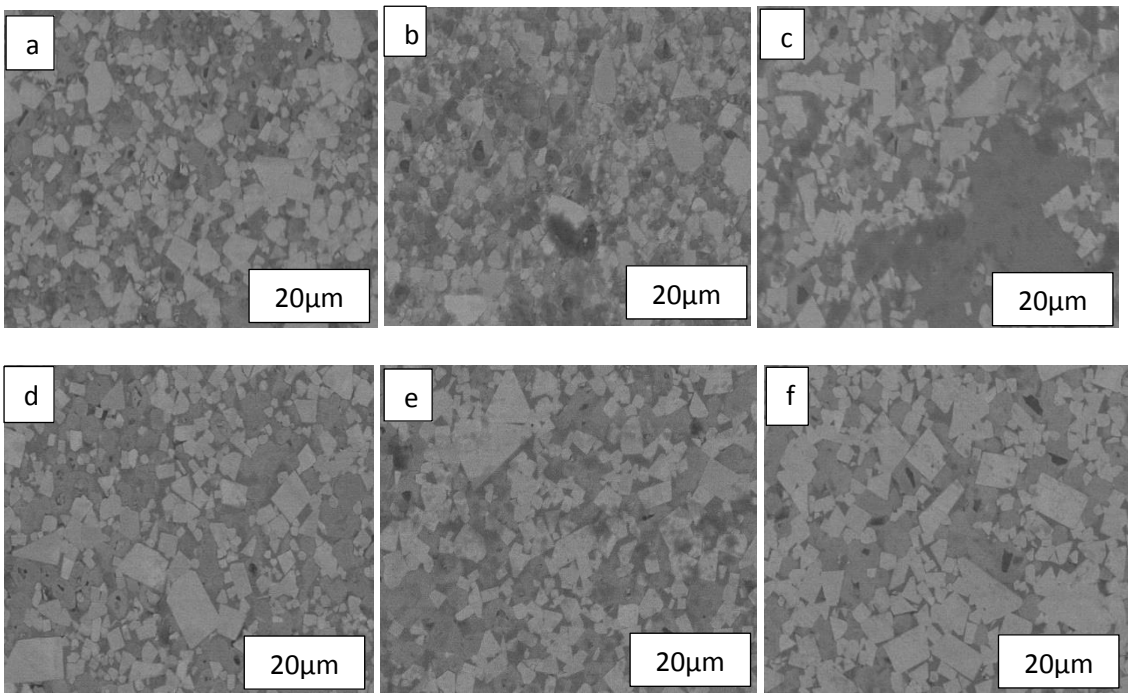


Fig. 4.20: Cross-sectional view SEM images of the sintered alloy D samples.

The average WC grain size for each of the alloys is listed in Table 4.7. The grains size of alloy-A was fluctuating as the C level increased and as the sintering temperature increased, a large grain size is seen on the standard C level alloy at 1510°C. The grain size of alloy-B increased with an increase in C level. The grain size of alloy-C decreased with an increase in C level as well as with the sintering temperature, this is due to the grain growth inhibitor $Cr_3C_2$ added. The grain size of alloy-D was fluctuating with the increase in C level and sintering temperature. Comparing all the alloys alloy-C has the smallest grains on average, this was expected because grain growth inhibitors were added in this alloy.

Table 4.7: Average WC grain size of the alloys in μm.

| | **Alloy-A** | **Alloy-B** | **Alloy-C** | **Alloy-D** |
|---|---|---|---|---|
| **Def-1340** | 3.89 ± 0.19 | 1.98 ± 0.67 | | |
| **Std-1340** | 3.06 ± 0.08 | 3.16 ± 0.77 | | |
| **Exc-1340** | 3.92 ± 0.36 | 3.12 ± 1.00 | | |
| **Def-1430** | 5. 20 ± 0.12 | 2.36 ± 0.31 | 2.33 ± 0.01 | 2.62 ± 0.09 |
| **Std-1430** | 4.46 ± 0.87 | 2.78 ± 0.72 | 2.18 ± 0.15 | 2.98 ± 0.06 |
| **Exc-1430** | 6.40 ± 0.45 | 3.54 ± 0.12 | 1.64 ± 0.06 | 2.06 ± 0.15 |
| **Def-1510** | 3.43 ± 0.01 | 2.43 ± 0.12 | 2.63 ± 0.19 | 1.94 ± 0.04 |
| **Std-1510** | 6.82 ± 1.26 | 2.77 ± 1.12 | 2.46 ± 0.53 | 1.99 ± 0.09 |
| **Exc-1510** | 4.47 ± 0.61 | 3.94 ± 0.98 | 1.84 ± 0.11 | 3.15 ± 0.11 |

The Co binder mean free path and WC contiguity was calculated for the straight WC-Co system represented by Alloy A and these values are listed in Table 4.8. These properties were not measured for the alloys containing mixed crystals. The BMFP and the WC contiguity of the alloy does not show a defined trend, however comparing the standard C level alloy with the other C levels individually, the WC contiguity of the standard C is higher than that of the other two C levels meaning there are more WC-WC interfaces in the alloy. The BMFP of the standard C is higher than the excess C alloy and less than the deficient C alloy.

Table 4.8: Contiguity and Co binder mean free path and WC contiguity for Alloy A in μm.

| | **Def-1340** | **Std-1340** | **Exc-1340** | **Def-1430** | **Std-1430** | **Exc-1430** | **Def-1510** | **Std-1510** | **Exc-1510** |
|---|---|---|---|---|---|---|---|---|---|
| **BMFP** | 0.48 ± 0.002 | 0.46 ± 0.003 | 0.45 ± 0.003 | 0.48 ± 0.004 | 0.52 ± 0.009 | 0.59 ± 0.013 | 0.52 ± 0.003 | 0.74 ± 0.020 | 0.49 ± 0.009 |
| C | 0.48 ± 0.008 | 0.57 ± 0.006 | 0.44 ± 0.009 | 0.31 ± 0.001 | 0.45 ± 0.010 | 0.30 ± 0.003 | 0.58 ± 0.005 | 0.41 ± 0.001 | 0.42 ± 0.004 |

### 4.3.2. Phase identification

Phase identification of the sintered alloys was achieved by XRD analysis. The analyses were done on one sample per sintering condition. The XRD graphs are shown for each alloy at the three different sintering temperatures.

Figs.4.21 to 4.23 are the XRD patterns for Alloy A. It can be seen that at all the sintering temperatures there are peak shifts, when using the standard C level alloy as a reference. At 1340°C the peaks of the C deficient alloys have shifted to the left, although the peaks show the same phases as those of the Standards C alloy, except at about 60°. The peaks of the excess C alloys have shifted slightly to the right and show a higher Co concentration compared to the other two C levels. There is no evidence of the graphite phase which was seen on the SEM images. At 1430°C only the excess C alloy peaks have shifted to the left and again it showed a higher Co level than the other two C levels. As the sintering temperature increased the standard C and C deficient alloys become more aligned to each other while a shift to the left was observed for the excess C alloys.

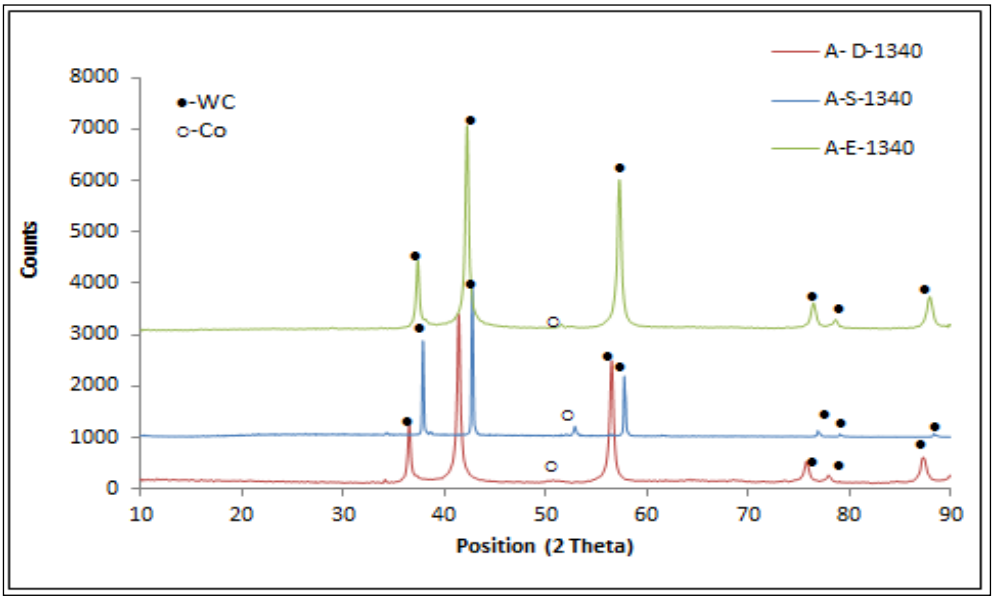


Fig. 4.21: XRD analyses of the Alloy-A samples sintered at 1340 °C.

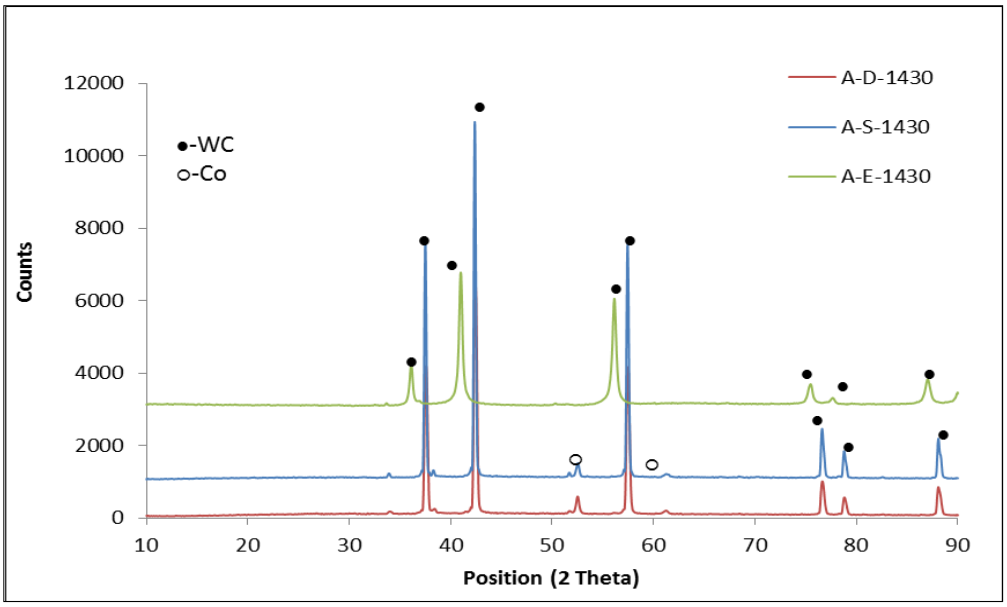


Fig. 4.22: XRD analysis of the sintered compacts for Alloy-A at 1430°C.

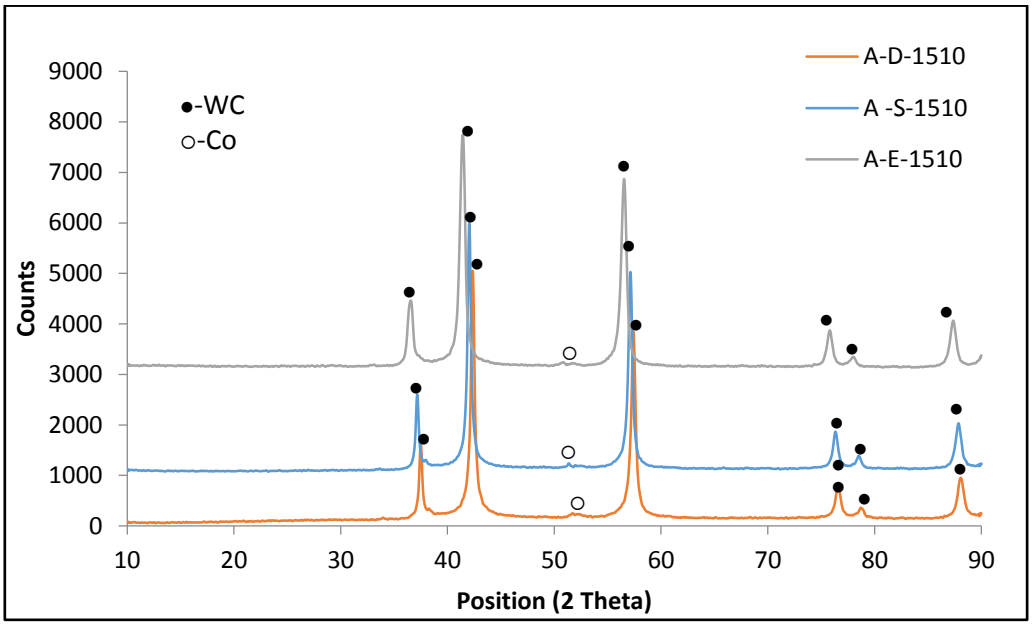


Fig. 4.23: XRD analysis of the sintered compacts for Alloy-A at 1510°C.

Figs. 4.24 to 4.26 are the XRD patterns for Alloy B. Peak shifts were observed with reference to the standard C level, at all the sintering temperatures. As the temperature increased, the peak intensity of the TiC increased. At 1340°C there were very small shifts of the C deficient alloy peaks to the right which are insignificant. However, at this temperature a greater peak shift to the right for the excess C alloys was observed. The Co appeared to be consistent.

At 1430°C there were small peak shifts for both the deficient and excess C alloys, while the Co peaks remained the same. The TiC peaks became more evident as the C content increased. At 1510°C peak shifts for the C deficient alloy were very small. Peak shifts were more evident on the excess C alloys. Once again, there was no change in the Co peaks as the C level increased, and the TiC peaks became more evident as the C content increased.

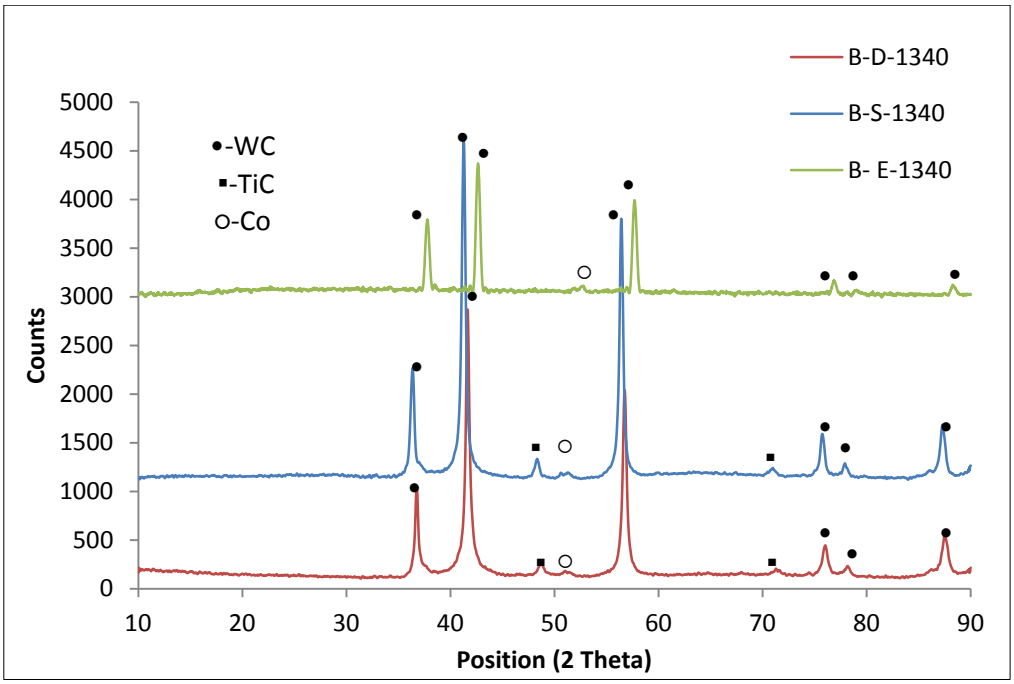


Fig. 4.24: XRD analysis of the sintered compacts for Alloy-B at 1340°C.

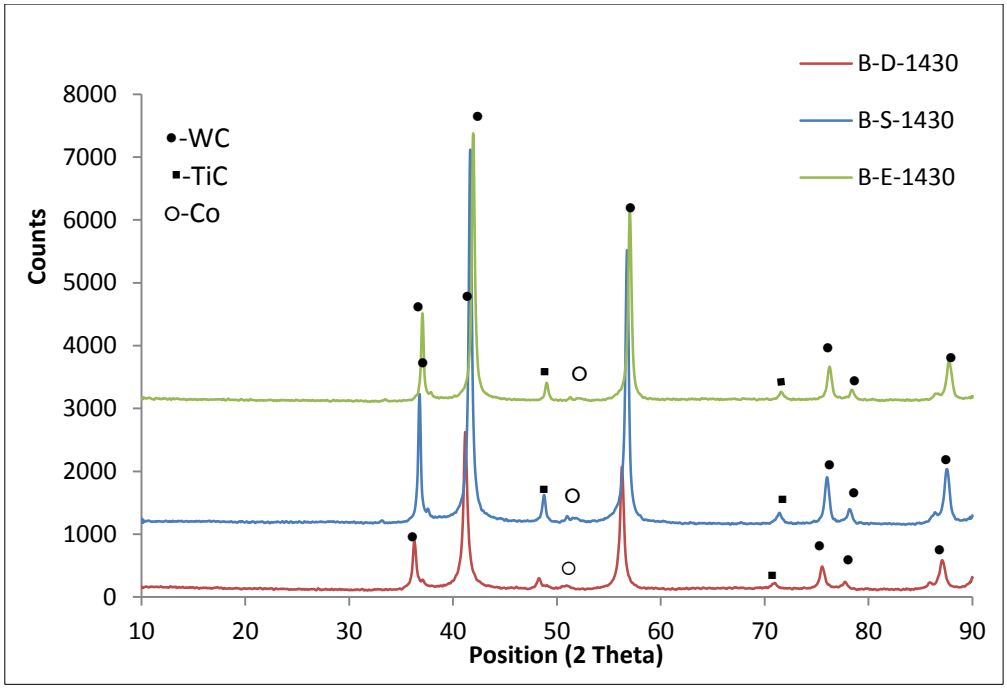


Fig.4.25: XRD analysis of the sintered compacts for Alloy-B at 1430°C.

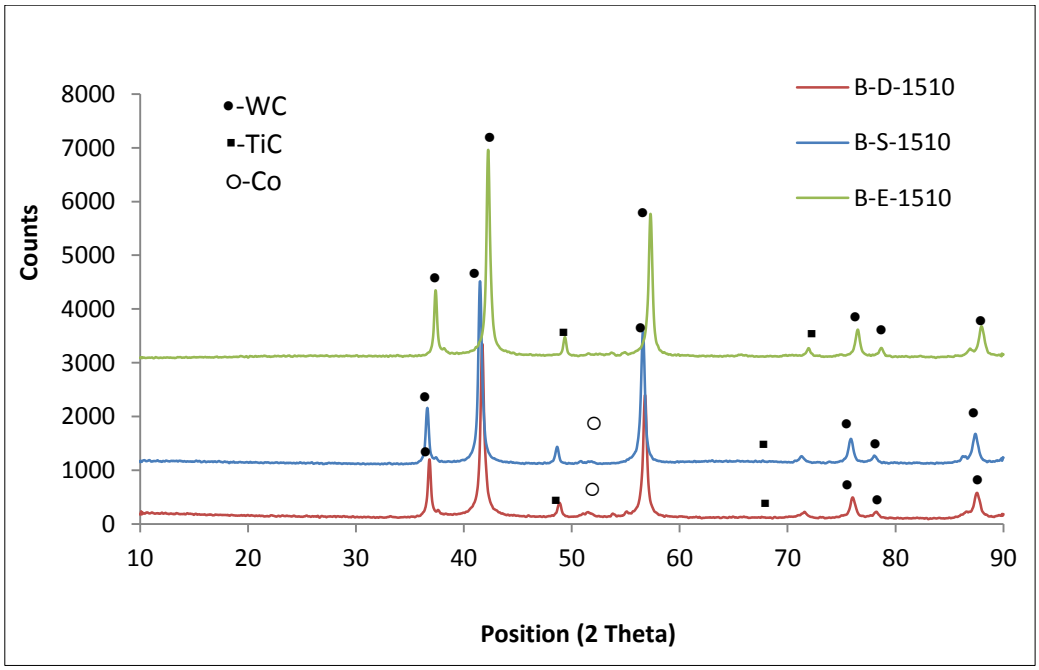


Fig. 4.26: XRD analysis of the sintered compacts for Alloy-B at 1510°C.

Fig. 4.27 and 4.28 are the XRD patterns for Alloy C. At 1430°C there is only a peak shift on the C deficient alloy to the left, with reference to the standard C alloy, while the peaks of the excess C alloy is aligned with those of the standard C. The Cr peak was seen only on the excess C alloy pattern. As the C level increased the intensity of the peaks increased.

At 1510°C the excess C alloy peaks were still aligned with those of the standard C alloy while the peaks of the C deficient alloys have shifted to the right. There was no change in the Co peak as the C level increased, and the TiC peaks were more evident as the C content increased.

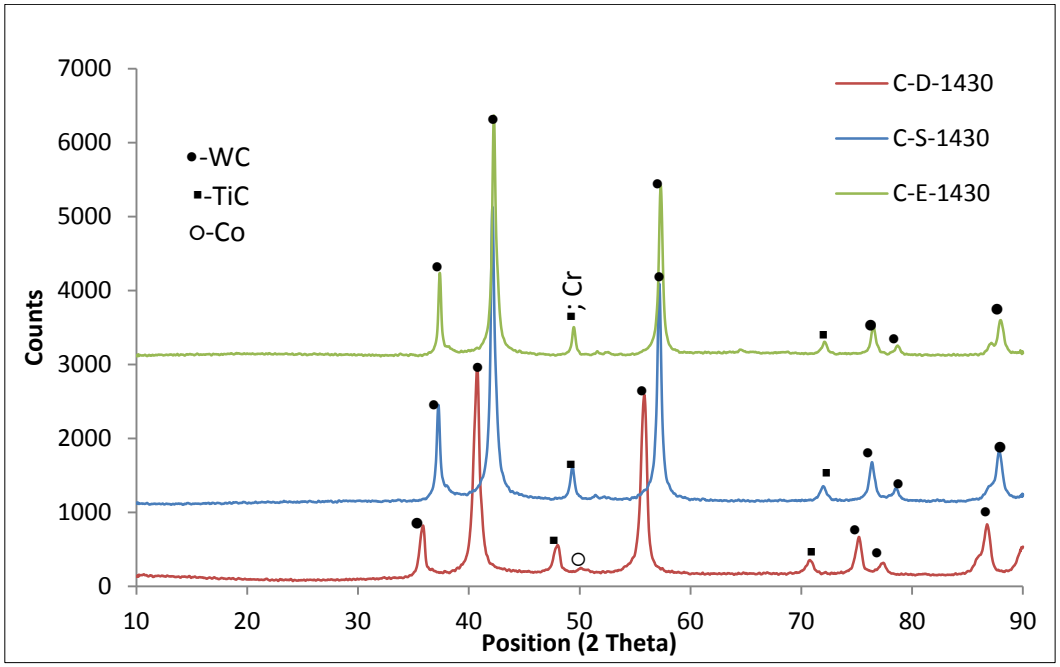


Fig. 4.27: XRD analysis of the sintered compacts for Alloy-C at 1430°C.

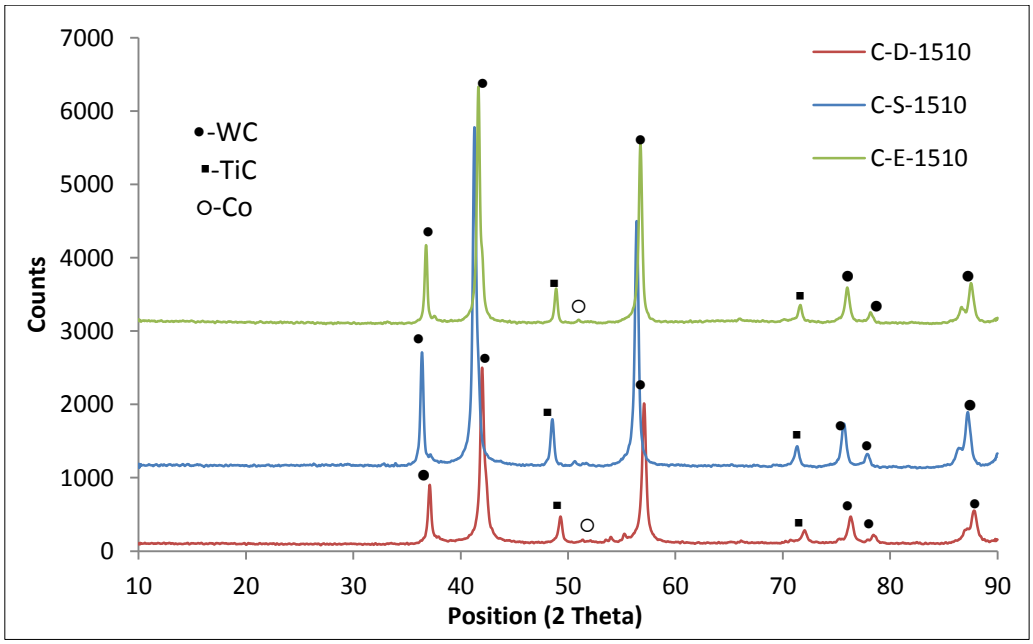


Fig. 4.28: XRD analysis of the sintered compacts for Alloy-C at 1510°C.

Figs. 4.29 and 4.30 are the XRD patterns for Alloy D. At 1430°C there is only a peak shift on the C deficient alloy to the left, with reference to the standard C alloy, while the peaks of the excess C alloy is aligned with those of the standard C. As the C level increased the intensity of the peaks increased. At 1510°C the excess C alloy peaks were still aligned with those of the standard C alloy while the peaks of the C deficient alloys have shifted to the right. There was no change in the Co peak as the C level increased, and the TiC peaks were more evident as the C content increased. The $Co_6W_6C$ peak was seen only on the deficient C alloy pattern.

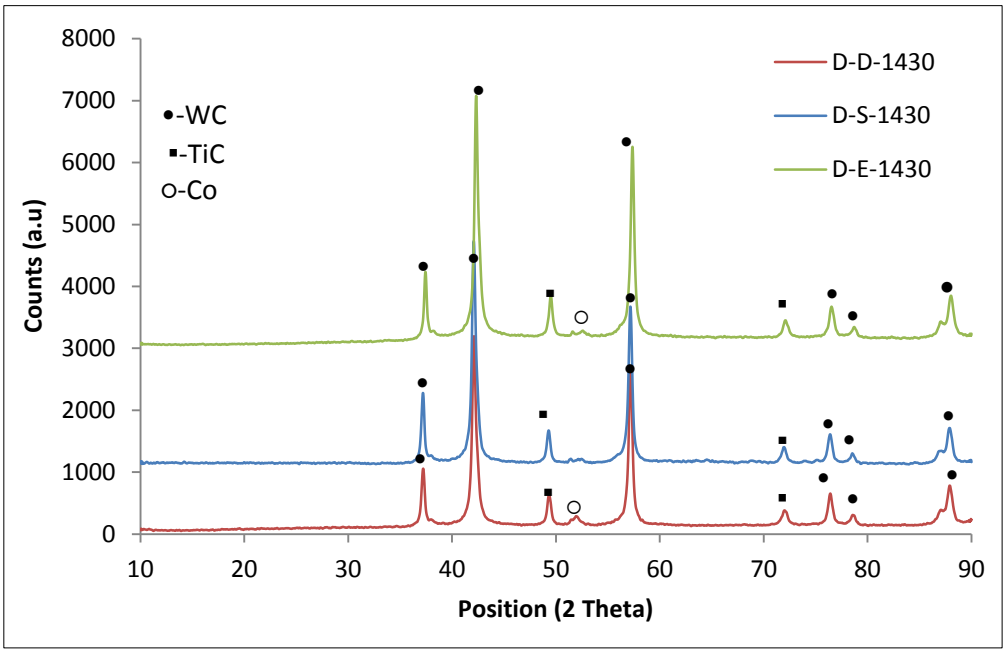


Fig. 4.29: XRD analysis of the sintered compacts for Alloy-D at 1430°C.

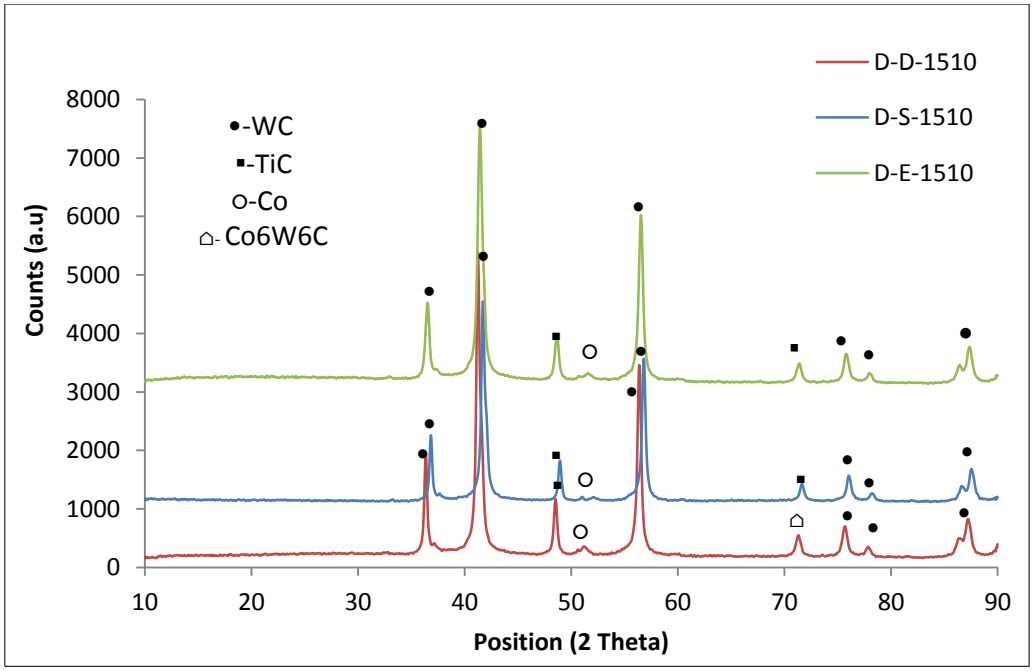


Fig. 4.30: XRD analysis of the sintered compacts for Alloy-D at 1510°C.

### 4.3.3. Density

The density and porosity of the alloys is listed in Tables 4.9 and 4.10. For some of the alloys the density decreased with an increase in the C content, while for other alloys the reverse was found. A similar trend was observed for an increase in sintering temperature. Alloy-D has the lowest density and alloy-A has the highest density. This is due to the amount of heavy WC present in the alloy; as the amount of total WC in the alloy decreased the density decreased.

Porosities of alloy-A and alloy-B did not show a defined trend. However as the sintering temperature increased the standard C values of both alloys was less porous compared to the values from the other carbon levels. Alloy-C and alloy-D showed a defined trend; as the C content increased the porosity of the alloys also increased. This corresponds to the decrease in the density of these alloys. For alloy-C and alloy-D it can be said that density is inversely proportional to the porosity of the alloys.

Table 4.9: Density and porosity for alloy-A and alloy-B.

| **Alloy-A** | | | | | | |
|---|---|---|---|---|---|---|
| | **1340°C** | | **1430°C** | | **1510°C** | |
| | **Density (g/cm3)** | **Porosity (%)** | **Density (g/cm3)** | **Porosity (%)** | **Density (g/cm3)** | **Porosity (%)** |
| **Def. C** | 14.95±0.136 | 0.07±0.160 | 14.99±0.020 | 0.35±0.129 | 14.96±0.019 | 0.15±0.089 |
| **Std C** | 15.02±0.011 | 0.53±0.269 | 14.95±0.027 | 0.07±0.181 | 14.92±0.023 | 0.10±0.161 |
| **Exc C** | 15.01±0.051 | 0.49±0.340 | 14.89±0.023 | 0.35±0.150 | 14.82±0.011 | 0.79±0.070 |
| **Alloy-B** | | | | | | |
| **Def. C** | 12.85±0.127 | 6.33±0.93 | 13.69±0.023 | 1.10±0.07 | 13.63±0.03 | 0.68±0.21 |
| **Std C** | 13.54±.008 | 1.34±0.06 | 13.57±0.010 | 0.25±0.17 | 13.49±0.03 | 1.66±0.22 |
| **Exc C** | 13.52±0.021 | 1.43±0.15 | 13.59±0.018 | 0.91±0.13 | 13.48±0.09 | 1.74±0.68 |

Table 4.10: Density and porosity for alloy-C and alloy-D.

| **Alloy-C** | | | | |
|---|---|---|---|---|
| | **1430°C** | | **1510°C** | |
| | **Density (g/cm3)** | **Porosity (%)** | **Density (g/cm3)** | **Porosity (%)** |
| **Def. C** | 13.08±0.052 | 0.32±0.387 | 13.02±0.020 | 0.34±0.170 |
| **Std C** | 13.02±0.016 | 0.72±0.121 | 13.04±0.020 | 0.59±0150 |
| **Exc C** | 12.97±0.023 | 1.12±0.173 | 12.92±0.020 | 1.54±0.120 |
| **Alloy-D** | | | | |
| **Def. C** | 12.41±0.088 | 1.44±0.701 | 12.44±0.010 | 1.22±0.060 |
| **Std C** | 12.41±0.015 | 1.42±0.120 | 12.43±0.020 | 1.29±0.170 |
| **Exc C** | 12.35±0.022 | 1.91±0.211 | 12.35±0.020 | 1.91±0.140 |

### 4.3.4. Coercivity

The coercivity of the alloys is listed in Tables 4.11 and 4.12 respectively. In general the coercivity decreased as the C content increased for all the alloys, except for Alloy A when sintered at 1340°C and 1430°C, where the reverse trend was observed. As the sintering temperature increased the coercivity decreased for all the alloys except Alloy B, which showed the highest values at a sintering temperature of 1430°C.

Table 4.11: Coercivity for alloy-A and alloy-B (Oe).

| | | | |
|---|---|---|---|
| **Alloy-A** | | | |
| | **1340°C** | **1430°C** | **1510°C** |
| **Def. C** | 153.10±1.370 | 147.50±0.533 | 141.30±2.581 |
| **Std C** | 163.00±0.520 | 150.60±0.971 | 128.50±1.841 |
| **Exc C** | 161.50±0.710 | 152.80±0.630 | 126.20±1.621 |
| **Alloy-B** | | | |
| **Def. C** | 183.30±2.797 | 218.00±1.943 | 173.40±5.816 |
| **Std C** | 146.20±1.874 | 167.00±0.738 | 150.00±1.000 |
| **Exc C** | 155.60±2.797 | 159.80±1.312 | 137.40±0.843 |

Table 4.12: Coercivity for alloy-C and alloy-D (Oe).

| | | |
|---|---|---|
| **Alloy-C** | | |
| | **1430°C** | **1510°C** |
| **Def. C** | 241±1.30 | 182.5±1.43 |
| **Std C** | 209±1.18 | 167±1 |
| **Exc C** | 183.2±1.23 | 165.3±0.48 |
| **Alloy-D** | | |
| **Def. C** | 185±1.34 | 127.5±1.27 |
| **Std C** | 144±1.27 | 106±3 |
| **Exc C** | 127±0.667 | 102.1±0.876 |

### 4.3.5. Magnetic Co

The results of the magnetic Co tests are listed in Tables 4.13 and 4.14 respectively. As the C level increased the amount of magnetic Co increased for all the alloys except alloy C. This alloy showed the highest value at the standard C level, at a sintering temperature of 1510°C, while the values at a sintering temperature of 1430°C were found to be similar for the standard and excess C alloys. Each alloy showed a varied trend in the amount of magnetic Co as the sintering temperature increased.

Table 4.13: Magnetic Co data for alloy-A and alloy-B (%).

| Alloy-A | | | |
|---|---|---|---|
| | **1340°C** | **1430°C** | **1510°C** |
| **Def. C** | 5.14±0.028 | 5.57±0.078 | 4.92±0.083 |
| **Std C** | 6.04±0.028 | 5.98±0.025 | 5.92±0.057 |
| **Exc C** | 6.15±0.031 | 6.06±0.025 | 6.14±0.041 |
| **Alloy-B** | | | |
| **Def. C** | 4.73±0.045 | 4.53±0.013 | 5.21±0.081 |
| **Std C** | 5.70±0.045 | 5.89±0.021 | 6.10±0.040 |
| **Exc C** | 6.24±0.032 | 6.29±0.050 | 6.43±0.032 |

Table 4.14: Magnetic Co data for alloy-C and alloy-D (%).

| Alloy-C | | |
|---|---|---|
| | **1430°C** | **1510°C** |
| **Def. C** | 3.52±0.070 | 3.89±0.021 |
| **Std C** | 4.63±0.020 | 4.83±0.050 |
| **Exc C** | 4.64±0.060 | 4.65±0.020 |
| **Alloy-D** | | |
| **Def. C** | 7.81±0.120 | 8.31±0.130 |
| **Std C** | 8.98±0.030 | 9.18±0.142 |
| **Exc C** | 9.55±0.220 | 9.36±0.211 |

### 4.3.6. Vickers hardness

The results of the Vickers hardness tests for alloy-A are represented in Tables 4.15 and Fig.4.31. As the C level increased the hardness of the alloy decreased at 1340°C. This alloy showed the highest value at the standard C level, at a sintering temperature of 1430°C and 1510°C. The alloy showed a varied trend on the hardness values as the sintering temperature increased.

Table 4.15: Summary of Vickers' hardness for alloy-A (HV).

| | **1340°C** | **1430°C** | **1510°C** |
|---|---|---|---|
| **Def. C** | 1620 ±26 | 1432 ± 5 | 1386±16 |
| **Std C** | 1504 ± 9 | 1455 ± 3 | 1399±5 |
| **Exc C** | 1493 ± 1 | 1424 ±28 | 1384±42 |

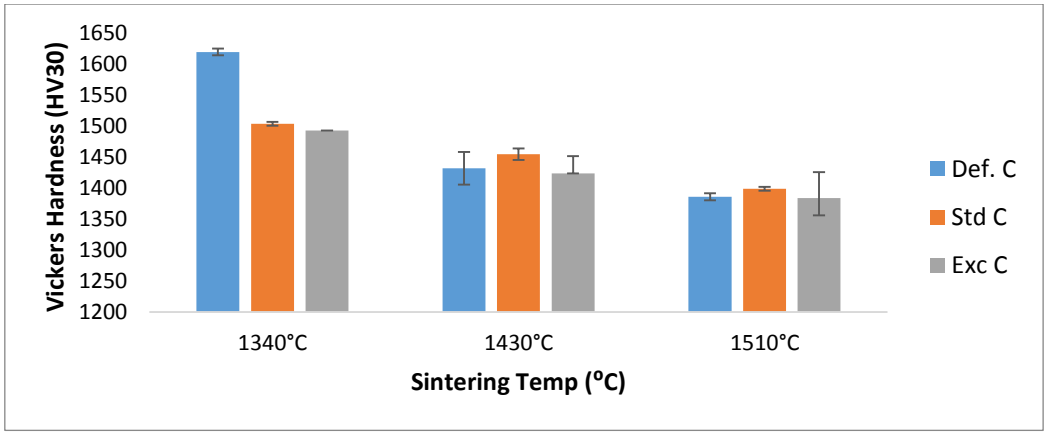


Fig. 4.31: Graphic summary of Vickers' hardness for alloy-A.

The micro-hardness profile results of alloy-A in Fig. 4.32 shows similar trend to the Vickers' hardness results.

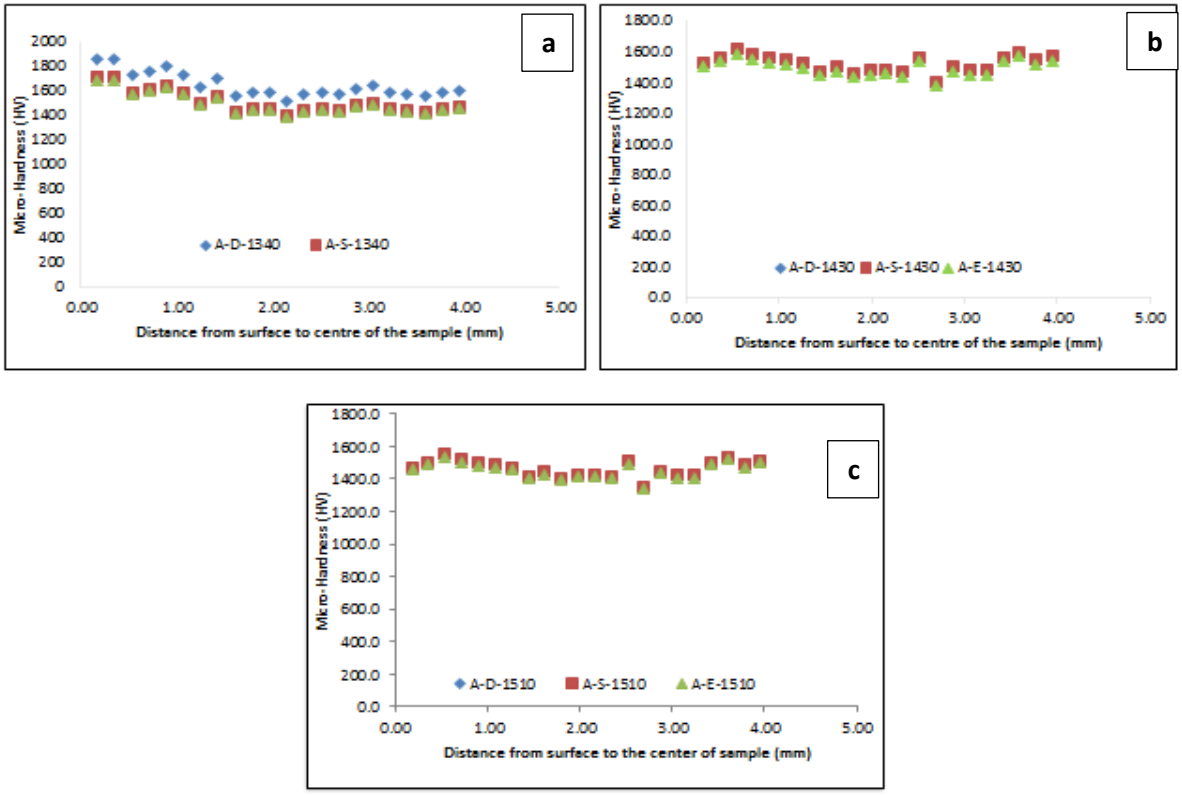


Fig. 4.32: Graphic summary of micro-hardness for alloy-A at different sintering temperatures (a) 1340 °C, (b) 1430 °C and (c) 1510 °C.

The results of the Vickers hardness tests for alloy-B are represented in Tables 4.16 and Fig. 4.33. As the C level increased the hardness of the alloy decreased. The hardness at 1340$^0$C for deficient C is low as compared to all the hardness of this alloy. The alloy showed a varied trend on the hardness values as the sintering temperature increased.

Table 4.16: Summary of Vickers' hardness for alloy-B (HV).

| | **1340°C** | **1430°C** | **1510°C** |
|---|---|---|---|
| **Def. C** | 898±51 | 1580±10 | 1591±1 |
| **Std C** | 1580±26 | 1497±21 | 1497±19 |
| **Exc C** | 1591±17 | 1536±9 | 1563±34 |

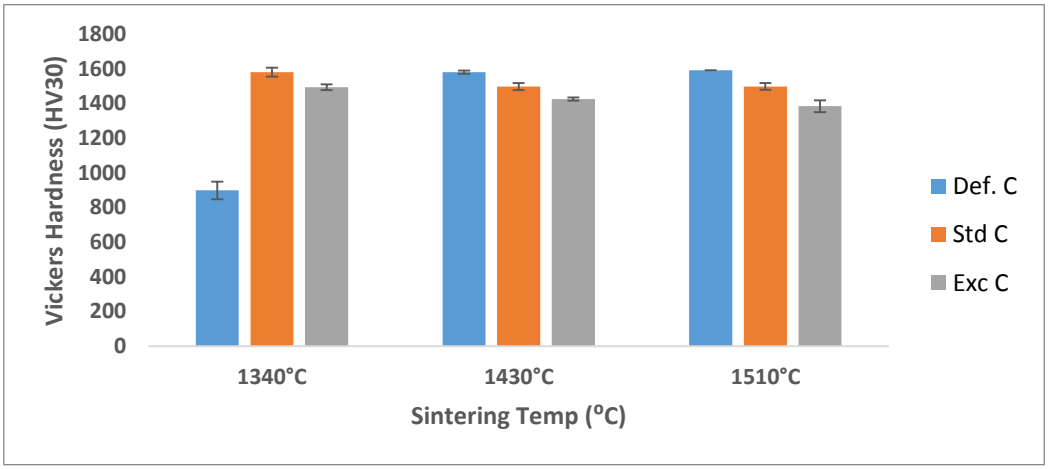


Fig. 4.33: Graphic summary of Vickers' hardness for alloy-B.

The results of the Vickers hardness tests for alloy-C are represented in Tables 4.17 and Fig. 3.34. As the C level increased the hardness of the alloy overall increased for both sintering temperatures. This alloy showed the lowest value at the standard C level, at a sintering temperature of 1430°C and 1510°C. The alloy showed an increasing trend on the hardness values as the sintering temperature increased, this is due to the grain growth inhibitor that was added in this alloy.

Table 4.17: Summary of Vickers' hardness for alloy-C (HV).

| | **1430**°C | **1510°C** |
|---|---|---|
| **Def. C** | 1763±41 | 1838±21 |
| **Std C** | 1743±12 | 1783±31 |
| **Exc C** | 1790±42 | 1852±45 |

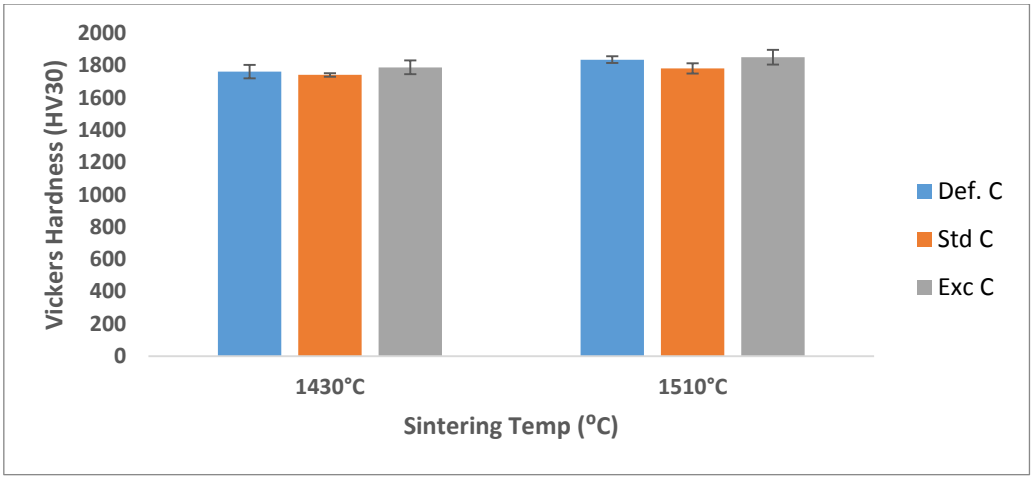


Fig. 4.34: Graphic summary of Vickers' hardness for alloy-C.

The micro-hardness profile results of alloy-C in Fig. 4.35 showed asimilar trend to the Vickers' hardness results.

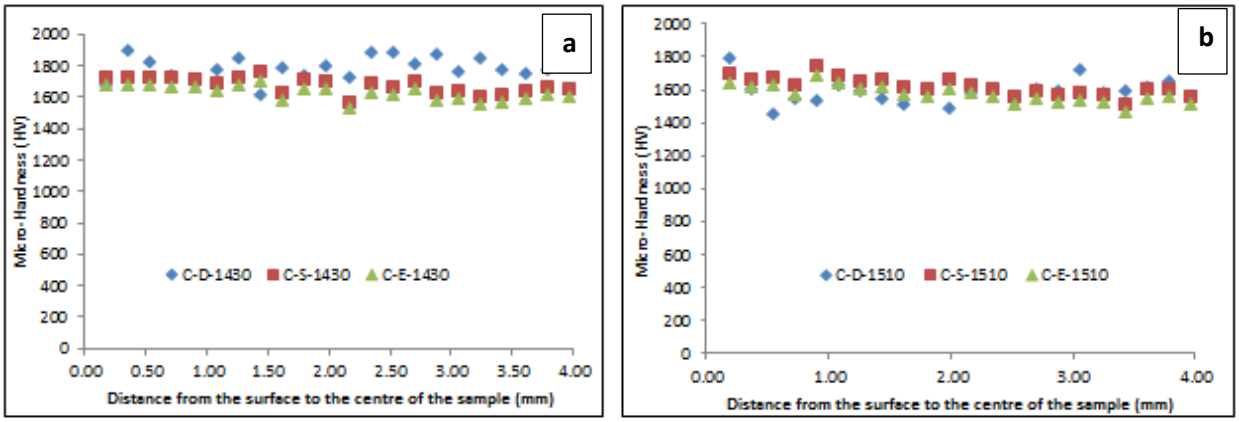


Fig. 4.35: Graphic summary of micro-hardness for alloy-C at different sintering temperatures (a) 1430°C and (b) 1510°C.

The results of the Vickers hardness tests for alloy-D are represented in Tables 4.18 and Figure 4.36. As the C level increased the hardness of the alloy decreased at 1430°C. This alloy showed the lowest value at the standard C level, at a sintering temperature of 1430°C and 1510°C. The alloy showed a varied trend on the hardness values as the sintering temperature increased.

Table 4.18: Summary of Vickers' hardness for alloy-D (HV).

| | **1430 °C** | **1510 °C** |
|---|---|---|
| **Def. C** | 1580±20 | 1515±59 |
| **Std C** | 1458±17 | 1469±53 |
| **Exc C** | 1425±20 | 1565±84 |

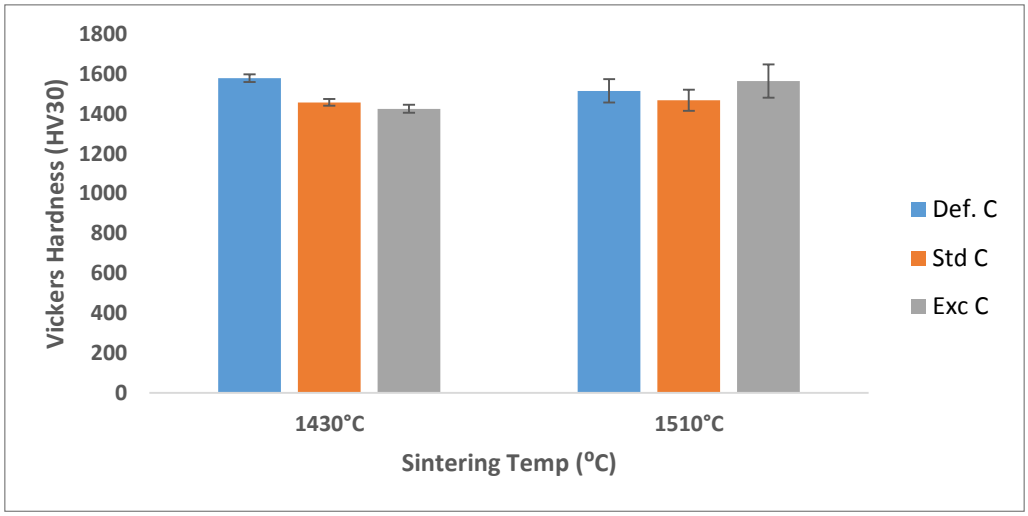


Fig. 4.36: Graphic summary of Vickers' hardness for alloy-D.

### 4.3.7. Fracture toughness

The results of the fracture toughness tests for alloy-A are represented in Tables 4.19 and Fig. 4.37. As the C level increased the toughness of the alloy decreased at 1430°C. The alloy showed avaried increasing trend on the toughness values as the sintering temperature increased, except for Def C at 1510°C.

Table 4.19: Summary of fracture toughness for alloy-A ($MPa.\sqrt{m}$).

| | **1340°C** | **1430°C** | **1510°C** |
|---|---|---|---|
| **Def. C** | 10.28±0.55 | 11.97±0.43 | 11.72±0.82 |
| **Std C** | 10.53±0.41 | 11.00±0.24 | 11.90±0.38 |
| **Exc C** | 10.21±0.80 | 10.90±0.54 | 11.71±0.41 |

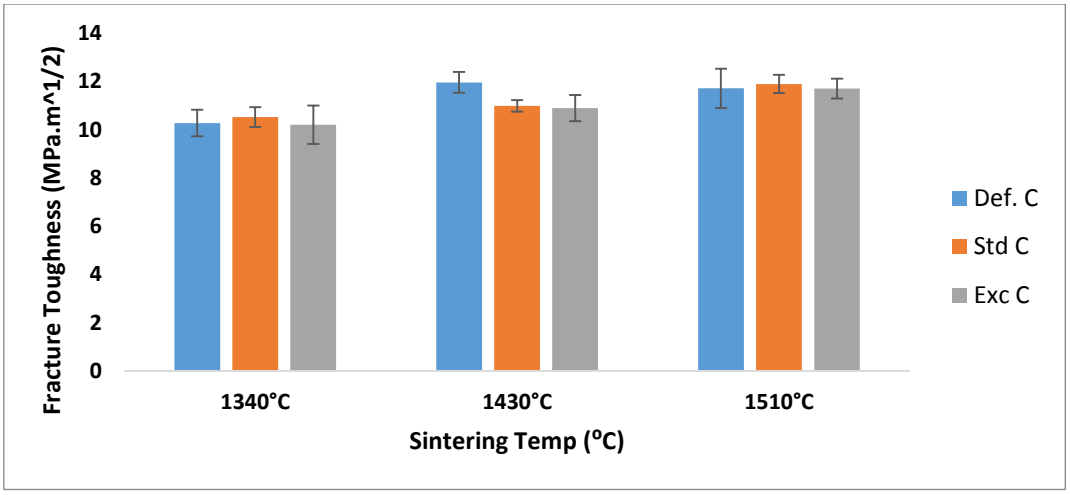


Fig.4.37: Graphic summary of fracture toughness for alloy-A.

The results of the fracture toughness tests for alloy-B are represented in Tables 4.20 and Fig. 4.38. As the C level increased the overall toughness of the alloy decreased for 1510°C while, it increased at 1340 and 1430°C. This alloy showed the highest value at the standard C level, at a sintering temperatures of 1430 and 1510°C. The alloy showed an increasing trend on the toughness values as the sintering temperature increased.

Table 4.20: Summary of fracture toughness for alloy-B ($MPa.\sqrt{m}$).

| | **1340 °C** | **1430 °C** | **1510 °C** |
|---|---|---|---|
| **Def. C** | 9.06±0.01 | 9.25±0.18 | 9.89±0.18 |
| **Std C** | 8.72±0.35 | 10.38±0.43 | 10.71±0.48 |
| **Exc C** | 9.51±0.19 | 9.86±0.22 | 9.54±0.18 |

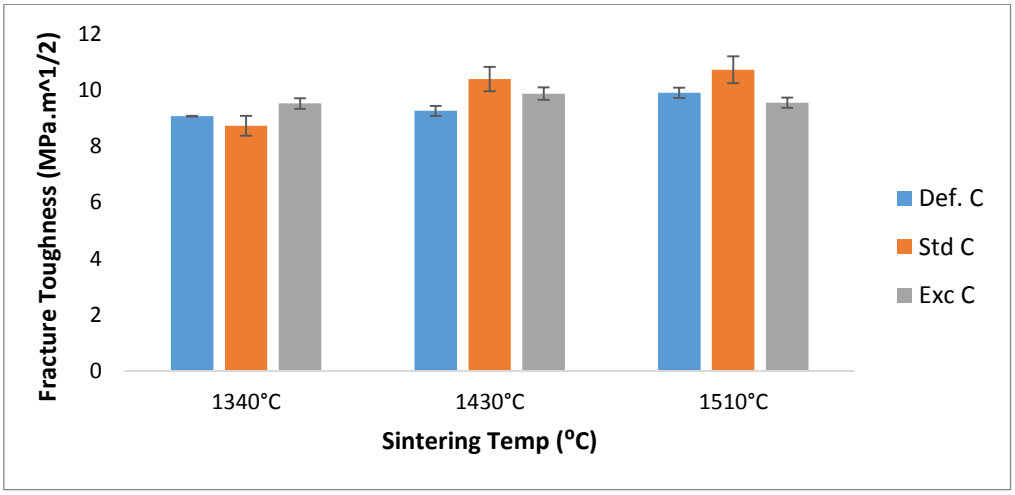


Fig. 4.38: Graphic summary of fracture toughness for alloy-B.

The results of the fracture toughness tests for alloy-C are represented in Tables 4.21 and Fig. 4.39. As the C level increased the toughness of the alloy increased at 1430°C. This alloy showed the lowest values at the standard C level, at a sintering temperature of 1430 and 1510°C. The alloy showed a varied trend on the toughness values as the sintering temperature increased.

Table 4.21: Summary of fracture toughness for alloy-C ($MPa.\sqrt{m}$).

| | **1430 °C** | **1510 °C** |
|---|---|---|
| **Def. C** | 9.63±0.50 | 10.91±0.09 |
| **Std C** | 9.77±0.03 | 9.69±0.26 |
| **Exc C** | 11.15±0.19 | 10.81±0.67 |

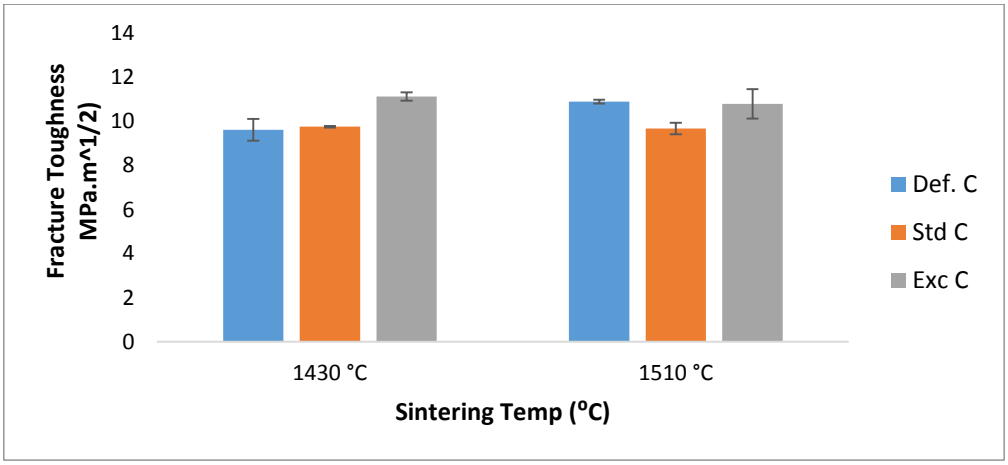


Fig. 4.39: Graphic summary of fracture toughness for alloy-C.

The results of the fracture toughness tests for alloy-D are represented in Tables 4.22 and Fig. 4.40. As the C level increased the toughness of the alloy decreased at 1510°C, while it increased at 1430°C. The alloy showed a varied trend on the toughness values as the sintering temperature increased.

Table 4.22: Summary of fracture toughness for alloy-D ($MPa.\sqrt{m}$).

| | **1430°C** | **1510°C** |
|---|---|---|
| **Def. C** | 11.10±1.05 | 12.73±0.86 |
| **Std C** | 11.38±0.34 | 12.17±0.90 |
| **Exc C** | 11.43±0.58 | 11.50±0.59 |

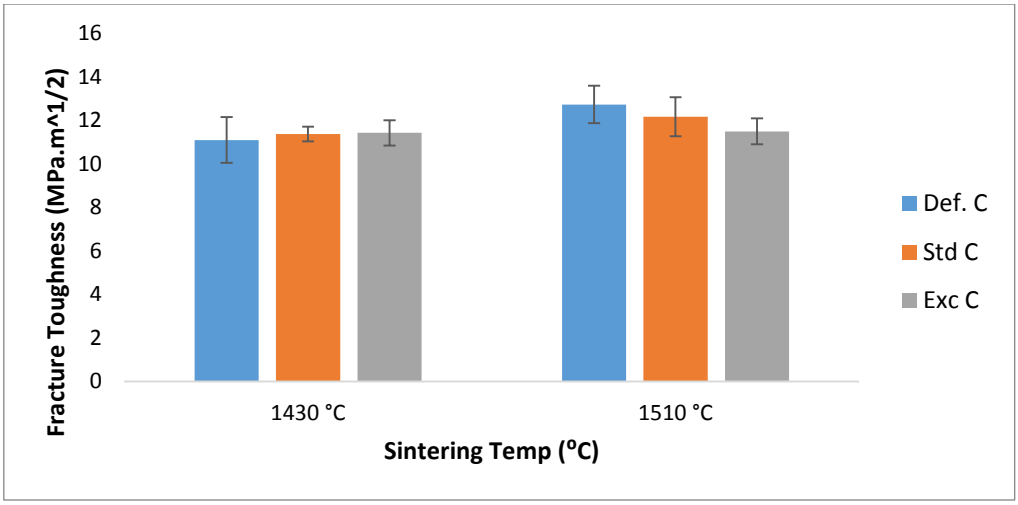


Fig. 4.40: Graphic summary of fracture toughness for alloy-D.

# Chapter 5

## Discussion

This chapter reports on the deeper analysis of the test work results in Chapter 4 to assist in answering the aim of the project. This chapter is divided into three sections namely:

- Characterization of powder
- Characterization of green compacts
- Characterization of sintered compacts

### 5.1. Characterization of powder

The starting powders were mixed and milled to produce four alloy grades. The difference between the three distinct powders used for each alloy is their carbon levels. The C contents were designated as “deficient C”, “standard C” and “excess C”. “Deficient C” means insufficient carbon in the WC-Co system; XRD analysis showed this aspect with an extra W peak, which was seen in all the alloys. “Standard C” for each alloy refers to the standard amount of C (6.12 wt. %) in the WC-Co system. The “excess C” on the WC-Co alloys indicates there is more C than required. All these C levels favour different mechanical and physical properties of the sintered alloy, which will be discussed later in the chapter.

All the alloy powders were milled to the same particle size of 1.8 µm. According to Fig. 4.3 the milling time of all the alloys was not the same. This is due to the elements present in the alloy. The addition of carbides other than WC reduced the milling time as seen with some of the alloys, the grindability of the alloys increased. The cobalt content also played a role in the milling time of the alloys. The more Co added in the system the shorter the milling time. Refer to alloy-C and alloy-D in Fig. 4.3, where alloy-D (9.5 wt. % Co) took about 6 hours to reach the targeted particle size while alloy-C (5 wt. % Co) took about 14 hours to reach the particle size.

Chemical analysis of the milled powders was conducted using XRF and ICP methods. From the results, a distinct difference between the two methods was observed. The differences were seen on both the starting and the milled powders. The chemical compositions of the starting powders were given by the manufacturer, and the ICP analysis showed similar compositions while the XRF results were different. In the XRF data, higher oxygen values were recorded compared to ICP. This may be due to the fact that XRF chemical analysis is done using the oxides of the elements and then this data is converted into elemental compositions. The advantage of the ICP method is that one can analyse the total sulphur and carbon in the samples, whereas the XRF can only identify elements from F upwards in the periodic table and provides no details on carbon analysis. The XRD and EDS (SEM) results agreed with the ICP results, although some elements such as Ta and Nb were not detected due to the low concentrations.

### 5.2. Characterization of green compacts

The densities of the alloys were not the same. As the fraction of additional carbides such as TiC, NbC and TaC increased, the density and porosity of the alloys decreased.. The addition of Co and mixed carbides reduced the number of large and heavy WC, leading to lighter materials.

The XRD results were similar for the three different C levels of each tool grade. The one similarity between all four C-deficient grades was the presence of a W peak, which is attributed to the extra W powder that was added to the C-deficient grades to lower the C content. The microstructures in Fig. 4.9 to 4.12 show that the granules of alloy-C and alloy-D are more closely packed as compared to the other two alloys. This is due to more voids being filled in these alloys.

## 5.3. Sintered alloy characterization

The discussion on the characterization of the sintered alloys is divided into two main sections, namely the effect of carbon content and then the effect of sintering temperature on the properties of the tool grades.

### 5.3.1. Effect of carbon content

Carbon is said to have a very critical effect on the properties of cemented carbide tools [1, 2]. Hence, the effect of C on the sintered alloy properties will first be discussed for each of the tool grades separately and thereafter a comparison between the tool grades will be made.

#### 5.3.1.1. Alloy A

Alloy A was a standard 94 wt. % WC - 6wt. % Co grade. The density of the alloy decreased with an increase in C content. The coercivity and the magnetic Co level of the alloy increased with the increase in C content. A deficiency of C in the alloy system, leads to excess W that will dissolve into the binder, decreasing the magnetism of the alloy.

The hardness increased with a decrease in C content at a sintering temperature of 1340°C. At sintering temperatures of 1430 C and 1510 C, the highest hardness was recorded using the standard C level, while the ‘deficient’ and ‘excess’ C alloys showed similar hardness values at each temperature. On the micro-hardness profiles of the cross-sections, the hardness from the surface to the centre of the samples remained fairly constant at each sintering temperature. The only notable difference was the higher average hardness of the ‘deficient C’ alloys sintered at 1340°C. According to literature [2] it has been said that as the C level is reduced the formation of eta phase becomes more likely. Eta phase is very hard therefore it will increase the hardness of the bulk alloy. However, on alloy-A there was no eta phase evident, yet the hardness of the alloy increased with decreasing C level. This increase may be attributed to the lower actual Co content and porosity levels compared to the other two alloys.

According to literature [2] as the C level in the cemented carbide system is added in excess of the stoichiometric level it promotes the formation of graphite that precipitates on the WC grains, see Fig. 4.13 c. As the C level increased the fracture toughness of the alloy increased, whereas the hardness was decreasing.

From the calculated WC grain sizes shown in Table 4.7; there was no defined trend as the carbon level increases. The binder mean free path and the WC contiguity of the alloy does not show a defined trend, however comparing the standard C level alloy with the other C levels individually, the WC contiguity of the standard C is higher than that of the other two C levels meaning there are more WC-WC interfaces in the alloy. The BMFP increased with decreasing C content. From literature [13] excess C lowers the melting point of Co, which increase the binder distribution within the WC particles, hence lowering BMFP values.

#### 5.3.1.2. Alloy B

Alloy-B is not a simple WC-Co system but has some additions of mixed carbides, thus, the effect of C is not only on the adjusted C forming the different C contents, but it is also due to these added carbides. As explained in Section 2.1 that the additions of TiC improves hardness of the material and the addition of (Ta, Nb)C improves high temperature properties of the alloy. It was seen that the density of alloy-B decreased with an increase in C level as well as the porosity of the alloy increased at 1510°C, and at the other temperatures there was no defined trend.

Coercivity decreased with an increase in C level, resulting to an easy demagnetization of the alloy. At "deficient C" the excess W dissolved in the Co, as mentioned above, however, not only WC was present in the alloy, also Ti, Ta and Nb carbides dissolved in the binder phase resulting in higher values of coercive forces to demagnetise the alloy. EDS analysis was done on the binder phase for the composition of the phase, see Fig. 5.1. Literature [14] states that "as the carbon content of a cemented carbide alloy is increasing the magnetic Co content also increases toward the amount of Co added during milling and mixing."

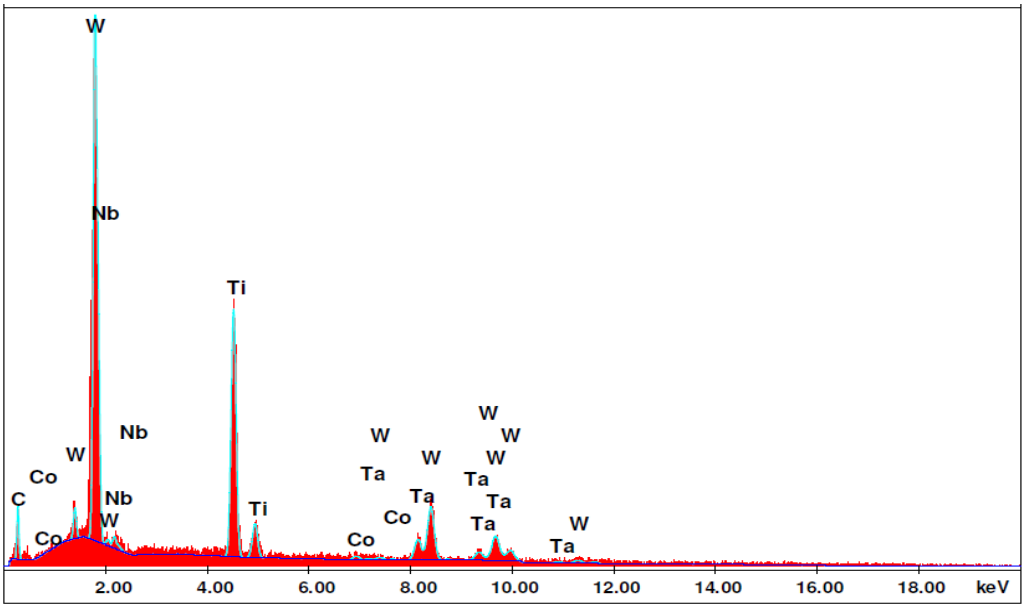


Fig. 5.1: EDS analysis of binder phase with dissolved Ta, Ti, W and Nb.

Hardness of the alloy increased with an increase in the C level at 1340°C, with the average hardness at the standard and excess C levels being within experimental error to each other. At sintering temperatures of 1430 ºC and 1510°C the standard C levels showed the lowest average hardness, with a higher average hardness measured at the deficient C levels. The toughness follows the inverse trend to hardness, with higher toughness values being associated with lower hardness values. This follows the well-established relationship between hardness and fracture toughness for hardmetals [2,14].

The XRD analysis showed the expected major phases of WC, Co and TiC, for the different carbon levels. From the SEM images there is not much change in grain size as the carbon level increases, whilst also the calculated grain size proves that there was not much of grain growth in the alloy. Binder mean free path and WC-WC contiguity were not calculated for this grade because of the complexity of the present carbides.

#### 5.3.1.3. Alloy C

Alloy-C had the lowest Co content of all the other alloys discussed. The density of the alloy decreased with an increase in C level, the alloy became lighter and closer to it's theoretical density (13g/l). The porosity of the alloy increased with an increase in the C level. The coercivity of alloy showed very high values as compared to the other two alloys that have been discussed above due to its low Co content as expected. However, as the C level increased the coercive forces required to demagnetize the alloy was decreasing, which is confirmed by literature [1]. The magnetic Co content of alloy-C in general increased with an increase in C level.

Hardness of alloy-C was fluctuating as the C level increased, it started high at deficient C and dropped at standard C and went up again at excess C, with the highest average hardness found at the excess C level. The high hardness at the deficient C level is attributed to the lower Co content measured at both sintering temperatures for this alloy. The high hardness at the excess C level is attributed to the finer WC grain size measured at both sintering temperatures. This grain refinement was achieved with the addition of Cr, known to be a grain growth inhibitor for hardmetals [29]. It appears that the effectiveness of grain growth inhibition increased as the sintering temperature increased. The micro-hardness profiles at both temperatures remained fairly constant from surface to center for all C levels, except the standard C level at 1430 C. The toughness showed the same trend as the hardness and this is not what literature generally reports, however the presence of the grain growth inhibitor Cr toughened the alloy [29]. It has been shown that the toughening mechanisms change when the WC grain size is small [30] and this may be the reason for the observed trends in the current research, but requires further investigation

The XRD analysis showed that as the C level increased the peaks of all the added carbides appeared. As the C level was increased the Co peaks were more visible. . The SEM micrographs showed that as the C level increased the (Ti, TiN) C areas became fewer and lighter. The grain size decreased with an increase in carbon content,which was due to the presence of Cr as the grain growth inhibitor [13], the calculated grain size concurs the same observation.

#### 5.3.1.4. Alloy D

Alloy-D had the highest Co content of all the other alloys present in this investigation. The effect of C level on the density of the alloyed showed a similar trend for both sintering temperatures.. As the C level increased the density of the alloy decreased. The density decreased to values (12.35 g/cm$^3$) which are less than the theoretical density (12.44 g/cm$^3$) of this alloy by about 1%. This may be due to the presence of high Co content in the alloy.

The coercivity of alloy-D decreased with an increase in C level. The coercive force that was needed to demagnetize the alloy became lower and lower. The magnetic Co increased with an increase in C level, more C present to bond with the likes of W, Ti, and the other elements the higher is the magnetic Co exposed and making the alloy to be more magnetic.

Hardness of alloy at 1430 °C decreased with an increase of the C level, and the toughness at the same temperature increased with increasing C level, which is what is expected. At 1510 °C the hardness fluctuated; compared with the "standard C", it was 3% higher at "deficient C" and 6.5% higher at "excess C", while the toughness decreased as the C level increased.

The XRD analysis; for all the sintering temperatures, showed that as the C level increased all the mixed carbides that were introduced in the beginning of the mixing stage are seen in the peaks. And there was high intensity Co peaks that were seen at excess C level and were seen in more than one position. The SEM micrographs showed that as the C level increased the Co pool areas increased and the TiC/ TiNC grains reduced and grains growth did not increase significantly, whilst the calculated grain sizes shows 37% increase of the grain size for the excess C level compared to the other two carbon levels.

### 5.3.2. Effect of sintering temperature

Alloy-A and alloy-B were sintered at three different temperatures (1340, 1430 and 1510°C), whilst, alloy-C and lloy-D were sintered only at two temperatures (1430 and 1510°C).

This section will discuss the effect of these sintering temperatures on different sintered properties that were are reported in Chapter 4. The effect of sintering temperature on the sintering properties will be discussed for each of the tool grades and thereafter compared against each other.

#### 5.3.2.1. Alloy-A

The density of alloy-A for all C level decreased as the temperature increased, this means as the sintering temperature increased the porosity in the material decreased and densification comes to completion.

The coercivity of the alloy also decreased with an increase in the sintering temperature for all the C levels.. For the magnetic Co, there is no defined trend as the temperature increases with all the C levels. At excess C the magnetic Co started high at 1340 then dropped at 1430°C with about 1.4% and then increased at 1510°C by 1.4%, for the standard C sample the magnetic Co content decreased with increase in sintering temperature.

As the sintering temperature increased the hardness of alloy-A decreased for all the C level and the toughness decreased as the temperature increased for the C levels except for "deficient C". This corresponds to literature which stipulate as the sintering temperature increased the hardness of the material will decrease [29]. This has also been proven by the grain growth that has been observed, which also relates to literature that hardness is influenced also by the grain size of the alloy [2], which is backed up by the calculated grain size. For the larger grain sizes the hardness of the alloy decreased. The XRD of the Alloy for all the C contents did not show any change, the peaks are aligned almost parallel to each for all the conditions.

#### 5.3.2.2. Alloy-B

The density of alloy-B for all the C levels was fluctuating as the sintering temperature increased. At deficient C the density started low at 1340°C and then increased by about 6% at 1430°C and dropped by 0.4% at 1510°C.

At standard C the density started low at 1340°C then increased by 0.2% at 1430°C and at 1510°C it dropped by 0.6%. With excess C a similar observation was made as with the other C level as the sintering temperature increased. There were cracks that were seen on some of the samples after sintering on the deficient C at 1340°C, these may be the cause of the fluctuating density values.

As the sintering temperature increases the Coercivity values for alloy-B were fluctuating. At 1430°C higher Coercivity values than on the other sintering temperatures were observed. So the trend that is followed in all the C level, the coercive forces started low at 1340°C, thereafter shoots up at 1430°C and dropped again at 1510°C. The magnetic Co increased with an increase in temperature for both Std and excess C levels and alternated for the deficient C as temperature increased at 1340 $^0$C; its started high then dropped at 1430°C by about 4% and shoot up again at 1510°C with about 13%. This implies that there is more W that has precipitated out on the Co solid solution at 1430 $^0$C than in all the other sintering temperatures.

Hardness of alloy-B increased as the temperature increases for both deficient and standard C levels, which was not what is generally expected. From literature [1] it has been said that as the sintering temperature of a material increases its overall hardness decreases, but in this case the opposite was evident; this may be due to the presence of the mixed carbides which require higher temperatures to sinter to the expected structures. This is proven by the XRD peaks that do not show all the main elements present in the alloys. Hardness of the alloy was very low at 1340°C for deficient C, which was not what was expected. From literature [2] it is said that deficient C lead to the formation of a hard brittle phase, which increases the overall hardness of the alloy, however, in this instance a different scenario is observed. This may be due to the possibility that the alloy at this temperature is not fully dense, hence, it does not attain the potential hardness required. Toughness increases with increase in sintering temperature for the different C levels, which is not what is expected. This shows that the increase in the sintering temperature improves both mechanical properties, which is an advantage for the cutting tool industry.

From the SEM micrographs as the sintering temperature increased the grains in the microstructure became more defined in shape, and there was no grain growth observed, which supports hardness that had been seen to increase with an increase in sintering temperature. Also as the temperature increaseed the (Ti, TiN) C phases disapated on the microstructure, and dissipated towards the edges of the microstructure to create the gradient zone as mensioned in Section 2.1 (Fig. 2.5).

#### 5.3.2.3. Alloy-C

As the sintering temperature increased the density of alloy-C was quite constant for all the C levels. The alloy became lighter as the sintering temperature increased then the porosity of the material reduced and the density was getting closer to the theoretical density of 13.05 $g/cm^3$ and even less as the temperature increases. Densification has reached its completion.

The Coercivity of alloy-C decreased with increase in temperature for all the different C levels. As the temperature goes high there is less coercive forces required to demagnetize the alloy. Although the values are very high as compared to the other alloys above, it shows that the Co content plays a very big role on the Coercivity of hard metals. Magnetic Co increases with the increase in sintering temperature as it is expected because all the mixed carbide at higher temperatures has the opportunity to form to completion and leaving the Co as purer as possible along the grain boundary.

Hardness of alloy-C increased with an increase in sintering temperature, this was because of the same reason as observed in alloy-B, as well as the addition of the cubic carbides. It was also said that as the Co content increased the hardness decreased, this had been proven to be true on this alloy, the hardness of this alloy was very high. The toughness of the alloy however was affected as the temperature increased in both standard and excess C levels the toughness of the alloy decreased and only with the deficient C level where the toughness was seen to increase with an increase in sintering temperature.

The Co rich phases increase with an increase in sintering temperature and the grain size did not increase due to the presence of the grain growth inhibitor in the alloy. The grain size of the alloy also supports the high hardness values that have been seen. For the XRD analysis it clear that the peaks of all the added carbides become more visible as the temperature increases as it is expected.

#### 5.3.2.4. Alloy-D

As the sintering temperature increases the density of alloy-D for deficient and standard C levels increases, this has not been seen this work. The density of alloy-D remained constant as the sintering temperature increased, this tells us that sintering temperature has an effect on the density of the alloy up to a certain point. The lowest density point that was seen for "excess C" was lower than the theoretical density of the alloy, whilst with the other C levels the density increased to exactly the theoretical density of 12.44 g/ $cm^3$.

The coercivity of the alloy decreased with an increase in the sintering temperature leading to the lower value of the coercive forces required to demagnetize the alloy. The magnetic Co increased with an increase in the sintering temperature, more of the Co is exposed.

The hardness of the alloy increased with an increase in the sintering temperature for the standard and excess C levels. However the deficient C level showed the opposite trend. The high hardness for this alloy is also attributed to the presence of the mixed carbides. The toughness of the alloy also increased with an increase in sintering temperature.

# Chapter 6

## Conclusions

The main aim of this project was to determine the optimum carbon level and sintering temperature for four cemented carbide tool grades. These are listed in Table 6.1. The values listed for the C content correspond to the initial level of C added to the powder mixture, to ensure proper composition selection during production, in order to manufacture a sintered material having optimum properties.

Table 6.1 Optimum C level and sintering temperature for all tool grades.

| | | **Option 1** | **Option 2** |
|---|---|---|---|
| **Alloy-A** | **C level** | Standard | Deficient |
| | **Temp($^{o}$C)** | 1430 | 1510 |
| **Alloy-B** | **C level** | Standard | Excess |
| | **Temp($^{o}$C)** | 1510 | 1430 |
| **Alloy-C** | **C level** | Standard | Standard |
| | **Temp($^{o}$C)** | 1430 | 1510 |
| **Alloy-D** | **C level** | Standard | Excess |
| | **Temp($^{o}$C)** | 1510 | 1430 |

The general conclusions for this research are:

- As the C level increased the density of the alloys remained fairly similar at each sintering temperature, with minor deviations observed for some of the alloys. The coercivity of the alloys decreased as the C level increased, except for alloy-A at the two lower sintering temperatures. The magnetic Co present was generally highest at the highest C level. There was no overall trend of increasing hardness and decreasing fracture toughness for all the alloys, as the C level increased. Each alloy showed its own specific trends in this regard, which was shown to be dependent on composition and microstructure. No direct relationship could be established between WC grain size and C content.
- As the sintering temperatures increased the density of the some of the alloys decreased while others remained similar. The porosity levels did not follow any specific trends. The coercivity decreased for all alloys except alloy-B, as the temperature increased, while the magnetic Co showed varying trends.

- XRD analysis did not show any phase evolution. Some evidence of grain growth was found at the higher sintering temperature for some of the alloys. However no consistent and direct relationship could be established for all the alloys. The hardness and fracture toughness relationships for all the alloys showed varying trends with respect to sintering temperature.

# Chapter 7

## Recommendations

- Additional characterization of the sintered compacts, e.g. TEM studies, and different microscopic techniques to provide deeper analysis of the effect of C.
- Repetition of the XRF analysis using a different model than the one used in this work.
- Sintering alloys C and D at 1340°C so that the effect of sintering temperature can be compared for all the alloys at all temperatures.
- Investigate the influence of C content on the green properties in further detail. Manufacture cutting tools from the powders for testing in commercial applications.

# References


1. P. Schwarzkopf, *Powder Metallurgy: Its Physics and Production*, Macmillan, New York, 1947.
2. G.S. Upadhyaya, *Cemented Tungsten Carbides: Production, Properties, and Testing*, Noyes Publications, New Jersey, 1998.
3. T.R. Sharer, *The designer's guide to Tungsten Carbide,* www.generalcarbide.com August 2012
4. http://users.encs.concordia.ca/~mmedraj/mech421/lecture%2012%20PM.pdf January 2013
5. A. Peterson, *Cemented Carbide Sintering: Constitutive relations and microstructural evolution*, PhD thesis, KTM, Stockholm, 2004.
6. R. Frykholm, M. Ekroth, B. Jansson, H.-O. Andren, J. Agren, *Effect of cubic phase composition on gradient zone formation in cemented carbides*, International Journal of Refractory Metals and Hard Materials**,** Volume 19, Issues 4–6, 527–538
7. www.hardmetals.sandvik.com
8. H.E. Exner, *Physical and chemical nature of cemented carbide*, Int. Mater. Rev., 4, 149-173, 1979.
9. L. Zhang, T.E. Madey, *Initial Stages of Sintering of Nanostructured WC-7wt.%Co*, Nano-Structured Materials, 2, 487-493, 1993.
10. S. Luyckx, *Nucleation and propagation of fracture in WC-Co alloys*, Ph.D. thesis, University of the Witwatersrand, Johannesburg, 1967.
11. Wilson Acchar, Cordt Zollfrank, Peter Greil, *Microstructure and Mechanical Properties of WC-Co reinforced with NbC*, Mat. Res. vol.7 no.3 São Carlos July/Sept. 2004
12. S.G. Huang, L. Li, O. Van der Biest , J. Vleugels , *VC- and Cr3C2-doped WC–NbC–Co hardmetals*, Journal of Alloys and Compounds**.** Volume 464, issues 1-2, 205–211
13. M. Hashiva, Y. Kubo, *The Influence of Carbon Content and Additions of Growth Inhibitors (V, Cr) on the Formation of Melt in WC-Co and WC-Ni alloys*, 17 Plansee Seminar 2009", issued by: Plansee Group, Austria; Plansee Group, Reutte, Austria, Reutte, Tirol, 2009, HM 55/1 - HM 55/17.

14. G.S. Upadhyaya, *Powder Metallurgy Technology,* Cambridge international Science publication, 2002
15. A.T. Santhanam, P. Tierney, J. L. Hunt, *Cemented Carbide*", Metals Handbook, ASM Int., 10th Ed., 2, 950-977, 1990.
16. J.D. Schell, K.P. Taylor, *Wear of Jet Engine Components*, ASM Handbook, 18, 588-592, 1992.
17. www.subtech.com, November 2012.
18. R.M. German, *Liquid Phase Sintering*, Plenum Press, New York, 1985.
19. W.B. Eisen, B.L. Ferguson, R.M. German, *Powder metal technologies and applications,* ASM Handbook, 7, 1154-1156, 1998.
20. ASTM Standard B276-91(2000), *Standard Test Method for Apperant Porosity in Cemented Carbides,* developed by Subcommittee: B09.06, Book of Standards vol 02.05
21. R.M. German, S*intering Theory and Practice,* John Wiley & sons, Inc., USA, 1996.
22. D. Tabor, *The Hardness of Metals,* Oxford University Press Inc., New York, 1951.
23. Ashby et al, *Materials: Engineering, Science, Processing and Design*, Elsevier Ltd publication, Ed 1, Chapter 8,2007
24. M.T. Laugier, *Coercivity, hardness and microstructure in WC-Co composites*, J. Mater. Sci. , 4, 211-216, 1985.
25. D.K. Shetty, I.G. Wright, P.N. Mincer, A.H. Clauer, *Indentation fracture of WC-Co cermets*, J. Mater. Sci., 20, 1873-1882, 1985.
26. MPIF Standard 42, *Determination of Density of Compacted or Sintered Powder Metallurgy products,* Metal Powder Industries Federation, 1980.
27. ISO standard 3326:2013, *Hardmetal-Determination of (the magnetization) coercivity*, Ed 2, ICS: 77.040.99.
28. ISO standard 3878:2013, *Hardmetal-Vickers hardness test*, Ed 3, ICS: 77.040.10.
29. M. Mahmoodan, H. Aliakbarzadeh, F. Shahri, *Effect of Cr3C2 and VC on the Mechanical and Structural Properties of Sintered WC-%10wt Co Nano Powders,* World Journal of Nano Science and Engineering, Vol.3 No.2(2013)
30. A.M. Soleimanpour, P. Abachi , A. Simchi '*Microstructure and mechanical properties of WC–10Co cemented carbide containing VC or (Ta, Nb)C and*

*fracture toughness evaluation using different models*' Int. Journal of Refractory Metals and Hard Materials 31 (2012) 141–146

# Appendix-A

## Carbon balance calculations

For the different carbon levels calculations were done to determine how much carbon had to be added or subtracted prior to mixing. Below is the summary of the calculations for all grades.

***Alloy-A***

Std C level:

WC = W + C

$$C = \frac{M_C}{M_C + M_W} \times 100 = \frac{12.01\ g/mol}{(12.01 + 183.84)\ g/mol} = 6.14\%$$

Assuming 1000 g of total powder mixed, WC is 94%

$$moles\ of\ C_{std} = \frac{1000\ g \times 94\% \times 6.14\%}{12.01\ \frac{g}{mol}} = 4.7996\ mol$$

Deficient C level

$$moles\ of\ C_{def} = \frac{1000\ g \times 94\% \times 5.9\%}{12.01\ \frac{g}{mol}} = 4.6178\ mol$$

$$Mole\ difference\ C = moles\ of\ C_{std} - moles\ of\ C_{def} = 4.7996 - 4.6178 = 0.1818\ mol$$

From the reaction stoichiometric $n_c = n_W = 0.1818$ mol

Tungsten is added to reduce the carbon level and mass added was:

$$mass\ of\ W_{added} = mole\ difference\ C \times M_W = 0.1818\ mol \times \frac{183.84\ g}{mol} = 33.4221\ g$$

Excess C level

$$moles\ of\ C_{exc} = \frac{1000\ g \times 94\% \times 6.3\%}{12.01\ \frac{g}{mol}} = 4.9309\ mol$$

$$Mole\ difference\ C = moles\ of\ C_{exc} - moles\ of\ C_{std} = 4.9309 - 4.7996 = 0.1313\ mol$$

Because it is excess level, carbon is added to the mixture, and the mass is:

$$mass\ of\ C_{added} = mole\ difference\ C \times M_C = 0.1313\ mol \times \frac{12.01\ g}{mol} = 1.6\ g$$

***Alloy-B***

Std C level:

It was assumed that the mixed crystals will be kept constant for all the carbon variations to simplify the calculations.

WC = W + C

$$C = \frac{M_C}{M_C + M_W} \times 100 = \frac{12.01\ g/mol}{(12.01 + 183.84)\ g/mol} = 6.14\%$$

Assuming 1000 g of total powder mixed, WC is 82.4%

$$moles\ of\ C_{std} = \frac{1000\ g \times 82.4\% \times 6.14\%}{12.01\ \frac{g}{mol}} = 4.2057\ mol$$

Deficient C level

$$moles\ of\ C_{def} = \frac{1000\ g \times 82.4\% \times 5.9\%}{12.01\ \frac{g}{mol}} = 4.0480\ mol$$

$$Mole\ difference\ C = moles\ of\ C_{std} - moles\ of\ C_{def} = 4.2057 - 4.0480 = 0.1577\ mol$$

From the reaction stoichiometric $n_c = n_W = 0.1577$ mol

Tungsten is added to reduce the carbon level and mass added was:

$$mass\ of\ W_{added} = mole\ difference\ C \times M_W = 0.1577\ mol \times \frac{183.84\ g}{mol} = 28.9989\ g$$

Excess C level

$$moles\ of\ C_{exc} = \frac{1000\ g \times 82.4\% \times 6.3\%}{12.01\ \frac{g}{mol}} = 4.3224\ mol$$

$$Mole\ difference\ C = moles\ of\ C_{exc} - moles\ of\ C_{std} = 4.3224 - 4.2057 = 0.1167\ mol$$

Because it is excess level, carbon is added to the mixture, and the mass is:

$$mass\ of\ C_{added} = mole\ difference\ C \times M_C = 0.1167\ mol \times \frac{12.01\ g}{mol} = 1.4\ g$$

***Alloy-C***

Std C level:

It was assumed that the mixed crystals will be kept constant for all the carbon variations to simplify the calculations.

WC= W + C

$$C = \frac{M_C}{M_C + M_W} \times 100 = \frac{12.01\ g/mol}{(12.01 + 183.84)\ g/mol} = 6.14\%$$

Assuming 1000g of total powder mixed, WC is 79.5%

$$moles\ of\ C_{std} = \frac{1000\ g \times 79.5\% \times 6.14\%}{12.01\ \frac{g}{mol}} = 4.064\ mol$$

Deficient C level

$$moles\ of\ C_{def} = \frac{1000\ g \times 79.5\% \times 5.9\%}{12.01\ \frac{g}{mol}} = 3.904\ mol$$

$$Mole\ difference\ C = moles\ of\ C_{std} - moles\ of\ C_{def} = 4.064 - 3.904 = 0.1588\ mol$$

From the reaction stoichiometric $n_c = n_W = 0.1588$ mol

Tungsten is added to reduce the carbon level and mass added was:

$$mass\ of\ W_{added} = mole\ difference\ C \times M_W = 0.1588\ mol \times \frac{183.84\ g}{mol} = 29.206\ g$$

Excess C level

$$moles\ of\ C_{exc} = \frac{1000\ g \times 79.5\% \times 6.3\%}{12.01\ \frac{g}{mol}} = 4.170\ mol$$

$$Mole\ difference\ C = moles\ of\ C_{exc} - moles\ of\ C_{std} = 4.170 - 4.064 = 0.1059\ mol$$

Because it is excess level, carbon is added to the mixture, and the mass is:

$$mass\ of\ C_{added} = mole\ difference\ C \times M_C = 0.1059\ mol \times \frac{12.01\ g}{mol} = 1.272\ g$$

***Alloy-D***

Std C level:

It was assumed that the mixed crystals will be kept constant for all the carbon variations to simplify the calculations.

WC= W + C

$$C = \frac{M_C}{M_C + M_W} \times 100 = \frac{12.01\ g/mol}{(12.01 + 183.84)\ g/mol} = 6.14\%$$

Assuming 1000g of total powder mixed, WC is 72.65%

$$moles\ of\ C_{std} = \frac{1000\ g \times 72.65\% \times 6.14\%}{12.01\ \frac{g}{mol}} = 3.714\ mol$$

Deficient C level

$$moles\ of\ C_{def} = \frac{1000\ g \times 72.65\% \times 5.9\%}{12.01\ \frac{g}{mol}} = 3.569\ mol$$

$$Mole\ difference\ C = moles\ of\ C_{std} - moles\ of\ C_{def} = 3.914 - 3.569 = 0.1452\ mol$$

From the reaction stoichiometric $n_c = n_W = 0.1452$ mol

Tungsten is added to reduce the carbon level and mass added was:

$$mass\ of\ W_{added} = mole\ difference\ C \times M_W = 0.1452\ mol \times \frac{183.84\ g}{mol} = 28.433\ g$$

Excess C level

$$moles\ of\ C_{exc} = \frac{1000\ g \times 72.65\% \times 6.3\%}{12.01\ \frac{g}{mol}} = 3.811\ mol$$

$$Mole\ difference\ C = moles\ of\ C_{exc} - moles\ of\ C_{std} = 3.811 - 3.714 = 0.0097\ mol$$

Because it is excess level, carbon is added to the mixture, and the mass is:

$$mass\ of\ C_{added} = mole\ difference\ C \times M_C = 0.0097\ mol \times \frac{12.01\ g}{mol} = 1.162\ g$$

# Appendix-B

## Powders chemical analysis

***Starting Powders***

Table B1: Starting powder XRF Chemical analysis.

| | W | WC | C | Co | HV3 | HV100 | TiCN |
|---|---|---|---|---|---|---|---|
| **F** | 0.0000 | 0.0000 | 0.0000 | 2.2195 | 0.0000 | 0.0000 | 0.0000 |
| **Cl** | 0.0000 | 0.0000 | 2.4733 | 0.0246 | 0.0000 | 0.0000 | 0.0000 |
| **Ca** | 0.0351 | 0.0455 | 1.3466 | 0.0000 | 0.0187 | 0.0129 | 0.0000 |
| **Ni** | 0.0000 | 0.0000 | 0.0000 | 0.0000 | 0.069229 | 0.0000 | 0.0100 |
| **Mg** | 0.0000 | 0.0000 | 0.1161 | 0.0000 | 0.0000 | 0.0000 | 0.0091 |
| **Na** | 0.0000 | 0.0000 | 2.0280 | 0.0000 | 0.0000 | 0.0000 | 0.0000 |
| **Si** | 0.0000 | 0.0019 | 0.7553 | 0.0124 | 0.0000 | 0.0000 | 0.0000 |
| **Zr** | 0.0000 | 0.0000 | 0.0000 | 0.0000 | 0.0000 | 0.0113 | 0.0100 |
| **Ti** | 0.0238 | 0.1944 | 1.0211 | 0.0210 | 13.4155 | 32.0811 | 58.9563 |
| **W** | 78.9690 | 78.8425 | 55.2804 | 0.6878 | 25.3441 | 36.6850 | 0.7249 |
| **S** | 0.0642 | 0.0000 | 3.6281 | 0.1405 | 0.0000 | 0.0194 | 0.0028 |
| **Mo** | 0.0553 | 0.0000 | 0.0000 | 0.0000 | 0.1142 | 0.0000 | 0.0189 |
| **Cr** | 0.0000 | 0.0000 | 0.0000 | 0.0000 | 0.0000 | 0.0000 | 0.0097 |
| **Fe** | 0.0449 | 0.0320 | 2.1313 | 0.0080 | 0.2815 | 0.0138 | 0.0776 |
| **Co** | 0.0000 | 0.0953 | 3.3886 | 67.8490 | 0.1584 | 0.0362 | 0.0962 |
| **Al** | 0.0000 | 0.0000 | 0.2914 | 0.0086 | 0.0083 | 0.0000 | 0.0086 |
| **Ga** | 0.0129 | 0.0000 | 0.0000 | 0.0000 | 0.0000 | 0.0000 | 0.0000 |
| **Ta** | 0.0000 | 0.0000 | 0.5896 | 0.0000 | 31.3401 | 0.0320 | 0.0117 |
| **V** | 0.0000 | 0.0000 | 0.0000 | 0.0000 | 0.203287 | 0.0000 | 0.1327 |
| **P** | 0.0000 | 0.0000 | 0.0000 | 0.0000 | 0.0000 | 0.0000 | 0.0004 |
| **Nb** | 0.0000 | 0.0000 | 0.0000 | 0.0000 | 4.2615 | 0.0130 | 0.0498 |
| **K** | 0.0000 | 0.0000 | 1.4004 | 0.0000 | 0.0000 | 0.0000 | 0.0000 |

Table B2: Starting powder ICP Chemical analysis.

| | W | WC | C | Co | HV3 | HV100 | TiCN |
|---|---|---|---|---|---|---|---|
| **C** | 0.033 | 6.420 | 98.000 | 0.084 | 9.020 | 12.940 | 10.440 |
| **S** | 0.077 | 0.070 | 0.103 | 0.022 | 0.074 | 0.067 | 0.077 |
| **Co** | 0.400 | 0.400 | 0.005 | 99.000 | 0.470 | 0.210 | 0.130 |
| **Zn** | 0.005 | 0.005 | 0.005 | 0.005 | 0.005 | 0.0005 | 0.005 |
| **Si** | 0.005 | 0.041 | 0.007 | 0.005 | 0.005 | 0.159 | 0.007 |
| **Cr** | 0.014 | 0.009 | 0.006 | 0.005 | 0.019 | 0.005 | 0.013 |
| **Mo** | 0.027 | 0.005 | 0.005 | 0.005 | 0.074 | 0.005 | 0.051 |
| **Ni** | 0.017 | 0.016 | 0.005 | 0.030 | 0.014 | 0.007 | 0.005 |
| **Cu** | 0.016 | 0.015 | 0.005 | 0.005 | 0.120 | 0.010 | 0.005 |
| **Nb** | 0.013 | 0.012 | 0.008 | 0.005 | 4.750 | 0.033 | 0.487 |
| **V** | 0.005 | 0.005 | 0.005 | 0.005 | 0.005 | 0.005 | 0.005 |
| **Ti** | 0.029 | 0.035 | 0.015 | 0.005 | 11.510 | 43.200 | 88.500 |
| **Ta** | 0.095 | 0.094 | 0.018 | 0.005 | 40.33 | 0.005 | 0.005 |
| **Fe** | 0.028 | 0.022 | 0.119 | 0.005 | 0.207 | 0.015 | 0.059 |
| **W** | 95.690 | 94.99 | 0.005 | 0.005 | 33.140 | 43.150 | 0.005 |
| **O** | 0.177 | 0.032 | 0.267 | 0.268 | 0.155 | 0.158 | 0.116 |

***Milled powders***

Table B3: Milled powder XRF Chemical analysis.

| | PA-d | PA-s | PA-e | PB-d | PB-s | PB-e | PC-d | PC-s | PC-e | PD-d | PD-s | PD-e |
|---|---|---|---|---|---|---|---|---|---|---|---|---|
| **F** | 0.896 | 0.673 | 0.593 | 0.589 | 0.638 | 0.615 | 0.179 | 0.251 | 0.635 | 0.632 | 0.077 | 0.504 |
| **Cl** | 0.000 | 0.000 | 0.019 | 0.000 | 0.000 | 0.000 | 0.000 | 0.000 | 0.000 | 0.000 | 0.000 | 0.000 |
| **Ca** | 0.040 | 0.063 | 0.042 | 0.030 | 0.044 | 0.027 | 0.035 | 0.036 | 0.034 | 0.028 | 0.026 | 0.038 |
| **Mg** | 0.000 | 0.000 | 0.000 | 0.000 | 0.000 | 0.010 | 0.000 | 0.000 | 0.000 | 0.003 | 0.000 | 0.000 |
| **Na** | 0.000 | 0.000 | 0.006 | 0.000 | 0.000 | 0.000 | 0.000 | 0.000 | 0.000 | 0.000 | 0.000 | 0.000 |
| **Si** | 0.000 | 0.000 | 0.002 | 0.000 | 0.000 | 0.000 | 0.000 | 0.001 | 0.000 | 0.007 | 0.000 | 0.000 |
| **Ti** | 0.000 | 0.072 | 0.069 | 4.361 | 4.145 | 5.024 | 6.556 | 6.721 | 6.877 | 6.990 | 7.016 | 6.744 |
| **W** | 71.320 | 71.302 | 71.369 | 62.690 | 63.443 | 62.328 | 63.120 | 62.280 | 61.804 | 57.133 | 58.460 | 57.832 |
| **S** | 0.048 | 0.055 | 0.046 | 0.039 | 0.041 | 0.037 | 0.000 | 0.041 | 0.036 | 0.037 | 0.051 | 0.049 |
| **Mo** | 0.000 | 0.000 | 0.000 | 0.016 | 0.009 | 0.011 | 0.000 | 0.000 | 0.000 | 0.000 | 0.000 | 0.000 |
| **Cr** | 0.000 | 0.020 | 0.000 | 0.000 | 0.000 | 0.000 | 0.286 | 0.320 | 0.312 | 0.000 | 0.000 | 0.000 |
| **Fe** | 0.020 | 0.108 | 0.031 | 0.059 | 0.050 | 0.040 | 0.028 | 0.034 | 0.039 | 0.063 | 0.060 | 0.129 |
| **Co** | 6.284 | 6.228 | 6.346 | 6.596 | 6.390 | 6.314 | 4.655 | 4.949 | 4.898 | 8.741 | 7.800 | 8.390 |
| **Al** | 0.012 | 0.010 | 0.010 | 0.008 | 0.011 | 0.000 | 0.000 | 0.008 | 0.007 | 0.006 | 0.008 | 0.008 |
| **Ta** | 0.000 | 0.000 | 0.000 | 2.256 | 2.178 | 2.277 | 1.519 | 1.614 | 1.661 | 1.930 | 1.995 | 1.926 |
| **V** | 0.000 | 0.005 | 0.000 | 0.147 | 0.000 | 0.000 | 0.000 | 0.000 | 0.000 | 0.168 | 0.215 | 0.187 |
| **P** | 0.000 | 0.000 | 0.000 | 0.000 | 0.000 | 0.000 | 0.000 | 0.000 | 0.000 | 0.000 | 0.000 | 0.000 |
| **Nb** | 0.000 | 0.000 | 0.000 | 0.293 | 0.299 | 0.298 | 0.211 | 0.213 | 0.209 | 0.225 | 0.228 | 0.230 |

Table B4: Milled powder ICP Chemical analysis.

| | PA-d | PA-s | PA-e | PB-d | PB-s | PB-e | PC-d | PC-s | PC-e | PD-d | PD-s | PD-e |
|---|---|---|---|---|---|---|---|---|---|---|---|---|
| **C** | 6.020 | 6.580 | 6.320 | 6.490 | 6.900 | 6.760 | 7.030 | 7.720 | 7.540 | 7.470 | 6.910 | 8.090 |
| **S** | 0.065 | 0.067 | 0.071 | 0.670 | 0.067 | 0.048 | 0.075 | 0.073 | 0.080 | 0.075 | 0.086 | 0.087 |
| **Co** | 6.230 | 6.000 | 6.380 | 6.540 | 6.280 | 6.520 | 4.790 | 4.720 | 4.380 | 9.180 | 9.640 | 9.740 |
| **Zn** | 0.005 | 0.005 | 0.005 | 0.005 | 0.005 | 0.005 | 0.005 | 0.005 | 0.005 | 0.005 | 0.005 | 0.005 |
| **Si** | 0.040 | 0.033 | 0.042 | 0.298 | 0.286 | 0.341 | 0.302 | 0.281 | 0.262 | 0.428 | 0.369 | 0.352 |
| **Cr** | 0.008 | 0.011 | 0.008 | 0.009 | 0.01 | 0.011 | 0.193 | 0.185 | 0.186 | 0.022 | 0.016 | 0.018 |
| **Mo** | 0.005 | 0.005 | 0.005 | 0.006 | 0.006 | 0.005 | 0.005 | 0.005 | 0.005 | 0.005 | 0.005 | 0.005 |
| **Ni** | 0.023 | 0.022 | 0.023 | 0.022 | 0.021 | 0.022 | 0.019 | 0.019 | 0.018 | 0.027 | 0.022 | 0.025 |
| **Cu** | 0.018 | 0.017 | 0.018 | 0.027 | 0.024 | 0.027 | 0.027 | 0.025 | 0.021 | 0.026 | 0.021 | 0.022 |
| **Nb** | 0.014 | 0.014 | 0.015 | 0.588 | 0.611 | 0.611 | 0.430 | 0.437 | 0.413 | 0.512 | 0.499 | 0.502 |
| **V** | 0.005 | 0.005 | 0.005 | 0.005 | 0.005 | 0.005 | 0.005 | 0.005 | 0.005 | 0.005 | 0.005 | 0.005 |
| **Ti** | 0.028 | 0.028 | 0.031 | 3.630 | 3.680 | 3.990 | 5.760 | 5.260 | 5.360 | 6.600 | 5.750 | 6.490 |
| **Ta** | 0.081 | 0.076 | 0.079 | 0.777 | 0.789 | 0.835 | 0.608 | 0.594 | 0.559 | 0.767 | 0.688 | 0.748 |
| **Fe** | 0.029 | 0.025 | 0.023 | 0.042 | 0.035 | 0.039 | 0.028 | 0.026 | 0.029 | 0.053 | 0.045 | 0.050 |
| **W** | 83.700 | 80.250 | 84.090 | 74.960 | 72.720 | 76.860 | 77.030 | 73.030 | 77.890 | 73.500 | 75.830 | 70.780 |
| **O** | 0.111 | 0.087 | 0.103 | 0.125 | 0.047 | 0.136 | 0.099 | 0.157 | 0.135 | 0.130 | 0.046 | 0.032 |

# Appendix-C

## EDS of powders

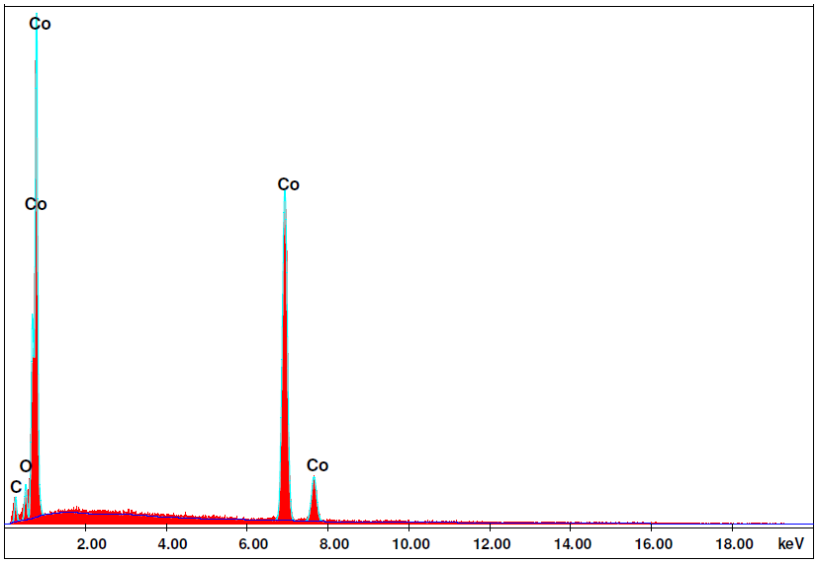


Fig. C1: EDS of Co powder.

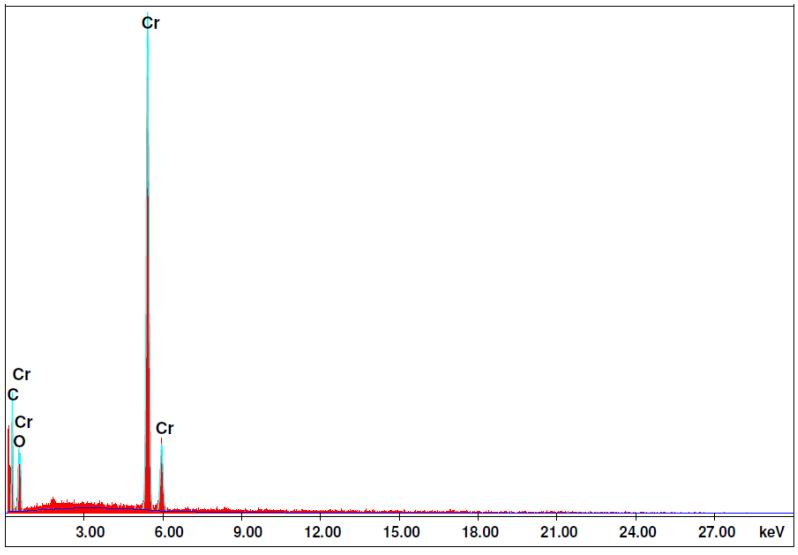


Fig. C2: EDS of $Cr_3C_2$ powder.

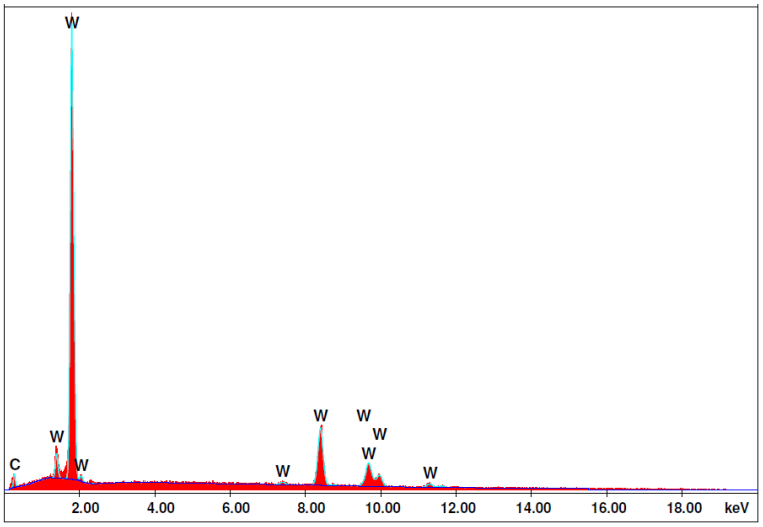


Fig. C3: EDS of WC powder.

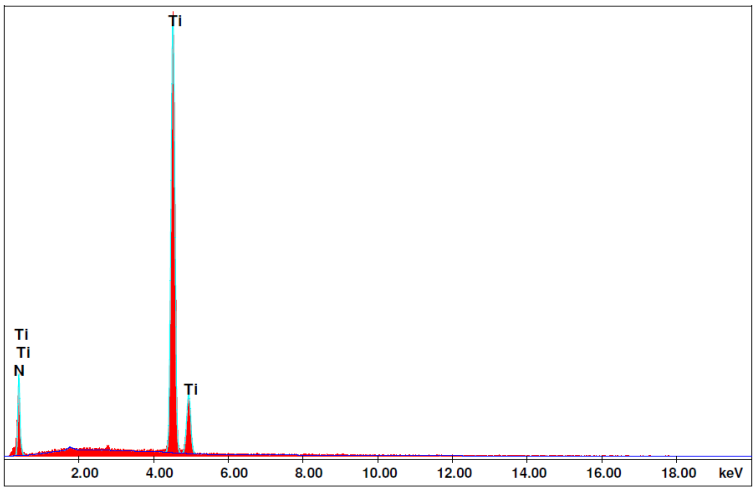


Fig. C4: EDS of TiCN powder.

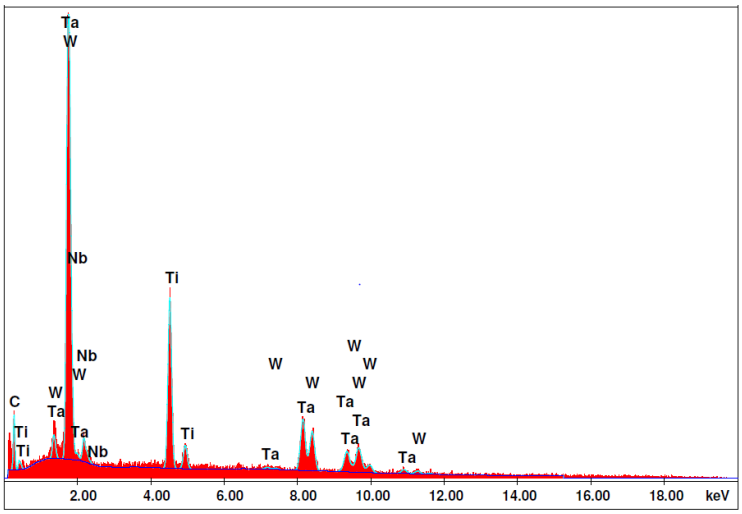


Fig. C5: EDS of MC-2 powder.

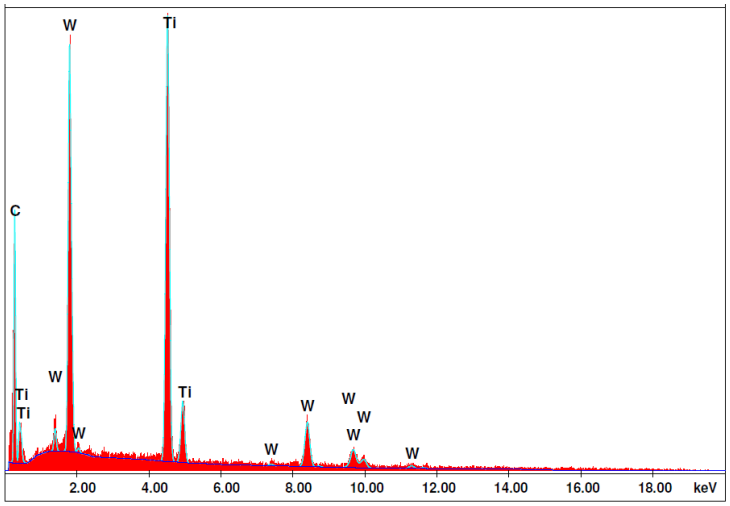


Fig. C6: EDS of MC-1 powder.

# Appendix-D

## XRD of milled powders

The letters on the diagrams represent the following:

- D: Deficient C level,
- S: Standard C level and
- E: Excess C level for all the alloys

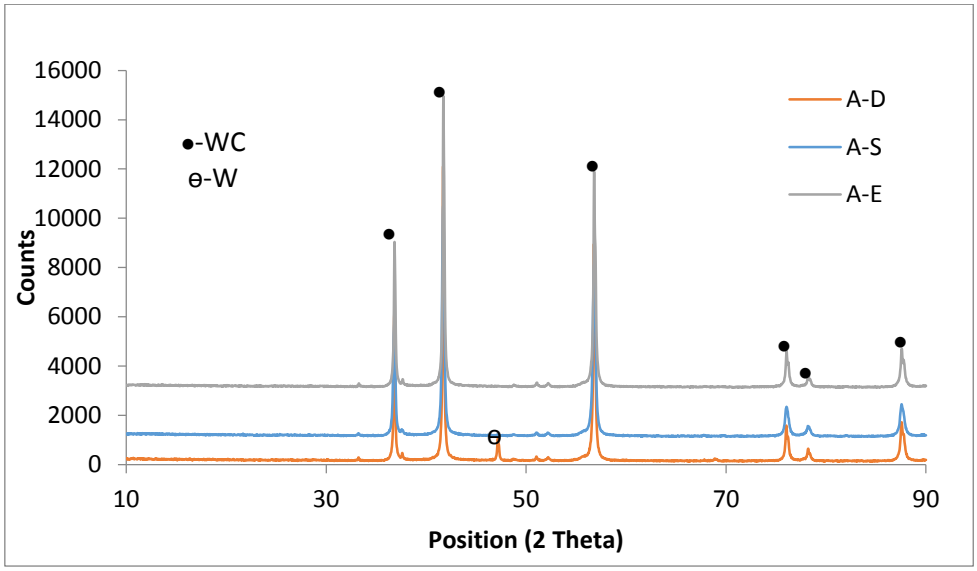


Fig. D1: XRD of alloy-A powder.

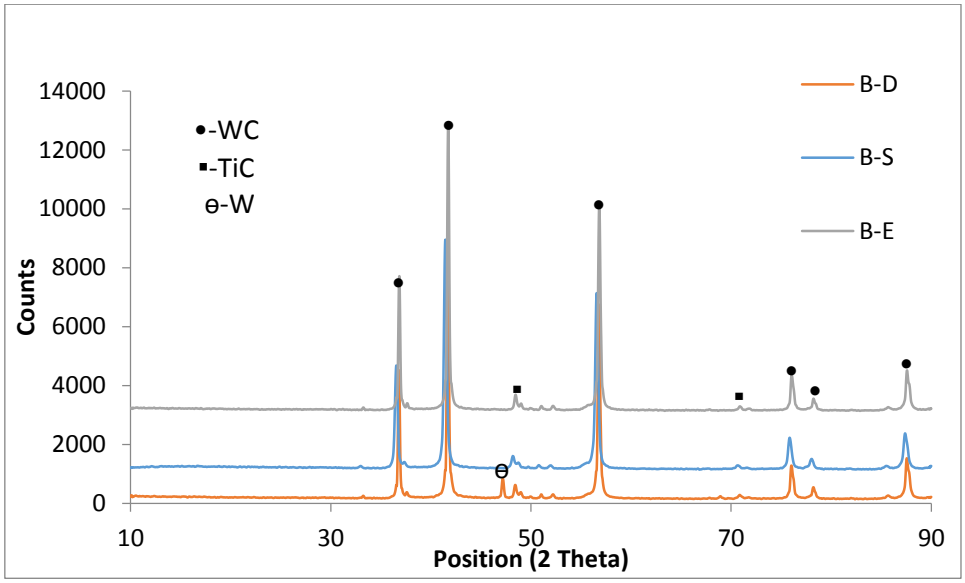


Fig. D2: XRD of alloy-B powder.

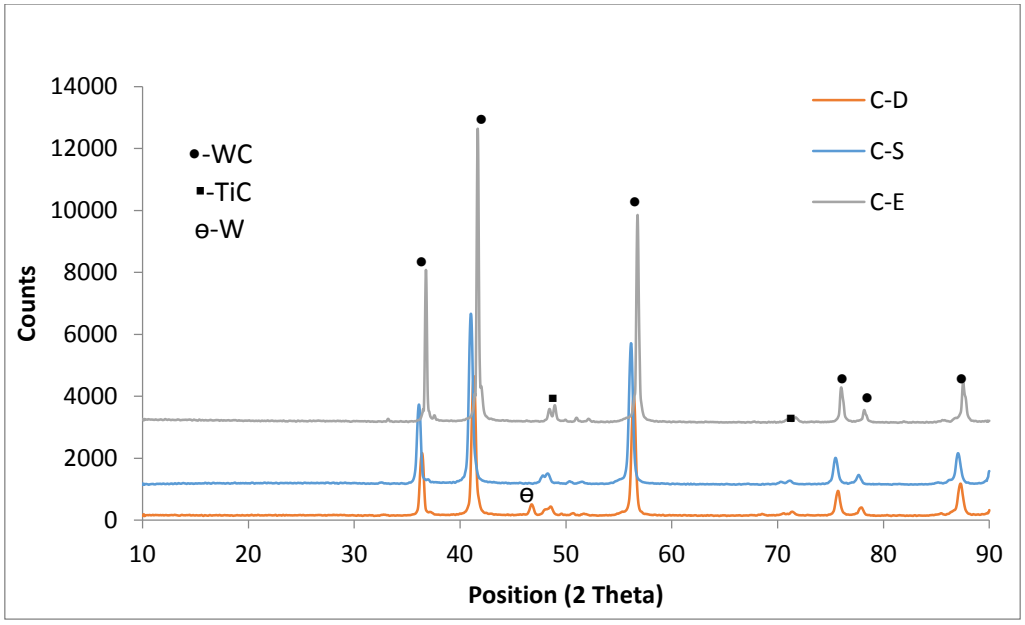


Fig. D3: XRD of alloy-C powder.

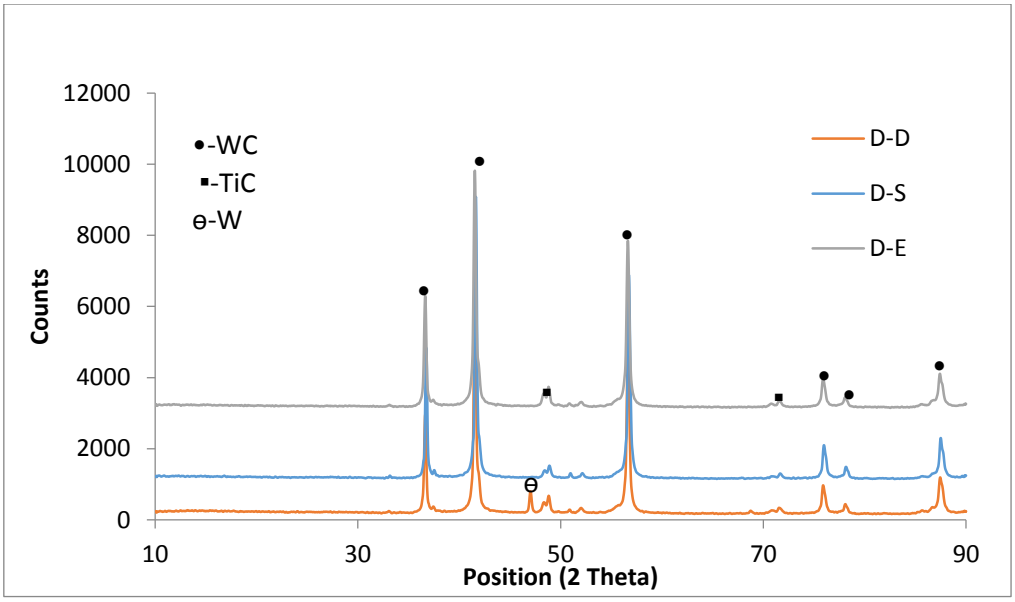


Fig. D4: XRD of alloy-D powder.

# Appendix-E

SEM images and EDS graphs of green compacts

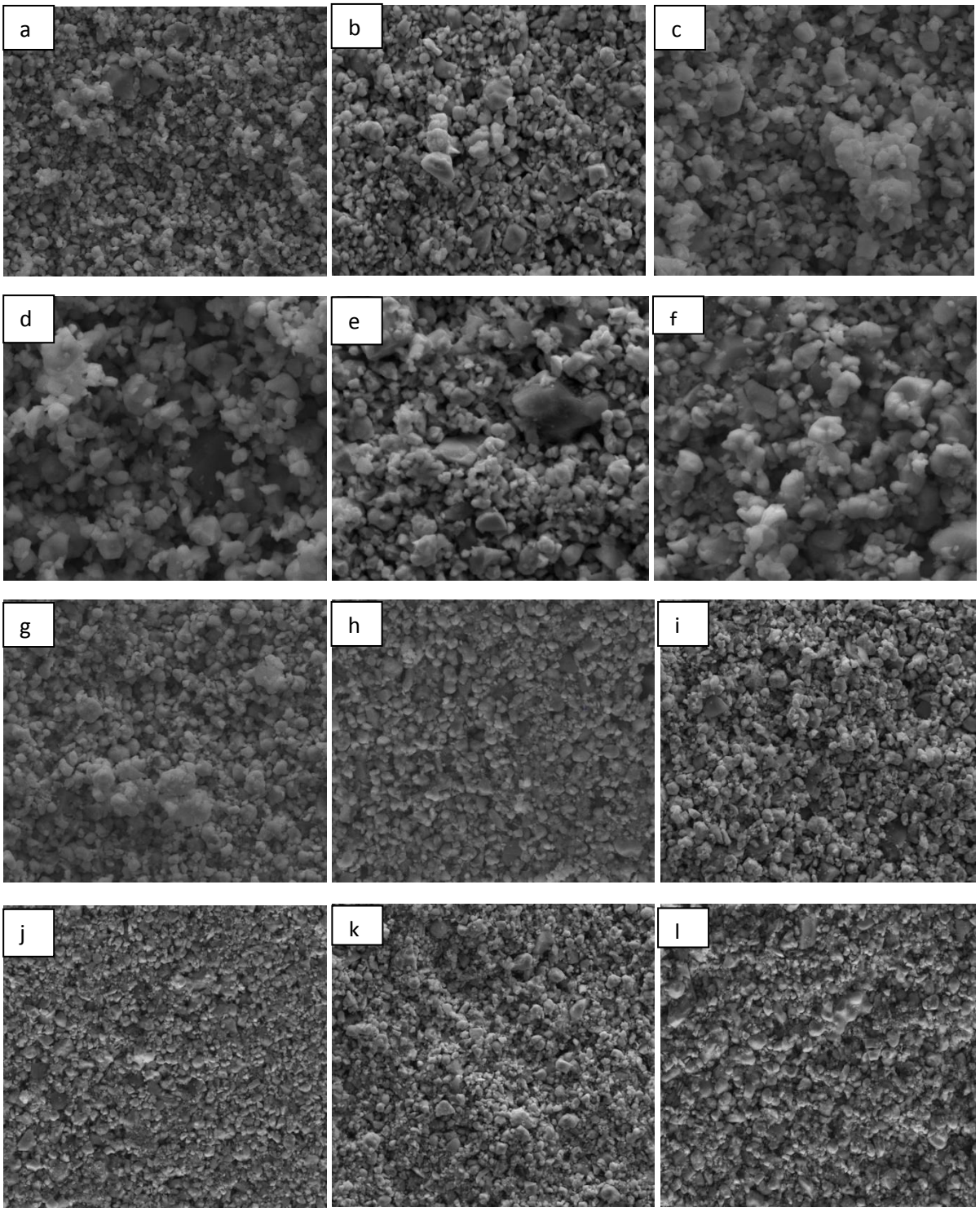


Fig. E1: SEM analysis for the green compacts: (a-c) Alloy-A with deficient to excess C, (d-f) Alloy-B with deficient to excess C, (g-i) Alloy-C with deficient to excess C, (j-l) Alloy-D with deficient to excess C.

***EDS***

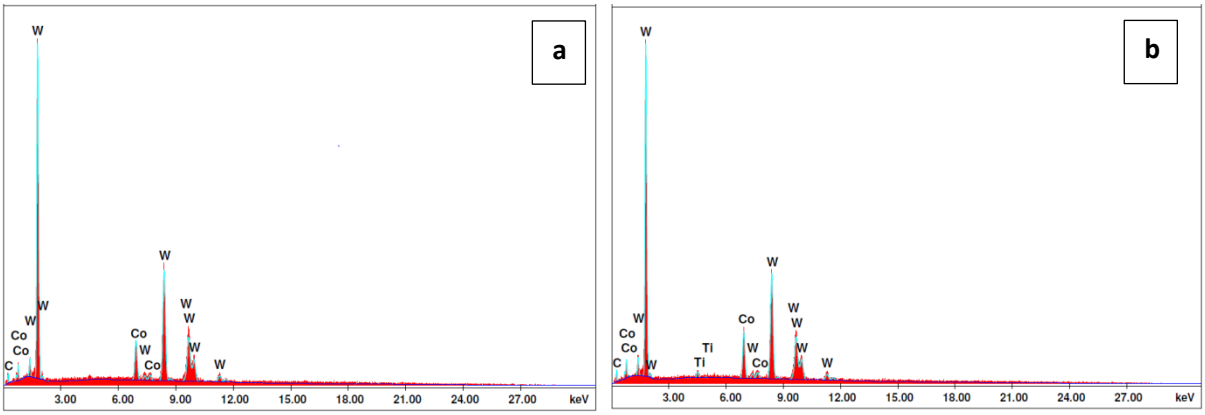


Fig. E2: EDS of alloy-A green compacts (a) Deficient C level and (b) Excess C level.

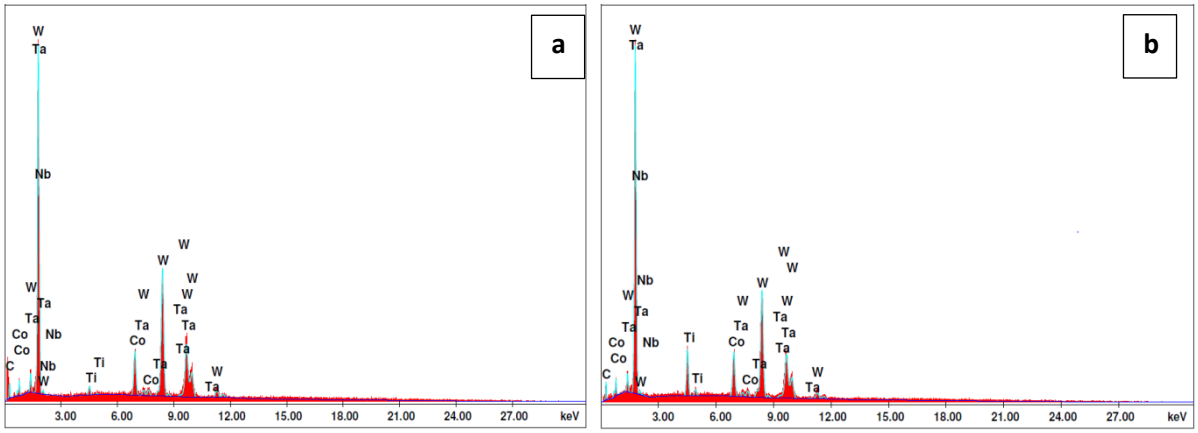


Fig. E3: EDS of alloy-B green compacts (a) Deficient C level and (b) Excess C level.

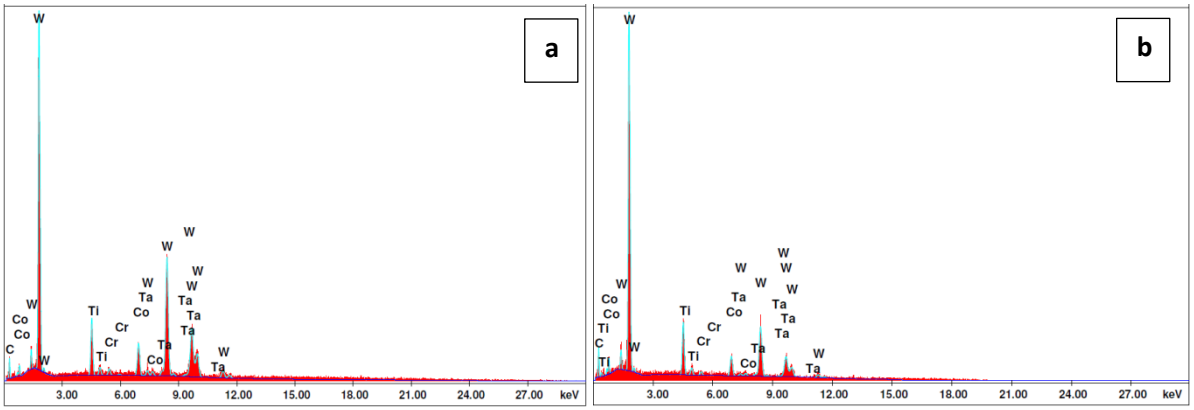


Fig. E4: EDS of alloy-C green compacts (a) Deficient C level and (b) Excess C level.

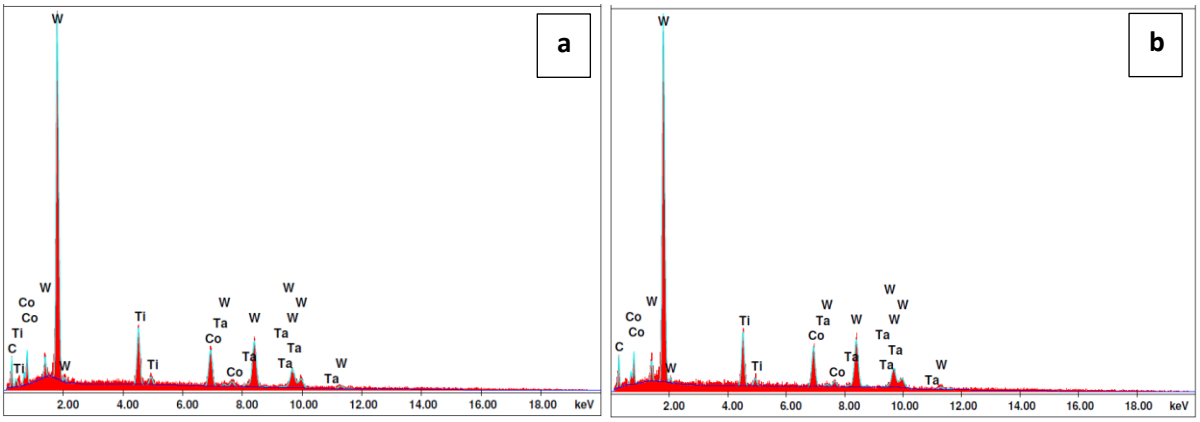


Fig. E5: EDS of alloy-D green compacts (a) Deficient C level and (b) Excess C level.